



Eva Maria Heider, BSc

Energy Dissipation between Seat and Vehicle:  
Analysis of Potential of a New Type of Operating Principle  
to Reduce Occupant Loads in Highly Automated Vehicles

## Master's Thesis

to achieve the University Degree of  
"Diplom-Ingenieurin"

submitted to  
Graz University of Technology  
Faculty of Mechanical Engineering  
Vehicle Safety Institute

Reviewer:  
Assoc.Prof. Dipl.-Ing. Dr.techn. Wolfgang Sinz

Supervisor:  
Dipl.-Ing. Felix Ressi, BSc

Graz, December 2020

*Energy Dissipation between Seat and Vehicle:  
Analysis of Potential of a New Type of Operating Principle to Reduce Occupant Loads in Highly  
Automated Vehicles*

Master's thesis submitted to

Graz University of Technology  
Faculty of Mechanical Engineering  
Vehicle Safety Institute  
Inffeldgasse 23/1  
8010 Graz, Austria

Copyright © 2020 by Eva Heider  
All rights reserved.

# Affidavit

I declare that I have authored this thesis independently, that I have not used other than the declared sources, and that I have explicitly indicated all material which has been quoted either literally or by content from the sources used. The text document uploaded to TUGRAZonline is identical to the present master's thesis.

Graz, 10 December 2020

---

Eva Maria Heider



# Acknowledgments

I would first like to thank my supervisor, Felix Ressi, who was there to offer me guidance at any time throughout my thesis. Together with Desiree Kofler you provided me with invaluable assistance and always had your door open when I had a question about my research. Thank you for guiding me in the right direction whenever I needed it!

I want to thank the Vehicle Safety Institute at Graz University of Technology with its members of staff who gave me the opportunity to work on this exciting topic and warmly welcomed me into their team.

In this context I would also like to acknowledge the use of HPC resources provided by the ZID of Graz University of Technology.

I wish to thank the colleagues I met throughout my studies that became friends for a lifetime and encouraged me whenever the going appeared so tough. Especially in times like the months of writing this thesis it was wholeheartedly appreciated to know you at my side.

Finally, I would like to express my deepest gratitude to my parents and family, who not only made my academic studies possible but also enabled my travels and personal growth during all these years. Thank you for your constant support, words of encouragement and invaluable advice! This accomplishment would not have been successful without you.

Eva Heider



# Abstract

As the introduction of automated vehicles is progressing, the possibilities for new interior concepts rise, too. With the driver becoming a passenger in the vehicle that can adopt new seating positions, a new consideration of occupant protection is required.

Within this thesis, a seat position longitudinally adjusted to the back was investigated. Allowing an in-crash-movement of the seat, a principle of energy dissipation to reduce the occupant loads was researched. The aim was to analyse the principle's potential for future highly automated vehicle concepts.

The principle was integrated into a simplified sled model, that was obtained from a finite element model of a 2014 Honda Accord mid-size sedan in the crash test procedure of an oblique moving deformable barrier test. Adaptations and modifications of the model included the transformation of the load case into a rigid wall test as well as the seat-integrated belt anchorage.

The pre-defined movement of the seat in the crash scenario was modelled with different force-displacement-characteristics. After simulation of various variants, injury assessment reference values were evaluated and compared to the biomechanical limits with a rating system that was partly adopted from NHTSA.

The assessment of the principle was done by comparison of the standard seat position with the position adjusted 400 mm to the rear and the adjusted seat with in-crash-movement.

The new operating principle resulted in a reduction of joint probability of injury of almost 27% compared to the firmly attached seat in a position 400 mm further back. Furthermore, the in-crash-movement led to even lower injury assessment reference values than the reference model with the standard seat in every case except chest deflection. However, a decrease compared to the backwards moved seat position was reached, with a chest injury risk decreased by 11%.

The analysis of the energy dissipating principle showed the potential to reduce occupant loads by one quarter in future highly automated vehicle concepts with a seat position adjusted further behind than the standard position.





# Kurzfassung

Mit der fortschreitenden Einführung von automatisierten Fahrzeugen und Systemen steigen auch die Auslegungsmöglichkeiten für neue Innenraumkonzepte. Da der Fahrer selbst zum Passagier im Fahrzeug wird, der neue Sitzpositionen einnehmen kann, ist eine erweiterte Betrachtung des Insassenschutzes erforderlich.

Im Rahmen dieser Arbeit wurde eine in Längsrichtung nach hinten verschobene Sitzposition untersucht. Ein Prinzip zur Energiedissipation um die Insassenbelastungen zu reduzieren wurde anhand einer in-Crash-Bewegung des Sitzes erforscht. Das Ziel war es, das Potential des Prinzips für zukünftige hochautomatisierte Fahrzeugkonzepte zu analysieren.

Das Prinzip wurde in ein vereinfachtes Schlittenmodell integriert, das aus einem finite Elemente Modell einer 2014-er Honda Accord Mittelklasse-Limousine im Crashtestverfahren eines schrägen Barrieretests gewonnen wurde. Anpassungen und Modifikationen des Modells umfassten die Transformation des Lastfalls in einen Frontalaufprall-Test sowie die sitzintegrierte Gurtverankerung.

Die vordefinierte Bewegung des Sitzes im Crash-Szenario wurde mit unterschiedlichen Kraft-Weg-Kennlinien modelliert. Nach der Simulation verschiedener Varianten wurden die Referenzwerte der Verletzungsbewertung ausgewertet und mit einem Bewertungssystem, das teilweise von der NHTSA übernommen wurde, mit den biomechanischen Grenzwerten verglichen.

Die Bewertung des Prinzips erfolgte durch Vergleichen der Standardsitzposition mit der um 400 mm nach hinten verstellten Position und dem verstellten Sitz mit in-Crash-Bewegung.

Das neue Funktionsprinzip führte zu einer Reduktion der Gesamt-Verletzungswahrscheinlichkeit um fast 27% im Vergleich zum fixierten Sitz in einer um 400 mm nach hinten verstellten Position. Darüber hinaus führte die in-Crash-Bewegung zu noch niedrigeren Referenzwerten in allen Fällen mit Ausnahme der Brusteindrückung als das Modell mit dem Standardsitz. Im Vergleich zur nach hinten verschobenen Sitzposition wurde jedoch trotzdem eine Reduktion des Risikos einer Brustverletzung um 11% erreicht.

Die Analyse des Prinzips zur Energiedissipation hat gezeigt, dass es Potential hat, die Insassenbelastungen in hochautomatisierten Fahrzeugkonzepten mit einer nach hinten verstellten Sitzposition um ein Viertel zu reduzieren.



# Contents

<b>List of Tables</b>	<b>xiii</b>
<b>List of Figures</b>	<b>xvii</b>
<b>1 Introduction</b>	<b>1</b>
1.1 Motivation . . . . .	1
1.1.1 Highly Automated Vehicles . . . . .	1
1.1.2 Seating Concepts . . . . .	3
1.2 Aim and Scope of the Thesis . . . . .	4
1.3 Approach . . . . .	6
<b>2 Method</b>	<b>7</b>
2.1 Source Model . . . . .	7
2.1.1 Anthropomorphic Test Devices . . . . .	8
2.1.2 Load Case . . . . .	9
2.1.3 Vehicle Model - Honda Accord . . . . .	10
2.2 Full Vehicle Model . . . . .	12
2.2.1 Load Case . . . . .	12
2.2.2 Vehicle Model . . . . .	13
2.2.3 Modification . . . . .	14
2.3 Integral Seat Model . . . . .	16
2.3.1 Headrest . . . . .	16
2.3.2 Seat Modifications . . . . .	18
2.3.3 Body Block Test . . . . .	18
2.4 Simplified Sled Model . . . . .	20
2.5 New Seat Position . . . . .	22
2.6 Principle for Energy Dissipation . . . . .	23
2.7 Simplified Model with Energy Dissipation . . . . .	24
2.8 Evaluation . . . . .	24
2.8.1 Injury Criteria . . . . .	25
2.8.2 Injury Severity . . . . .	27

2.8.3	Injury Risk Curves . . . . .	28
2.8.4	Joint Probability of Injury . . . . .	29
2.8.5	Relative Risk . . . . .	30
2.8.6	Star Rating Scheme . . . . .	30
2.8.7	Combined Crashworthiness Rating . . . . .	30
2.8.8	Applied Rating System . . . . .	31
<b>3</b>	<b>Results</b>	<b>35</b>
3.1	Full Vehicle Model . . . . .	35
3.2	Simplified Sled Model . . . . .	35
3.3	New Seat Position . . . . .	36
3.4	Adaptations . . . . .	38
3.4.1	Airbag Deployment Time . . . . .	38
3.4.2	Belt Force Scaling . . . . .	39
3.4.3	Principle for Energy Dissipation . . . . .	42
<b>4</b>	<b>Discussion</b>	<b>51</b>
<b>5</b>	<b>Conclusion</b>	<b>59</b>
<b>6</b>	<b>Summary</b>	<b>61</b>
<b>7</b>	<b>Outlook</b>	<b>63</b>
	<b>Bibliography</b>	<b>68</b>
<b>A</b>	<b>Appendix - List of Submodels</b>	
<b>B</b>	<b>Appendix - evaluated Diagrams</b>	
<b>C</b>	<b>Appendix - Simplified Sled Model</b>	
<b>D</b>	<b>Appendix - Diagrams for the Seat Belt Load Limiter Curve</b>	
<b>E</b>	<b>Appendix - Full Vehicle Model</b>	
<b>F</b>	<b>Appendix - RearPosSMED</b>	

# List of Tables

2.1	Proposed Critical Intercepts for the Neck Injury Criterion for the Hybrid III 50th percentile Adult male Dummy, (Eppinger et al., 1999) . . . . .	26
2.2	AIS Levels, (AAAM, 2015) . . . . .	28
2.3	Injury Risk Curves, (U.S. Department of Transportation, 2008) . . . . .	29
2.4	Adopted Injury Criteria with Limits, (NHTSA, 2015) . . . . .	32
3.1	Maximum Belt Forces - RearPosHOT Model . . . . .	40
3.2	Matrix for the Linear-Linear-Characteristic with initial Force Level (FL) . . . . .	47
4.1	Kinematic Analysis of Interaction between Dummy and Airbag . . . . .	56
4.2	Comparison of Dissipated Energy . . . . .	57



# List of Figures

1.1	U.S. Fatalities and Fatality Rate per 100 Million vehicle miles travelled, by Year, 1975-2018, (National Center for Statistics and Analysis, 2019) . . . . .	1
1.2	Society of Automotive Engineers Automation Levels, (NHTSA, 2020a) . . . . .	2
1.3	Flexible Seating Concepts . . . . .	4
1.4	New Occupant Seat Positions and schematic Configuration of Adapted Occupant Protection Technologies, (Laakmann et al., 2019) . . . . .	5
1.5	Approach . . . . .	6
2.1	Overview . . . . .	7
2.2	2014 Honda Accord Finite Element Model, (Singh et al., 2018) . . . . .	8
2.3	THOR 50% Male Dummy . . . . .	9
2.4	Oblique Moving Deformable Barrier Test - Left Side Impact, (NHTSA, 2014a) . . . . .	10
2.5	Oblique Moving Deformable Barrier Test - Simulation Model . . . . .	10
2.6	2014 Honda Accord Finite Element Model - Exploded View of the Vehicle Submodels - (Singh et al., 2018) . . . . .	11
2.7	2014 Honda Accord Finite Element Model - Seat Models With Deformed Cushions, (Singh et al., 2018) . . . . .	11
2.8	Frontal NCAP, (NHTSA, 2012) . . . . .	13
2.9	Full Vehicle Model . . . . .	13
2.10	Rigid Wall Test - Crash Pulse . . . . .	14
2.11	Node-Set for Prescribed Velocity Curve highlighted in orange . . . . .	14
2.12	Rigid Wall Test - Airbag Analysis, (NHTSA, 2012) . . . . .	15
2.13	Rigid Wall Test - Baseline Settings . . . . .	16
2.14	2012 Toyota Camry Detailed Finite Element Model, (CCS, 2016) . . . . .	17
2.15	Headrest - fitted onto the Seat Model . . . . .	17
2.16	Headrest Position . . . . .	17
2.17	Integral Seat Model . . . . .	18
2.18	Body Blocks for Combination Lap and Shoulder Belt Anchorage, (NHTSA, 1994) . . . . .	19
2.19	Body Block Test - Load Application, (Hessenberger, 2003) . . . . .	19
2.20	Body Blocks positioned within Seat Model in the Test Scenario . . . . .	20
2.21	Reduced body-in-white . . . . .	21
2.22	Adaptation of Contact Definition - Corrected Pelvic Restraint . . . . .	22

2.23	Simplified Sled Model - Baseline Model with Hands on Steering Wheel (BaselineHOS) . . . . .	22
2.24	Simplified Sled Model - Baseline Models . . . . .	23
2.25	Simple Force-Displacement-Characteristic . . . . .	23
2.26	Principle for Energy Dissipation - Position within the Model . . . . .	24
2.27	Neck Loading Modes . . . . .	27
2.28	Chest Deflection - Load Cells in the THOR Dummy . . . . .	28
2.29	Star Rating by means of the Relative Risk, (CARHS, 2020) . . . . .	30
2.30	Combined Crashworthiness Rating, (U.S. Department of Transportation, 2008) . . . . .	31
2.31	Distance between Dummy Head and Steering Wheel . . . . .	32
3.1	Baseline Rating Sheet . . . . .	36
3.2	BaselineHOT & RearPosHOT Rating Sheet . . . . .	37
3.3	Airbag Deployment Times - Analysis of Dummy Position at Time of Full Inflation . . . . .	38
3.4	Airbag Deployment Times - Analysis of HIC15 and Chest Deflection . . . . .	39
3.5	Shoulder Belt Force for different BL-Scaling Factors - Simulation . . . . .	40
3.6	Shoulder Belt Force in different Vehicle Models, (Keon, 2016) . . . . .	40
3.7	RearPosHOT Rating Sheet - Variation of Belt Force Scaling . . . . .	41
3.8	Constant-Linear Force-Displacement-Characteristic . . . . .	43
3.9	RearPosSMED Rating Sheet - Comparison of Constant-Linear-Characteristics . . . . .	43
3.10	Kinematic Analysis - RearPosSMED with Constant-Linear-EM-Characteristic . . . . .	44
3.11	Constant-Linear Force-Displacement-Characteristics with various Force Levels . . . . .	44
3.12	Linear-Linear Force-Displacement-Characteristic . . . . .	45
3.13	RearPosSMED Rating Sheet - Comparison of Linear-Linear-Characteristics . . . . .	45
3.14	RearPosSMED - Impact between Dummy and Steering Wheel . . . . .	46
3.15	Linear-Linear Force-Displacement-Characteristic with initial Force Level . . . . .	46
3.16	Linear-Constant-Linear Force-Displacement-Characteristic with initial Force Level . . . . .	48
3.17	RearPosSMED Rating Sheet - Comparison of Linear-Constant-Linear-Characteristics . . . . .	49
4.1	Reached Percentage of the respective Limits for the considered Variants . . . . .	54
B.1	Comparison of the Head Acceleration . . . . .	
B.2	Comparison of the Neck Axial Force . . . . .	
B.3	Comparison of the Neck Shear Force . . . . .	
B.4	Comparison of the Neck Moment . . . . .	
B.5	Comparison of the Femur Compression Force Left . . . . .	
B.6	Comparison of the Femur Compression Force Right . . . . .	
B.7	Comparison of the Chest Deflection UL . . . . .	
B.8	Comparison of the Chest Deflection UR . . . . .	
B.9	Comparison of the Chest Deflection LR . . . . .	



B.10	Comparison of the Chest Deflection LL	.....
B.11	Comparison of the Abdomen Deflection Left	.....
B.12	Comparison of the Abdomen Deflection Right	.....
B.13	Comparison of the Shoulder Belt Force	.....
B.14	Comparison of the Pelvis Belt Force	.....
C.1	RearPosHOT Rating Sheet - Variation of Airbag Deployment Time	.....
D.1	Unscaled Seat Belt Load Limiter Curve	.....
D.2	Scaled Seat Belt Load Limiter Curve - Scaling Factor 0.7	.....
E.1	Full Vehicle Model Rating Sheet - Comparison of Belt Force Scaling	.....
F.1	RearPosSMED Rating Sheet - Comparison of Linear-Linear-Characteristics with an Initial Force Level	.....
F.2	RearPosSMED Rating Sheet - Comparison of Linear-Linear-Characteristics with an Initial Force Level	.....



# 1 Introduction

## 1.1 Motivation

In 2018, 36,560 people were killed in motor vehicle crashes on U.S. roadways. The 2.4% decrease from 2017 describes the general downward trend in traffic deaths over the past decades (Figure 1.1). The European Union can account for a 1.0% reduction in this period, with 23,339 people killed in road accidents in 2018 (eurostat, 2020). In Austria, a total of 409 persons died in road traffic accidents in the same year. According to Statistik Austria (2019), this means a decrease in fatalities of 1.2% compared to the year before. The annual reduction in the previous years was 9.8% (2014-2015, 2015-2016) and 4.2% (2016-2017) (Statistik Austria, 2019), which shows that the downward trend is slowly stagnating. This overall reduction is not only a result of safety programs, but also of vehicle improvements and optimization of passive occupant crash protection systems. (National Center for Statistics and Analysis, 2019)

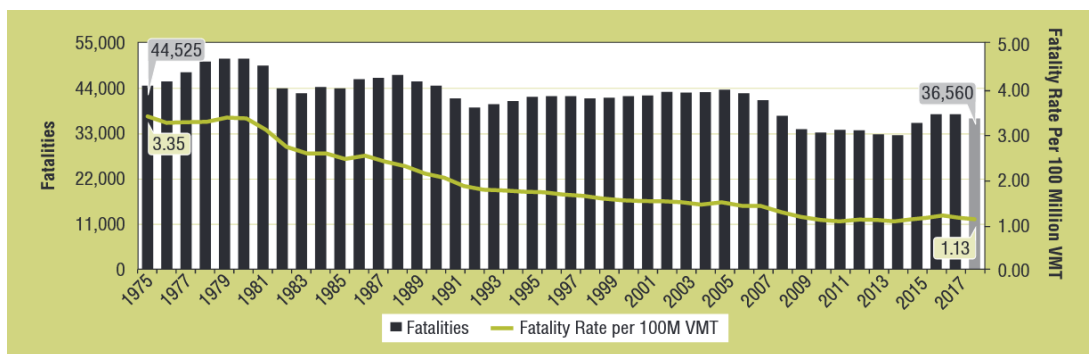


**Figure 1.1:** U.S. Fatalities and Fatality Rate per 100 Million vehicle miles travelled, by Year, 1975-2018, (National Center for Statistics and Analysis, 2019)

Today's new motor vehicles are already equipped with various driver assistance technologies that help to save lives and prevent injuries. These include advanced safety features, such as Lane Departure Warning or Blind Spot Detection, driver assistance features like Automatic Emergency Braking, up to partially automated safety features, for example self-parking technology. The potential of these passive systems is almost tapped so that in the future greater safety benefits can only be reached with fully automated features such as the highway autopilot. (NHTSA, 2020a)

### 1.1.1 Highly Automated Vehicles

The safety benefits of highly automated vehicles (HAVs) are enormous, considering the fact that 94% of serious crashes are due to human error (NHTSA, 2020a). The potential to save lives and reduce injuries will not only help to protect vehicle occupants, but also vulnerable road users, like motorcyclists, bicyclists and pedestrians. In addition, HAVs may also increase

mobility for elderly, visually- or physically-impaired individuals. Autonomous technologies further offer the possibility to improve traffic flow as well as reduce environmental impact. (NHTSA, 2020a)

With their potential to significantly reduce traffic accidents, highly automated vehicles have become one of the most discussed topics in automotive development. A variety of autonomous functions will be implemented with the overall aim of handling the complete task of driving. This can be resumed in six levels of driver assistance technology advancements, the so-called Society of Automotive Engineers (SAE) automation levels (Figure 1.2). (NHTSA, 2020a)

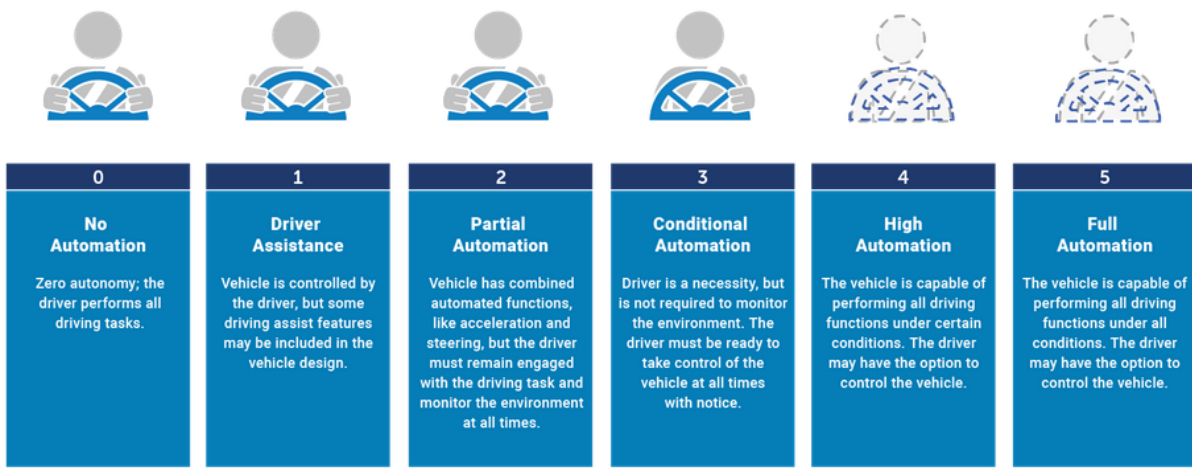


**Figure 1.2:** Society of Automotive Engineers Automation Levels, (NHTSA, 2020a)

In its Surface Vehicle Information Report, SAE International (2014) gives detailed information on automated driving systems. Their levels of automated driving can be explained as follows:

#### Level 0: No Automation

The driver performs all aspects of the driving task.

#### Level 1: Driver Assistance

The driver has full control of the vehicle at all times, but can activate the driving assistance system and hand over either the longitudinal (accelerating, braking) or lateral (steering) dynamic driving task. He is always in the position to immediately take over when required or requested by the system.

#### Level 2: Partial Automation

In contrast to level 1, the partial automation system can adopt both longitudinal and lateral driving tasks simultaneously. Still, the driver has to constantly supervise the task and immediately take over when required or requested by the system.

#### Level 3: Conditional Automation

The conditional automation system is capable of executing all dynamic driving tasks when activated under certain circumstances. However, a driver is still required and must be ready to take over control at all times when he is requested to do so by the vehicle. An example for a level 3 system is the Drive Pilot from Daimler AG (2020), which is expected to be ready for use

in suitable German motorway sections in the second half of 2021.

#### Level 4: High Automation

The automated driving system monitors the driving environment and is able to perform all driving tasks completely unsupervised in certain circumstances. This means that in specific situations no driver is required to pay attention or even be in the vehicle. As a level 4 system, Daimler AG (2020) presented their Intelligent Parking Pilot which is capable of driverless highly automated parking.

#### Level 5: Full Automation

The vehicle can perform all driving functions by itself at all times and under all conditions. The driver may request to take over control but the system is capable of working driverless.

Not all vehicle manufacturers go through all the levels with their development process. The president and chief executive at Volvo Car Group (2017), for example, criticises the conditional automation mode and considers it to be unsafe. Even though the car is in charge of the driving in this mode, the driver could only have a few seconds of time to take over control in case of an emergency. In his eyes, the role of the driver is not defined clearly enough, which is why Volvo wants to launch its first autonomous car at Level 4. (Volvo Car Group, 2017)

With cars driving themselves, the driver becomes an occupant in the vehicle which provides more degrees of freedom for possible activities and seating positions.

### 1.1.2 Seating Concepts

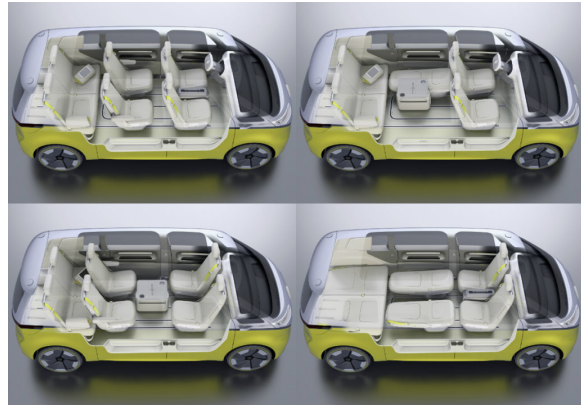
Ive et al. (2015), Jorlöv et al. (2017) and Östling and Larsson (2019) conducted studies in the U.S., Sweden and China to find out about possible future seating concepts in HAVs. To investigate their preferences, participants were confronted with a short drive and a long trip scenario in a hypothetical fully automated vehicle. They found that future occupants' activities might include working, reading, watching movies, relaxing or interacting with other occupants. Therefore, the living-room-position with swivel seats as well as a reclined backrest with backward moved seat track were identified as preferred positions. Participants also mentioned a horizontal position in order to sleep, as it can be found in the future concept of Volvo (2018) (Figure 1.3a).

Simultaneously, car manufacturers are introducing new interior concepts. The Volkswagen Group, for example, developed a self-driving concept car for autonomous driving (Volkswagen Group, 2017). In addition to their concept for mobility of the future in road traffic, they presented their fully autonomous multi-purpose vehicle I.D. BUZZ. Figure 1.3b shows VW's flexible seating concept, that is established when the driver becomes redundant. (Torque, 2017)

This leads to the conclusion that companies that design HAV technologies, as well as consumers desire further development of seating layouts for autonomous driving. Along with



(a) Horizontal Sleeping Position - Volvo 360C, (Volvo, 2018)



(b) Volkswagen I.D. Buzz, (Torque, 2017)

**Figure 1.3:** Flexible Seating Concepts

this comes the challenge to make flexible seating as safe as the seating in current vehicles. (Matsushita et al., 2019)

The introduction of HAVs will greatly reduce the amount and severity of crashes by eliminating human error. Even though the number of automated cars in the future vehicle fleet will increase, there will still be a majority of driver-controlled vehicles that are mostly of SAE level 0 (no automation), level 1 (active cruise control or lane keeping assist) or level 2 (driver is constantly supervising). Crashes will still occur in this transition period, however infrequent or severe, involving vehicles in which the actions of the driver are not predictable for the autonomous systems. Together with the changing vehicle interiors, this will lead to new challenges for occupant protection. (Filatov et al., 2019)

Therefore, a new consideration of occupant protection becomes necessary and composes the scope of this thesis.

## 1.2 Aim and Scope of the Thesis

The desired positions explained in 1.1.2 still have to be safe positions in order to allow the future implementation of these concepts. For investigating them with current systems, the layout that is the easiest to realise is formed by the seat moved to a backwards position. The rotation of seats, for example, is to a great extent not realisable in today's vehicle interiors due to a shortage of space.

The seat moved to a backwards position is better described as the standard seating position with upright back rest but longitudinally adjusted. Within this thesis, a seat position moved 400 mm to the rear was identified as the situation to be investigated. With the driver being in a 400 mm distance from the steering system and pedals, he is unable to execute any of the driving tasks and only has the option to control the vehicle by changing his position. Thus, the necessary automated driving system will presumably have to be of level 4.

Furthermore, a great percentage of today's occupants in the front passenger seat travel with the seat positioned rearward of the mid-track position and even up to full-rear on the seat track (Reed et al., 2020). So far, this rear position is not evaluated by legal crash test procedures,

which makes it even more relevant to examine the longitudinally adjusted seat. The seat position moved 400 mm to the back will therefore form a basis for further research on seating concepts, from reclined back rests to backwards facing seats and sleeping positions.

Two approaches for occupant load reduction seem possible to compensate the seat position further back at the present state of the art. Either the restraint systems are brought closer to the occupant or the occupant is brought closer to the restraint systems.

For the first option, the current occupant protection technologies need adaptation. This can be realised by integration of the seatbelt into the seat back or adaptation of the airbag in volume and shape. These adaptive system solutions to counteract the changing geometric conditions for safe relaxing and working seat concepts were developed by Laakmann et al. (2019) and are depicted in Figure 1.4.

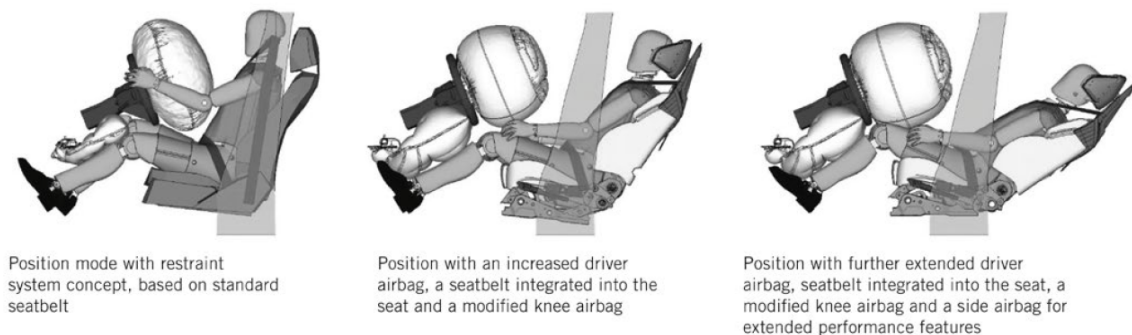


**Figure 1.4:** New Occupant Seat Positions and schematic Configuration of Adapted Occupant Protection Technologies, (Laakmann et al., 2019)

The second idea considers a seat that can move within the vehicle with a pre-defined motion. A principle investigated by Adomeit et al. (2009) uses the potential of sensor technology to identify accidents in advance. The vehicle sensor system permanently scans the environment and is able to detect a frontal accident not later than 100 ms before the crash start. It then triggers the developed pre-crash/crash restraint system that initiates movement of the occupant contrary to the impact direction 80 ms before the crash for a gain of time and energy. This energy compensates for part of the crash energy that burdens the occupant. The system showed a significant increase of the occupant protection level. (Adomeit et al., 2009)

Another approach uses the energy generated in an accident. By bringing the occupant closer to the original seat position it aims to dissipate this energy. This is done with an energy management system integrated in the longitudinal seat adjustment, as it was tested in Huf and Sengottu Velavan (2018).

To increase occupant protection for new seat and seating positions by reducing the occupant loads, the decision was made to bring the occupant closer to the restraint systems. Apart from the belt-integrated seat, the existing restraint systems will be used which does not entail a complete re-development of airbags. The investigated system allows the seat to absorb energy by moving forward and, thus, reduces the forces acting on the occupant. It will further be referred to as a seat with in-crash movement. This motivates the aim of this thesis, which is the

analysis of the potential of this new type of operating principle of energy dissipation.

### 1.3 Approach

For the central idea of the seat with in-crash movement, a finite element model was used. In the course of this thesis, the development process of the model is explained. Based on the source model, the methods used to obtain the adapted model are discussed in detail. On the one hand, a pure consideration of the seat model was necessary. Seatbelts are usually anchored in the b-pillar, which is not purposeful and potentially dangerous for the concept of a moving seat. Therefore, the belt was integrated into the seat back. On the other hand, the vehicle model with all its modifications is described. This includes the adaptations made in order to allow the energy dissipating principle to reduce loads.

The thesis contains information on U.S. legislation and NHTSA crash test procedures. By means of simulation, these vehicle crash tests were reproduced and virtually assessed. After the presentation of the evaluation process, the optimized simulation results are presented and discussed, subsequently. The end of the thesis is formed by a concluding summary and outlook in the form of requirements for an energy management system for improved occupant protection.

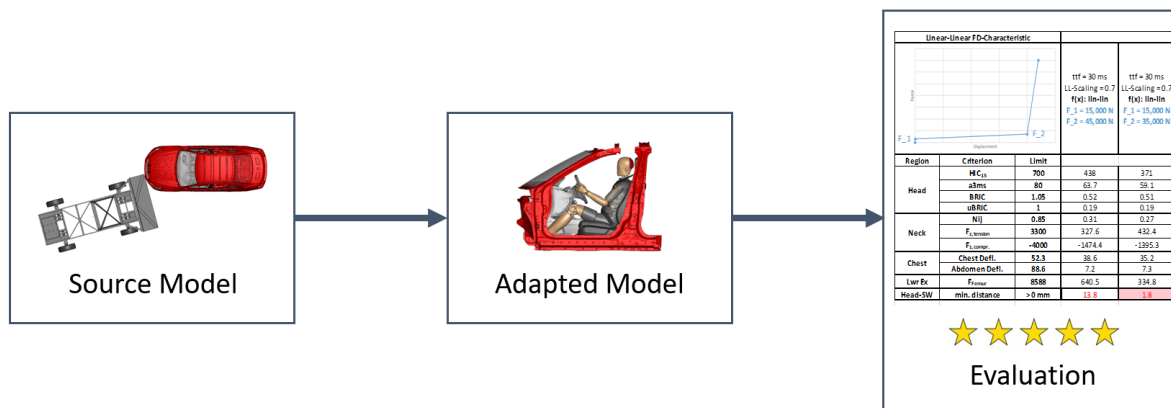


Figure 1.5: Approach



## 2 Method

Based on the LS-DYNA model of an oblique barrier test, two submodels were considered separately. This was on the one hand the full vehicle model and on the other hand the seat model. These two models were then combined to a simplified sled model which was designed to reduce computational cost. Finally, the connections between the seat and the relevant body-in-white parts were changed to allow the seat to move in a pre-defined way. The result was the simplified model with energy dissipation which was used to examine and evaluate the reduction of occupant loads.

Figure 2.1 gives an overview together with section references. This chapter also includes the initial definitions and specifications made.

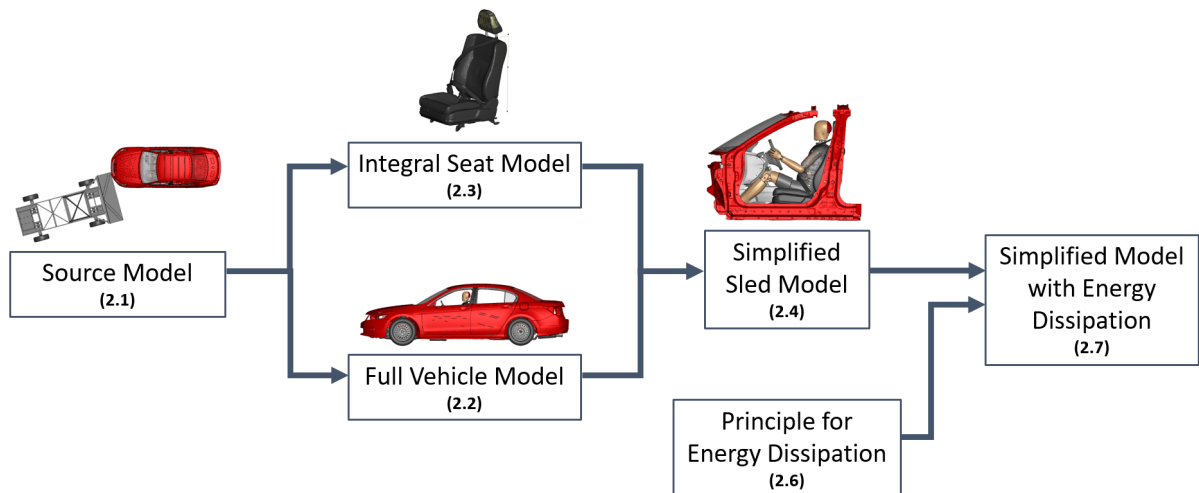
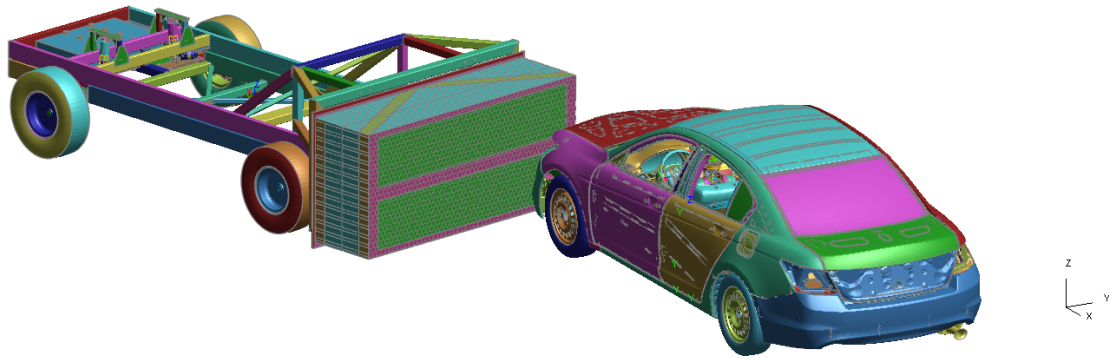


Figure 2.1: Overview

### 2.1 Source Model

One of the potential benefits of the new operating principle is that the belt and airbag system do not need to be changed depending on the seat adjustment. Therefore, a model of a current vehicle could serve as the basis for the model used in this thesis. This source model represents a 2014 Honda Accord mid-size sedan in the crash test procedure of an oblique moving deformable barrier test (Figure 2.2). The model includes the vehicle interior, two THOR 50th percentile male frontal dummy models for the driver and front seat passenger, as well as occupant restraint systems. (Singh et al., 2018)



**Figure 2.2:** 2014 Honda Accord Finite Element Model, (Singh et al., 2018)

The model with its components, as well as the load case are described in this section.

### 2.1.1 Anthropomorphic Test Devices

Anthropomorphic test devices (ATD), also known as crash test dummies, are used to measure loads occupants would be subjected to in vehicle crashes. Based on the dummy responses, the injury risk can be estimated through data modelling. Depending on the field of study and the test situation, there are dummies for frontal impact, side impact and rear impact as well as adult and child dummies with variation in size, age and gender. (Humanetics Group, 2020)

This thesis focuses on the 50th percentile male that represents an average male adult in size and weight.

For frontal impact test procedures, the Hybrid III 50th percentile male is the most commonly used dummy in the world. It is called a hybrid because it was created by combining parts of two different types of dummies (Haug et al., 2004). When developed in 1976, it was considered to have excellent biofidelity as well as instrumentation capability. It is also used in non-automotive applications. The dummy has a weight of 77.7 kg and seated height of 883.9 mm. (Humanetics Group, 2020)

The more recently developed frontal impact ATD is the Test device for Human Occupant Restraint (THOR) that incorporates major advancements in biofidelity and sensing. In addition to more human-like features, the dummy can assume various seating positions. (Haug et al., 2004) It can assess whole-body trauma in a variety of environments and is therefore expected to be the dummy of the future for the evaluation of automotive safety restraint systems. It has a weight of 76.6 kg and seated height of 906.5 mm. (Humanetics Group, 2020).

The THOR 50th percentile male is shown in Figure 2.3, together with its simulation model that is included in the source vehicle model. The THOR dummy finite element (FE) model is publicly available from the University of Virginia and was developed for use in LS-DYNA. (Singh et al., 2018)

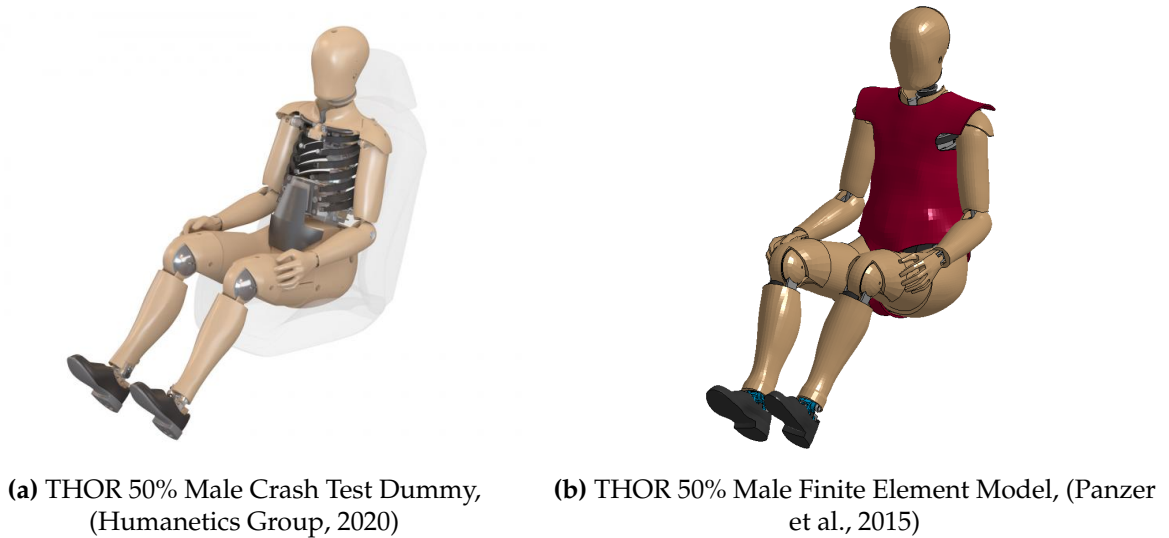


Figure 2.3: THOR 50% Male Dummy

### 2.1.2 Load Case

The National Highway Traffic Safety Administration (NHTSA) is part of the U.S. Department of Transportation with the objective of reducing vehicle-related crashes. In 1979, NHTSA developed the first New Car Assessment Program (NCAP) as a motivation for vehicle manufacturers to optimize the safety level of their vehicles beyond the legal minimum standards. (NHTSA, 2020b)

The main load cases for the U.S. NCAP to assess the vehicles' maximum crashworthiness are frontal, side, rollover and rear impact (Hershman, 2001). As part of the frontal NCAP evaluation, NHTSA intends to add a new frontal oblique crash test. (U.S. Department of Transportation, 2015).

This crash test procedure involves an oblique moving deformable barrier (OMDB) that hits the tested vehicle at 90.12 km/h. In the scenario, the vehicle is positioned 15° from the barrier's centerline with a 35% overlap (Figure 2.4). (Singh et al., 2018) It is equipped with two THOR 50th percentile adult male dummies for driver and front passenger. The barrier is 2.2 m wide, 1.2 m high and weighs 2490.2 kg. (NHTSA, 2014b)

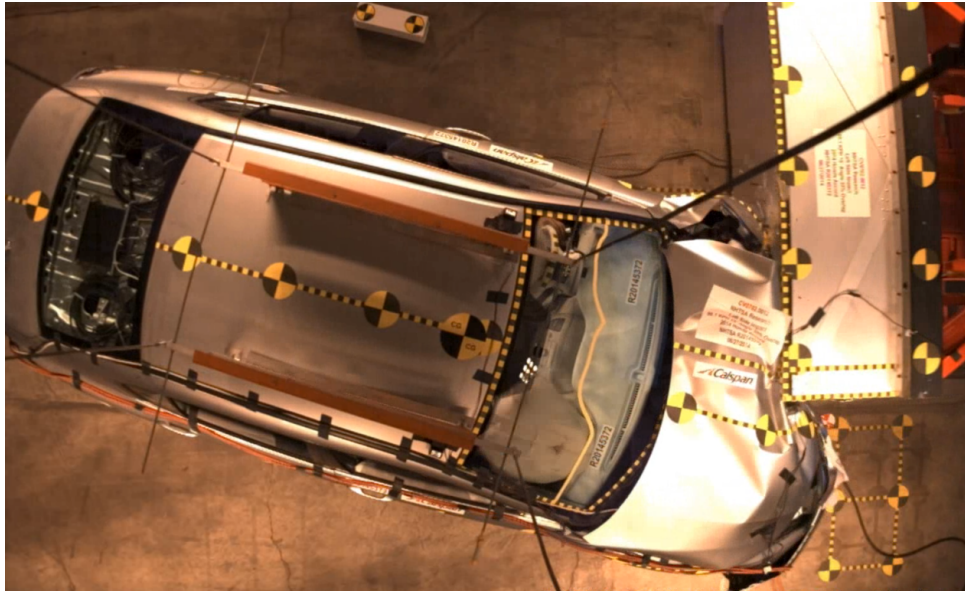


Figure 2.4: Oblique Moving Deformable Barrier Test - Left Side Impact, (NHTSA, 2014a)

### 2.1.3 Vehicle Model - Honda Accord

The FE model of an OMDB test was developed by NHTSA and EDAG to evaluate occupant injury potential (Singh et al., 2018). It was created for use with LS-DYNA and is publicly available from the NHTSA homepage (NHTSA, 2018). A top view of the model in the appropriate crash test scenario at a simulation time of 18 ms is shown in Figure 2.5. It shows its position relative to the coordinate system, which can also be seen in Figure 2.2. Noticeable is the x-axis, that points to the rear of the vehicle.

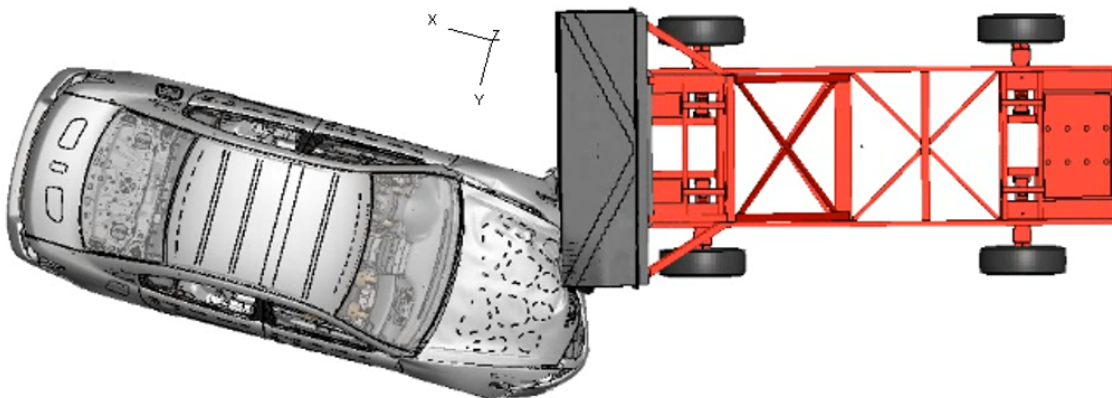
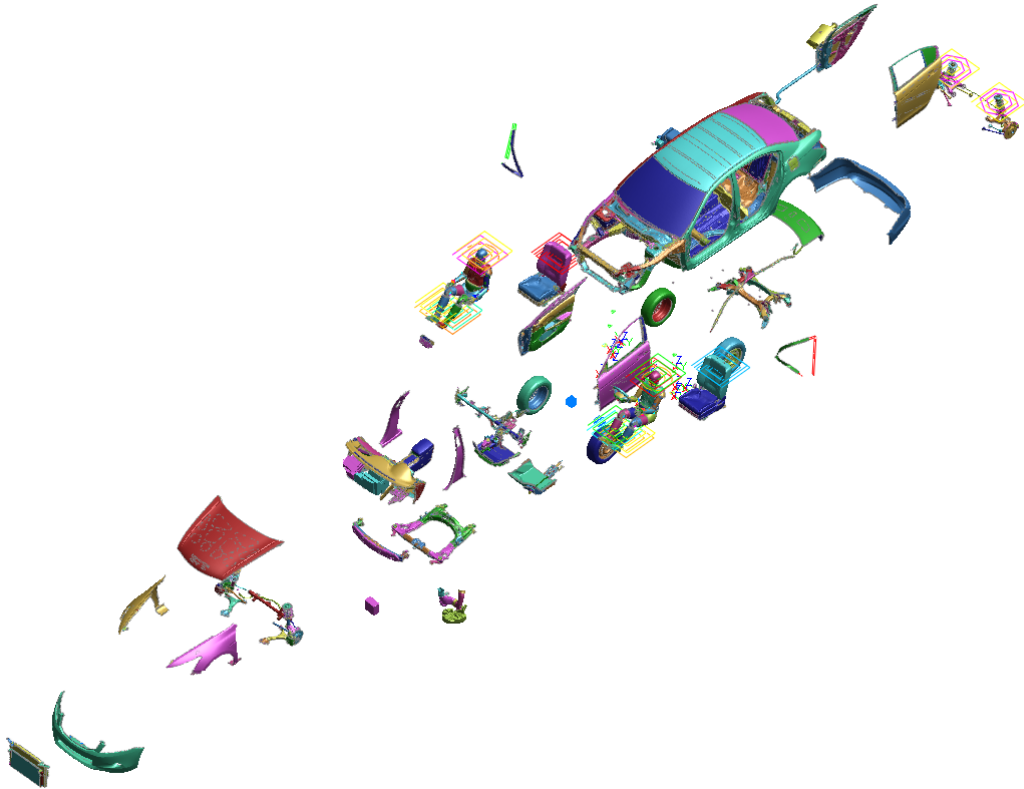


Figure 2.5: Oblique Moving Deformable Barrier Test - Simulation Model

The input deck consists of a main-file that reads the include-files of a separate folder. These files exist for various submodels, which are listed in Appendix A. Figure 2.6 shows an exploded view of the appropriate vehicle submodels.



**Figure 2.6:** 2014 Honda Accord Finite Element Model - Exploded View of the Vehicle Submodels - (Singh et al., 2018)

The included occupant restraint systems are composed of three point seat belts with pretensioners and load limiters, frontal airbags and a driver's side curtain airbag. The model does not contain headrests because it was purely developed for the oblique load case, which does not include headrests to allow an unobstructed view for all camera perspectives in the physical tests. (NHTSA, 2020b)

In order to obtain more realistic occupant kinematics the model was gravity settled prior to simulation. Figure 2.7 shows the pre-deformed seat cushions to the THOR shapes. (Singh et al., 2018)

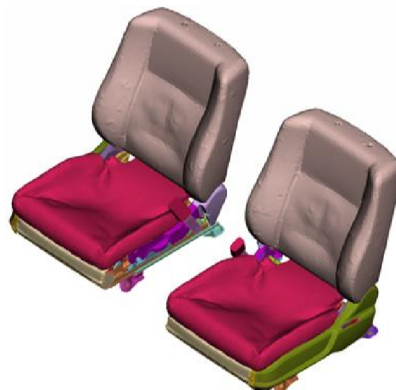


**Figure 2.7:** 2014 Honda Accord Finite Element Model - Seat Models With Deformed Cushions, (Singh et al., 2018)

Important to mention is the simulation time of 140 ms and the model units, which are defined as follows:

- mass in [t]
- length in [mm]
- time in [s]

The model was not functional in the state it was provided by NHTSA. It needed error correction, for example formatting style, to make the simulation executable. As the oblique barrier test was represented correctly, the model was adapted for further use.

## 2.2 Full Vehicle Model

The OMDB test procedure is by definition an oblique scenario and has therefore longitudinal and lateral velocity components. The resulting intrusion is, thus, very one-sided. For simplification, a purely longitudinal movement should be considered. This led to the changing of the load case to a frontal crash scenario. In that case, the vehicle can absorb energy across its full width and shows significantly less intrusion into the passenger compartment.

The decision for this new load case was additionally supported because NHTSA provides considerably more information on the rigid wall test in the form of videos, reports and measuring data in an online database. This allows an easier and better validation and verification.

The full vehicle model in the scenario of a rigid wall test was derived from the initial simulation deck. This process is described in the following.

### 2.2.1 Load Case

In the frontal NCAP or rigid wall test (RWT) the tested vehicle is crashed into a rigid wall with full overlap at a velocity of 56.3 km/h (Figure 2.8). The impact is equivalent to a vehicle moving at 112.7 km/h striking an identical parked vehicle, or equivalent to two identical vehicles each moving toward each other at 56.3 km/h. The vehicle is equipped with two Hybrid III 50th percentile adult male dummies which represent a driver and a front seat passenger. (Hershman, 2001)

In the future, NHTSA intends to change the occupant model and use the THOR 50th percentile male crash test dummy in the full frontal tests instead (U.S. Department of Transportation, 2015).



Figure 2.8: Frontal NCAP, (NHTSA, 2012)

## 2.2.2 Vehicle Model

For simulation of the frontal NCAP, the measured velocity plot from the test was applied to the vehicle. So to say, the crash scenario was modelled as a virtual sled test in order to have as little change as possible and maintain the comparability.

As a first step to reduce computational cost, the rigid wall was not modelled. All unnecessary include-files, such as the barrier, were excluded from the input deck. For all further simulations, only the driver was considered. (Figure 2.9)

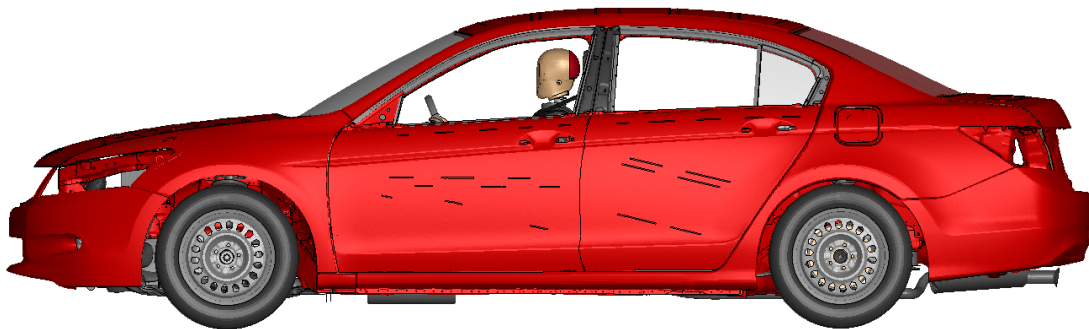
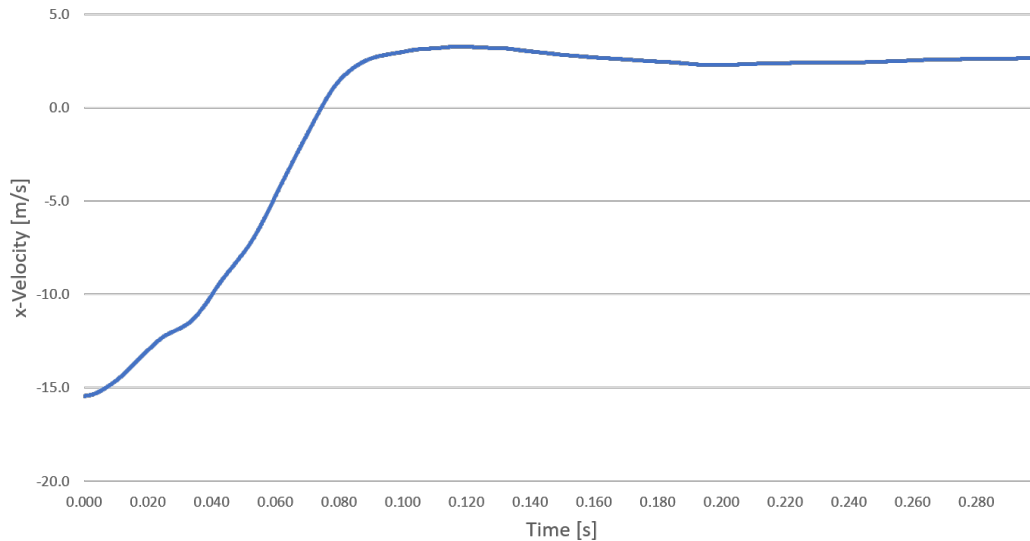


Figure 2.9: Full Vehicle Model

The frontal crash scenario was modelled by application of a prescribed velocity curve on the vehicle. The velocity time-history curve was obtained from NHTSA crash test data and is shown in Figure 2.10. It describes the deceleration and rebound. Negative values are due to the fact that the coordinate system has its negative x-axis in direction of the vehicle front. In addition, the vehicle's movement was restricted to the x-direction.



**Figure 2.10:** Rigid Wall Test - Crash Pulse

The crash pulse was applied to the vehicle via a set of nodes on the vehicle's underbody, which is highlighted in orange in Figure 2.11.

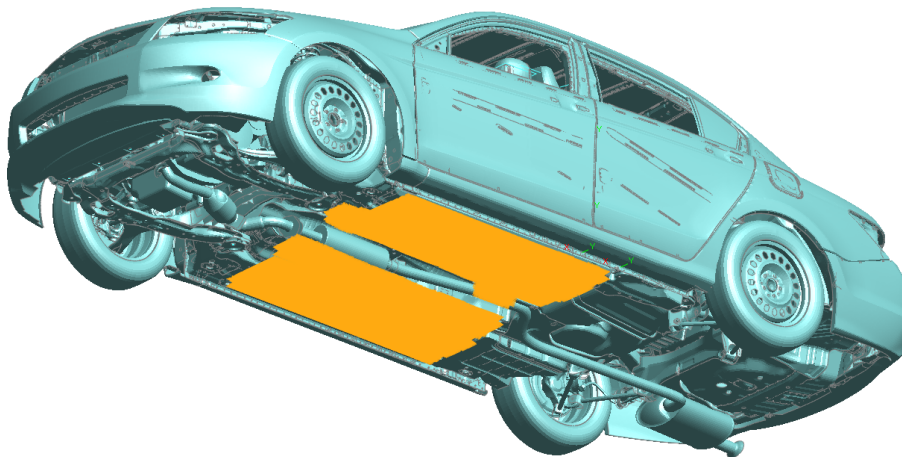


**Figure 2.11:** Node-Set for Prescribed Velocity Curve highlighted in orange

### 2.2.3 Modification

In order to facilitate meaningful comparisons between the occupant loads with and without the principle for energy dissipation, the baseline model should produce plausible results. However, as primarily relative comparisons to the baseline are drawn, no validation was performed. In this sense, the following modifications were aimed at obtaining a model which yielded plausible results for the RWT.

Therefore, the driver airbag deployment time as well as time of full inflation were estimated by video analysis. For the investigation NHTSA's test number 8035 for the 4-door-Sedan was considered. The final test report as well as videos can be found on their vehicle database website (NHTSA, 2012). Investigation gave an estimated time-to-fire (TTF) of 15 ms and a full airbag



inflation at 34 ms (Figure 2.12).

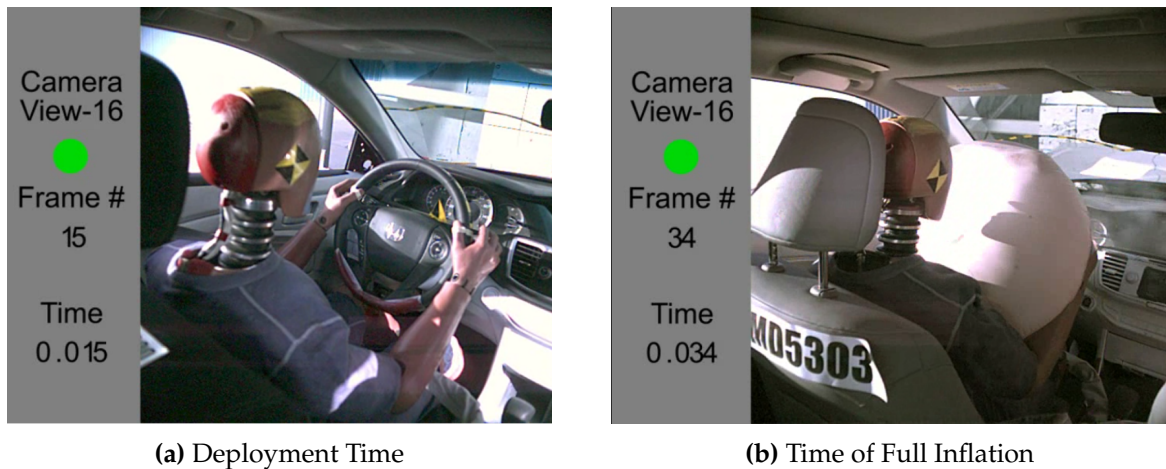


**Figure 2.12:** Rigid Wall Test - Airbag Analysis, (NHTSA, 2012)

With a TTF of 15 ms the simulation showed a fully inflated airbag at 54 ms. This deviation can be explained by the airbag inflation curve which was modelled to be valid for the oblique barrier load case. For more similarity in the airbag inflation, the TTF was set to 10 ms. An earlier trigger time was considered to be unrealistic and only rarely occurs in physical crash tests (Iraeus and Lindquist, 2016).

Because the source model was not validated for the frontal load case, the dummy head showed an impact with the steering wheel in the simulation. As a consequence, variation of the vent area was considered to increase the distance between the dummy head and the steering wheel. The initial setting was a vent area of 4000 mm<sup>2</sup>, which is equivalent to a radius of about 36 mm. An improvement of the observed distance was not to be found until a reduction of the radius to 30 mm. In order to have a margin for the further modifications of the model, the new vent area was set to 2463 mm<sup>2</sup> (which is equivalent to a radius of 28 mm) and resulted in a distance between dummy head and steering wheel of 71 mm.

The final configuration of airbag settings resulted in an acceptable distance between dummy head and steering wheel, and overall improved visual similarity to the NHTSA crash test videos. Thus, the reduced vent area in combination with an earlier TTF were set out to be the baseline parameters for further simulation.

Figure 2.13 shows the positioned dummy in the frontal load case with these baseline parameters at the time of full airbag inflation.

In the full vehicle model, the seatbelt is mounted on the b-pillar. To enable energy dissipation by means of a movable seat, this connection had to be converted into a seat-integrated anchorage which necessitated modifications to the seat.

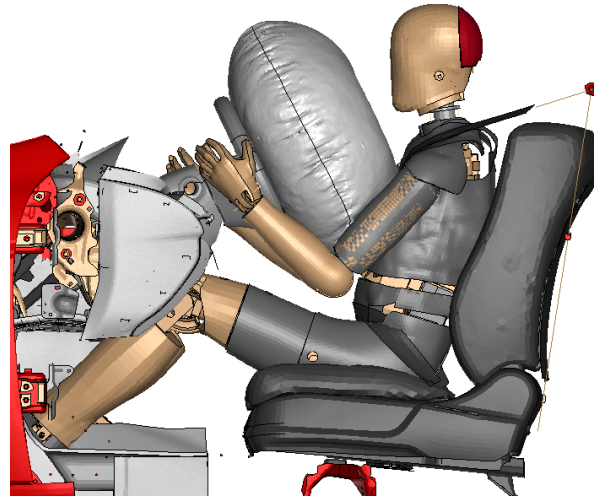


Figure 2.13: Rigid Wall Test - Baseline Settings

## 2.3 Integral Seat Model

The second submodel derived from the source model was the seat model. In order to make the seat adjustable in longitudinal direction, the seat belt could no longer be mounted into the b-pillar. Instead, it had to be integrated into the seat structure, which resulted in a belt integral seat. Therefore, the seat together with the belt and its connections were isolated from the model.

The modified load case represents a frontal crash situation, which does not necessarily need headrests. In order to obtain the possibility to use the model for rear impact scenarios, a headrest was added to the driver's seat. In FE models parts can easily be blanked and excluded, thus no disadvantage arises. For the headrest a second vehicle model was considered.

### 2.3.1 Headrest

The 2012 Toyota Camry detailed FE model was developed by the Center for Collision Safety and Analysis (CCSA) researchers. The process was sponsored by the Federal Highway Administration (FHWA). The model was also created for use with LS-DYNA and is publicly available and represents a rigid wall test (Figure 2.14a). It includes headrests, but neither an occupant model nor seat belts and airbags, as can be seen in Figure 2.14b. (CCS, 2016)

The headrest geometry from the Toyota Camry model was slightly modified and added to the Honda Accord seat model. Headrest and seat were joined with a rigid connection on both parts' posts and bars. The modification contained a scaling in y-direction to fit the headrest onto the seat as well as a transformation into the correct position (Figure 2.15). The positioning was based on the static head restraint geometry evaluation for rear crash protection from IIHS (2008). Figure 2.16a shows the position that is described to have "good geometry". It allows the headrest for an average-size adult male to be no farther than 6 cm below the top of the head and no farther than 7 cm behind it. The aim within this thesis was that the upper edge of head

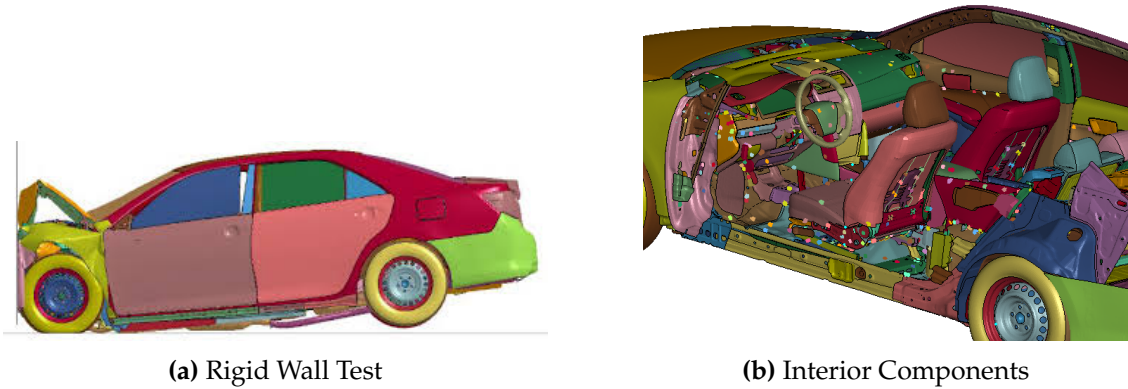


**Figure 2.14:** 2012 Toyota Camry Detailed Finite Element Model, (CCS, 2016)

and headrest end at approximately the same height. The measured distance in x-direction is 10.5 mm (Figure 2.16b).

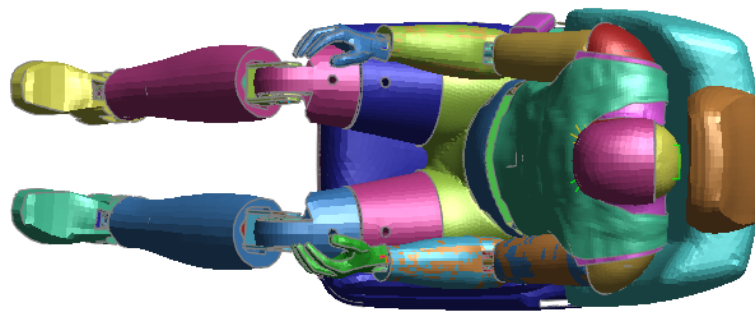


**Figure 2.15:** Headrest - fitted onto the Seat Model

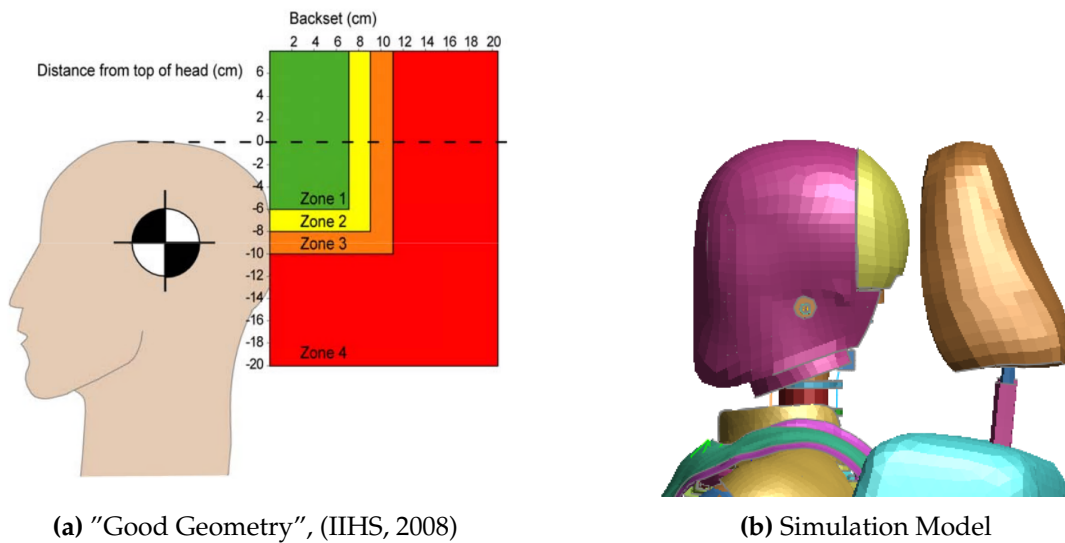


**Figure 2.16:** Headrest Position

With the new seat model, the transformation into a belt integral seat was conducted.

### 2.3.2 Seat Modifications

#### Seat-integrated Belt Anchorage

For the seat model to be movable, the seat belt anchorage was detached from the b-pillar and integrated into the seat back. As Figure 2.17a shows, the initial anchorage points, visible as green pieces on the red post beside the seat, were connected by constraints to rigid parts in the seat structure. The upper parts are tied to two of the green anchorage points, which is why the visible connection starts in between those two points.

#### Supporting Frame

For the seat to take the belt loading, it was strengthened and given additional stiffness both, in the seat back and seat area (Figure 2.17b). This supporting frame is made up from rigidly connected nodes within the structure. The crossing point in the lower connection gives the contact point, which is the generic mounting structure in preparation for the movable seat.

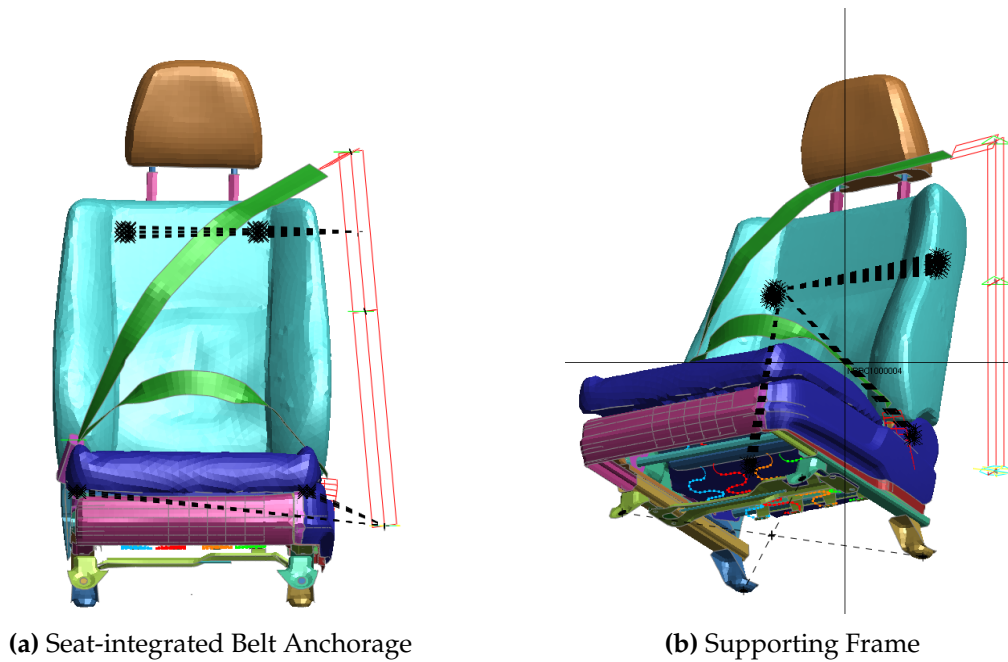


Figure 2.17: Integral Seat Model

As a result of these modifications, it had to be ensured that the seat belt assembly can withstand the loads and complies with the relevant legislation from NHTSA. This is often referred to as body block test (BBT) because body blocks are used to load the pelvis and shoulder belt. Conform with this test the modified seat was tested in simulation.

### 2.3.3 Body Block Test

#### Legislation

Part of NHTSA's duty is writing and enforcing the Federal Motor Vehicle Safety Standards (FMVSS). They are the pendant to the United Nations Economic Commission for Europe (UN/ECE)

regulations.

In the FMVSS Laboratory Test Procedure No. 210 (NHTSA, 1994), "requirements for seat belt assembly anchorages to insure their proper location for effective occupant restraint and to reduce the likelihood of their failure" are established.

This thesis discusses passenger cars with Type 2 seat belt assemblies, which is a combination of lap and shoulder belt. The test procedure is executed with two body blocks - one for the pelvic belt section (Figure 2.18a) and one for the upper torso belt section (Figure 2.18b).

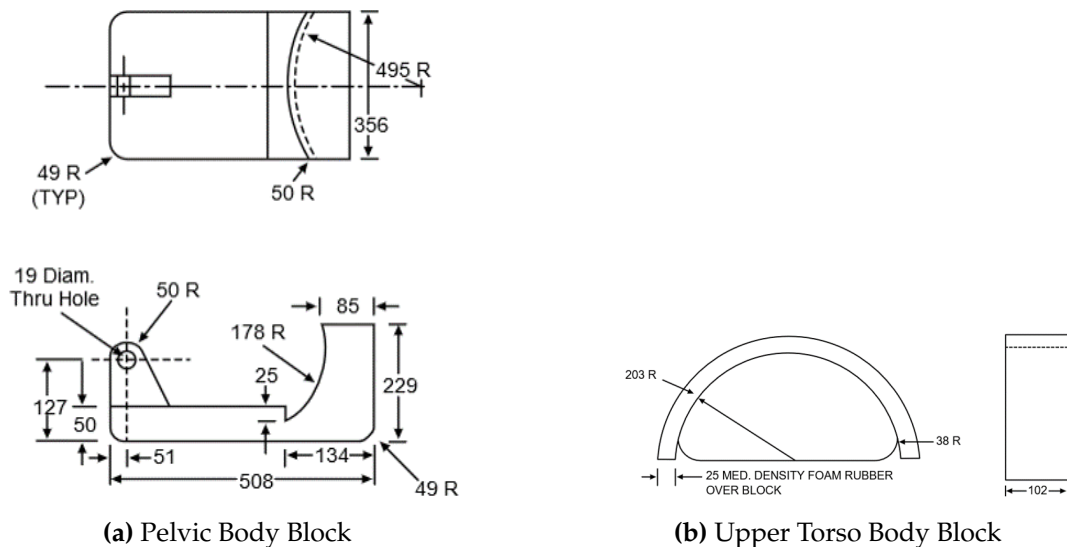


**Figure 2.18:** Body Blocks for Combination Lap and Shoulder Belt Anchorage, (NHTSA, 1994)

Both are loaded simultaneously with a force of 13,345 Newton in seating direction at an application angle of  $10 \pm 5$  degrees upgrade, as described in Figure 2.19. The full force has to be attained in not less than 0.1 seconds but not more than 30 seconds. In order to pass the test procedure, the force has to be sustained for 10 seconds. It is stated, that "permanent deformation or rupture of a seat belt anchorage or its surrounding area is not considered to be a failure". (NHTSA, 1994)

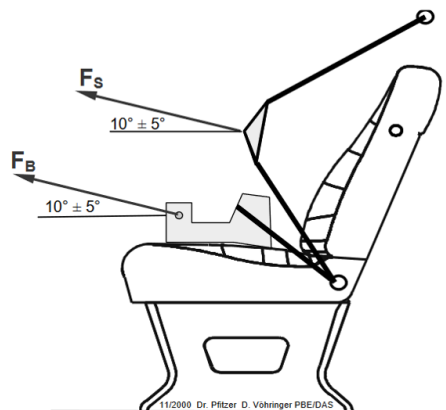


**Figure 2.19:** Body Block Test - Load Application, (Hessenberger, 2003)

## Simulation

The pelvic and upper torso block were modelled in CATIA V5R19 according to the geometry in Figure 2.18. The parts were transferred to and meshed in LS-PrePost-4.6-x64. With the correct positioning, the blocks were integrated into the seat model through file inclusion, as can be seen in Figure 2.20.

To reproduce the body block test, the set-up (Figure 2.19) was modelled as a load case. For simulation, the generic mounting structure (Figure 2.17b) was used for the application of force. Figure 2.20 also shows the initial position and position that is held for 10 seconds, in order to give a better understanding of the conducted body block test procedure.

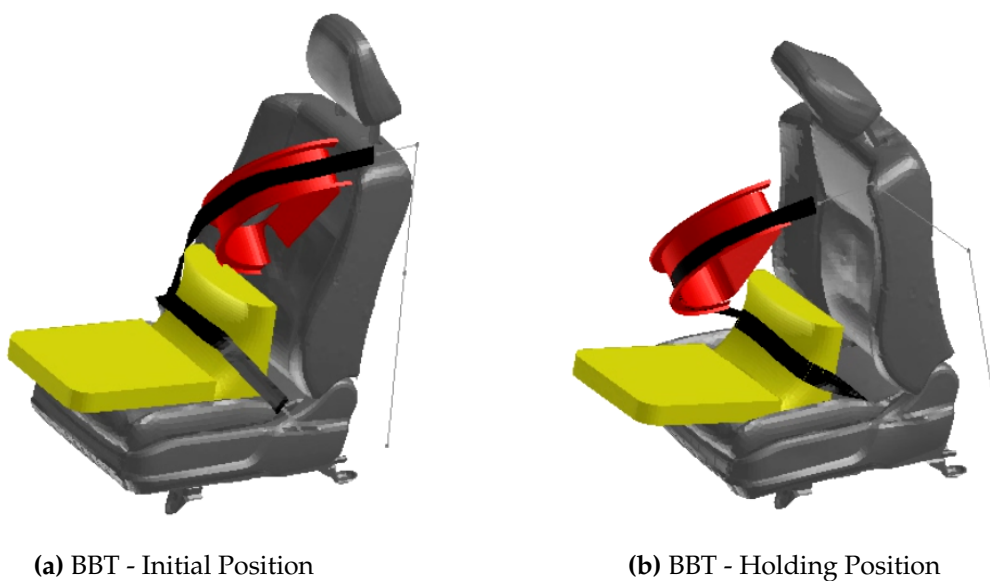


**Figure 2.20:** Body Blocks positioned within Seat Model in the Test Scenario

Simulation of the test procedure showed that the modified seat was in need of more stiffness. For the seat to withstand the loads for the full time duration, some of its structure had to be strengthened. Therefore, the material for some parts was changed to high-tensile steel.

With adaptation of both, the full vehicle model and the integral seat model, they were ready to be combined into a sled model.

## 2.4 Simplified Sled Model

The reduction and simplification of the model greatly reduced the number of deformable parts and, therefore, computational cost. That way, a sled model was received as a test environment for the further investigation of the operating principle.

Based on the full vehicle model, Figure 2.21 depicts the reduced body-in-white, in which all irrelevant parts were removed. All visible parts were combined to one rigid part that constitutes

the simplified body. This involved the modification of the point of application for the frontal crash pulse from Figure 2.10, that represents the RWT.

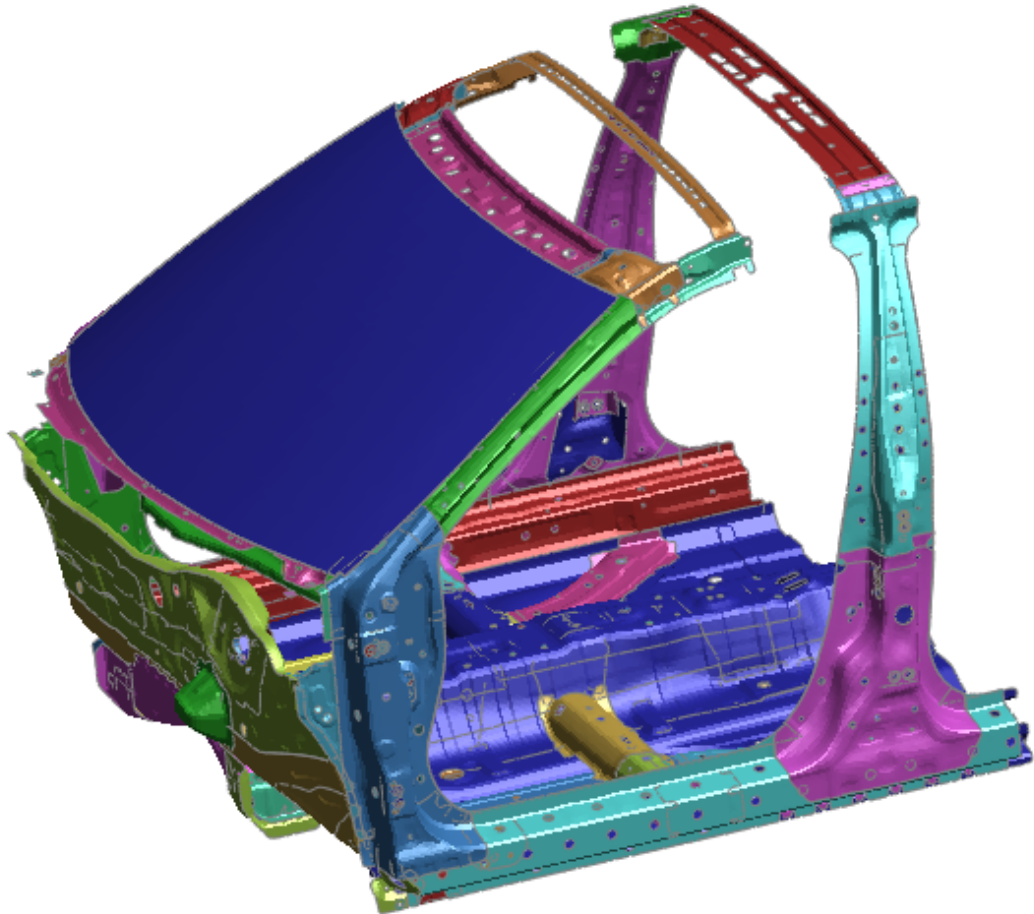


Figure 2.21: Reduced body-in-white

The combination of the two models, reduced vehicle and integral seat, was conducted by inclusion of the modified seat- and seatbelt-file and adaptation of connection- and contact-files. As an example for the adaptation of contact definition, the contact between dummy and seatbelt can be mentioned. Figure 2.22 depicts the difference of pelvic restraint in an early development stage and simulation with updated belt contacts. After 50 ms, the time of full airbag inflation, the contact treatment used in the original model version is unable to detect the edge on the side of the pelvis belt and lower dummy body (Figure 2.22a). With the correction in contact definition, the pelvis belt fits and slides smoothly on the dummy's pelvis during simulation, as Figure 2.22b shows.

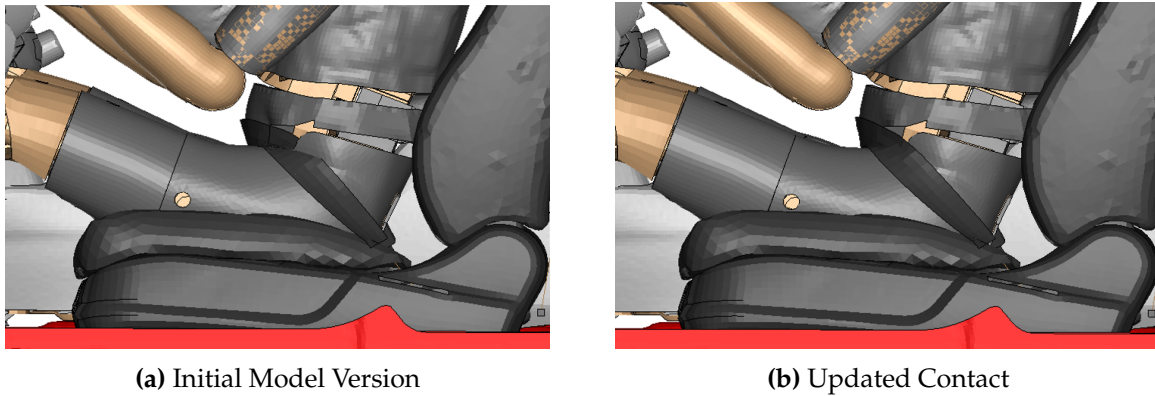


Figure 2.22: Adaptation of Contact Definition - Corrected Pelvic Restraint

The resulting simplified sled model is depicted in Figure 2.23. It forms the starting model for all further investigation.

In the following, it is referred to as the baseline model with hands on steering wheel (BaselineHOS).

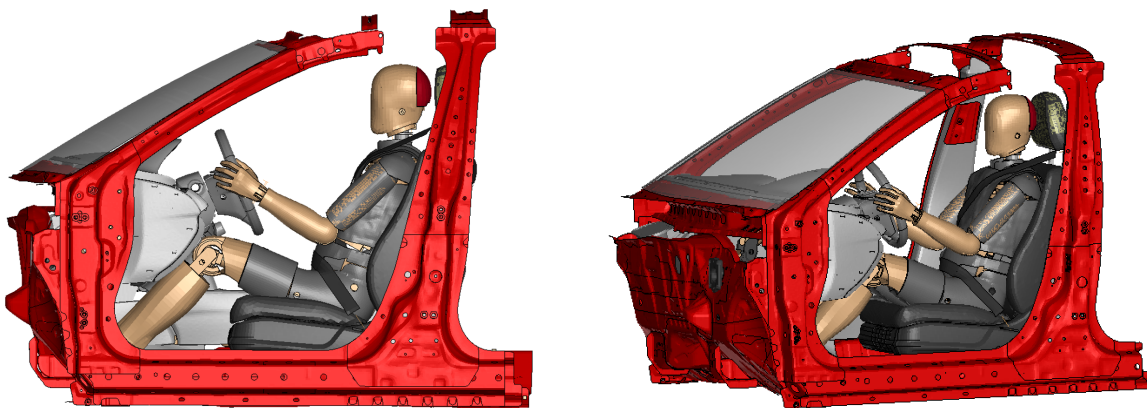


Figure 2.23: Simplified Sled Model - Baseline Model with Hands on Steering Wheel (BaselineHOS)

## 2.5 New Seat Position

The investigation of occupant loads in a seat position moved to the rear demands for adjustments of the seat including the dummy. In order to make the simulation model more realistic for automated driving scenarios, the position of the dummy arms was altered. Instead of the driving position, which means the dummy holding the steering wheel, the arms were moved on his thighs (Figure 2.24a).

As a prearrangement for the seat with in-crash movement, it was adjusted 400 mm to the back (Figure 2.24b). This longitudinal adjustment was reached by a simple transformation within the inclusion process of the files.



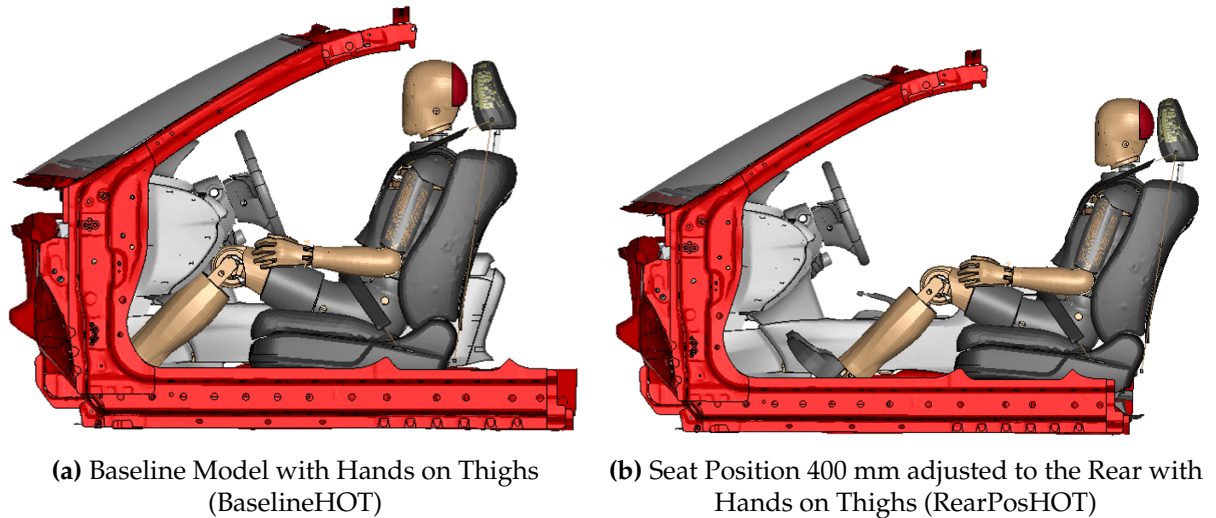


Figure 2.24: Simplified Sled Model - Baseline Models

Subsequently, the model shown in Figure 2.24a will be referred to as the baseline model with hands on thighs (BaselineHOT), whereas Figure 2.24b, as the starting model for all with in-crash-movable variants, is named the model adjusted to the rear with hands on thighs (RearPosHOT).

## 2.6 Principle for Energy Dissipation

The operating principle with the aim of reducing occupant loads is based on a relation between force and displacement of the seat. An example of a simple characteristic is given in Figure 2.25, with a constant sequence followed by a steep rising end. The characteristic can be adjusted by different force levels and mathematical functions.

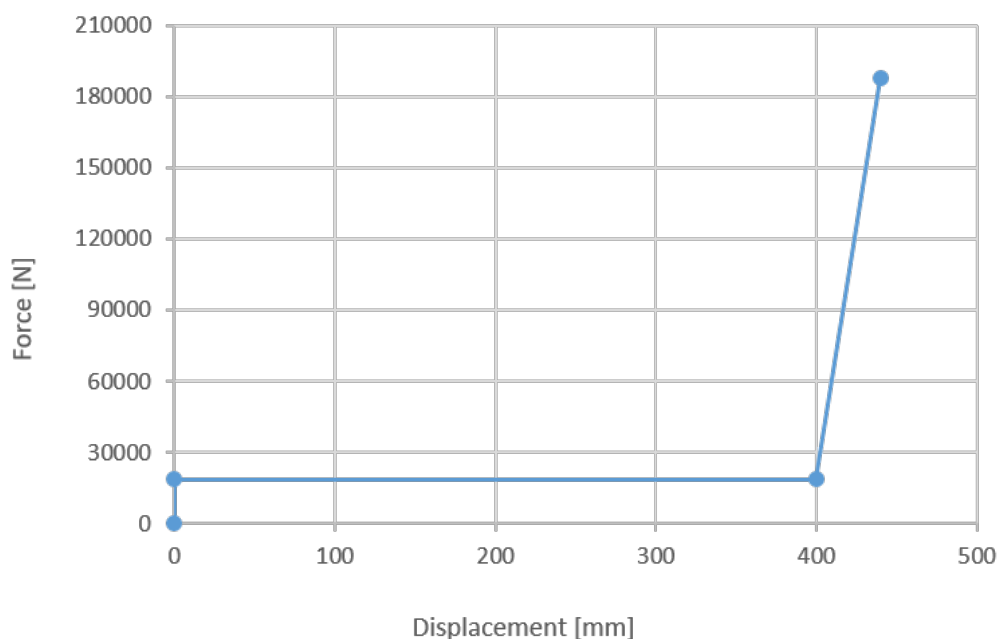


Figure 2.25: Simple Force-Displacement-Characteristic

For better visualization of the principle, it can be explained as a spring-damper-system. The plasticity of the spring is pre-set to 98% but is adaptable.

The principle within the vehicle and seat model are depicted in Figure 2.26. The system's front facing end is connected to the vehicle underbody, visible as the green part in the figure. The other end is mounted to the seat with the orange dotted lines depicting the modelled connections.

The principle for energy dissipation was integrated into the simplified sled model via an additional include-file.

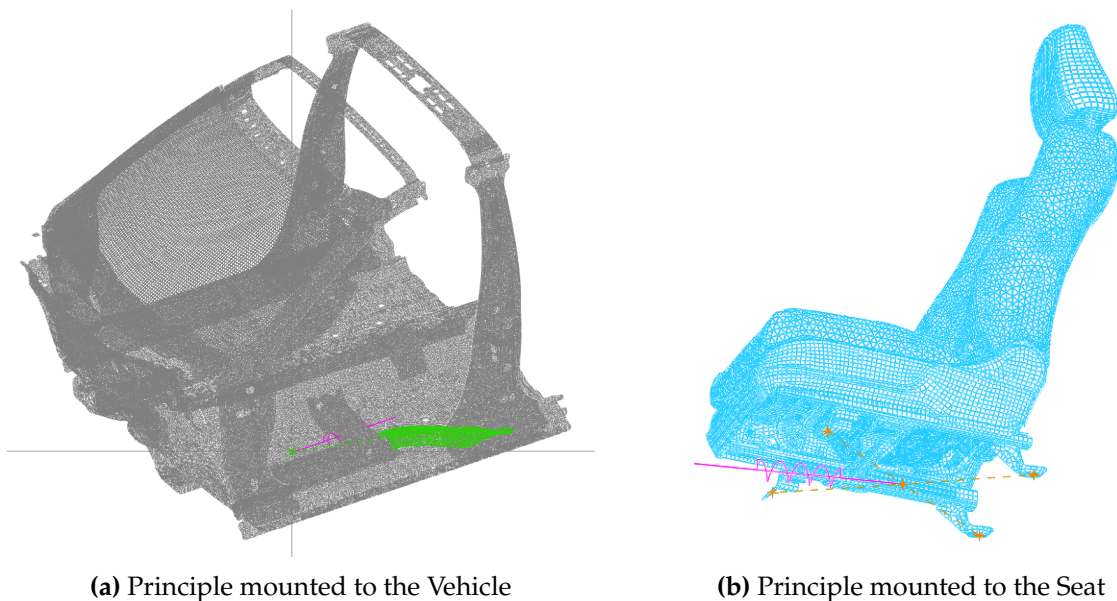


Figure 2.26: Principle for Energy Dissipation - Position within the Model

## 2.7 Simplified Model with Energy Dissipation

All further simulations to investigate and analyse the energy dissipation between seat and vehicle were conducted with the simplified sled model with hands on thighs and the seat moved 400 mm to the back, as it is shown in Figure 2.24b. The combined model is therefore called the simplified model with energy dissipation in rear position (RearPosSMED).

In order to optimize the principle and, therefore, the reduction of occupant loads, an evaluation of the simulation outcome was established.

## 2.8 Evaluation

To evaluate the new operating principle, a variation of the U.S. NCAP star rating was used. Therefore, this chapter presents the NHTSA rating scheme, starting with an introduction of injury criteria. At the end, the applied rating system is explained.

### 2.8.1 Injury Criteria

Injury criteria are meant to translate the mechanical responses of crash test dummies into a risk of life or injury to a living human (Eppinger et al., 1999). They are experimentally derived by determination of relationships between forces/motions and resulting injuries. The development of criteria is commonly done for one dummy size, e.g. the 50th percentile male, and then applied and translated to other size dummies, a process known as scaling (Kleinberger et al., 1998).

Because of the difference in human beings, the definition of injury tolerance levels or limits is difficult. Therefore, they are obtained through combination of information gained in indirect methods, such as human volunteer testing, cadaver testing, computer simulation or utilization of crash test dummies. (Eppinger et al., 1999)

The frontal NCAP rating system includes the body regions and criteria head (HIC15), neck (Nij, tension, and compression), chest (deflection), and femur (axial force) for the Hybrid III 50th percentile male. They are the same as in the FMVSS No. 208. This is to improve vehicle evaluation as well as to choose criteria consistent with those used in other frontal crash assessment programs, in order to generally improve restraint system development. (U.S. Department of Transportation, 2008)

NHTSA intends to change their rating scheme to a system that is similar to the one used in Euro NCAP in the future. The Euro NCAP test procedure uses a sliding scale which consists of a lower and upper limiting value. Injury criteria that reach a value beneath the lower limit result in a zero point rating while a value higher than the upper limit does not result in extra points. (U.S. Department of Transportation, 2015)

In the following, the injury criteria are described in more detail.

#### *Head - HIC15*

The Head Injury Criterion (HIC) is the standardized maximum integral value of the head acceleration. For the HIC15, the length of the time interval ( $T_2 - T_1$ ) is 15 ms. The HIC value is defined as

$$HIC = \left( \left[ \frac{1}{T_2 - T_1} \int_{T_1}^{T_2} a(t) dt \right]^{2.5} (T_2 - T_1) \right)_{max} \quad (2.1)$$

with  $a(t)$  being the time history for the resultant translational acceleration of the center of gravity of the head. (Laituri et al., 2016)

The HIC is based on translational accelerations only and, therefore, is the mechanism for bone-and/or otherwise-related injuries concerning the head. Takhounts et al. (2013) considered another category for head injury, namely brain-related injuries, which is why the BrIC (brain injury criterion) was developed. It is defined as

$$BrIC = \sqrt{\left( \frac{\omega_x}{\omega_{xc}} \right)^2 + \left( \frac{\omega_y}{\omega_{yc}} \right)^2 + \left( \frac{\omega_z}{\omega_{zc}} \right)^2} \quad (2.2)$$

with  $\omega_i$  being the peak rotational velocities about the x, y, and z axes, and  $\omega_{ic}$  the corresponding

critical rotational velocities. Important to point out is that BrIC uses the maximum values of head rotational velocities. (Takhounts et al., 2013)

A new kinematic-based metric was developed in a study from Gabler et al. (2018) to predict strain-based responses. The universal BrIC (UBrIC) is based on the relationship between brain deformation to rotational head motion.

$$UBrIC = \left\{ \sum_i \left[ \omega_i^* + (\alpha_i^* - \omega_i^*) e^{-\frac{\alpha_i^*}{\omega_i^*}} \right]^r \right\}^{\frac{1}{r}} \quad (2.3)$$

where  $\omega_i^*$  and  $\alpha_i^*$  are the directionally dependent ( $i = x, y, z$ ) maximum magnitudes of head angular velocity and angular acceleration, normalized by a critical value:

$$\omega_i^* = \frac{\omega_i}{\omega_{icr}} \text{ and } \alpha_i^* = \frac{\alpha_i}{\alpha_{icr}} \quad (2.4)$$

In the study,  $r = 2$  showed better performance than  $r = 1$ . (Gabler et al., 2018)

With these three criteria most brain injuries and skull fractures occurring in automotive environment can be captured. (Takhounts et al., 2013)

#### Neck

The used neck injury criterion  $N_{ij}$  includes four possible combined neck loading modes, namely tension-extension, tension-flexion, compression-extension and compression-flexion bending moment (Figure 2.27). These combinations are represented through the indices "ij" in the following formula:

$$N_{ij} = \frac{F_Z}{F_{int}} + \frac{M_Y}{M_{int}} \quad (2.5)$$

The resulting neck criterion is the sum of the normalized loads and moments, where  $F_Z$  is the axial force,  $F_{int}$  is the critical intercept value of load used for normalization,  $M_Y$  is the flexion/extension bending moment and  $M_{int}$  is the critical intercept value for moment used for normalization. The loads and moments are normalized with respect to critical intercept values defined for tension, compression extension and flexion, presented in Table 2.1. (Eppinger et al., 1999)

**Table 2.1:** Proposed Critical Intercepts for the Neck Injury Criterion for the Hybrid III 50th percentile Adult male Dummy, (Eppinger et al., 1999)

Tension	Compression	Flexion	Extension
4500 N	4500 N	310 Nm	125 Nm

#### Chest Deflection

The frontal NCAP focuses on the peak chest deflection, instead of the chest acceleration which was used prior for the assessment of thoracic injury risks. (U.S. Department of Transportation, 2008)

Figure 2.28 shows the four load cells within the THOR dummy model: upper left (element

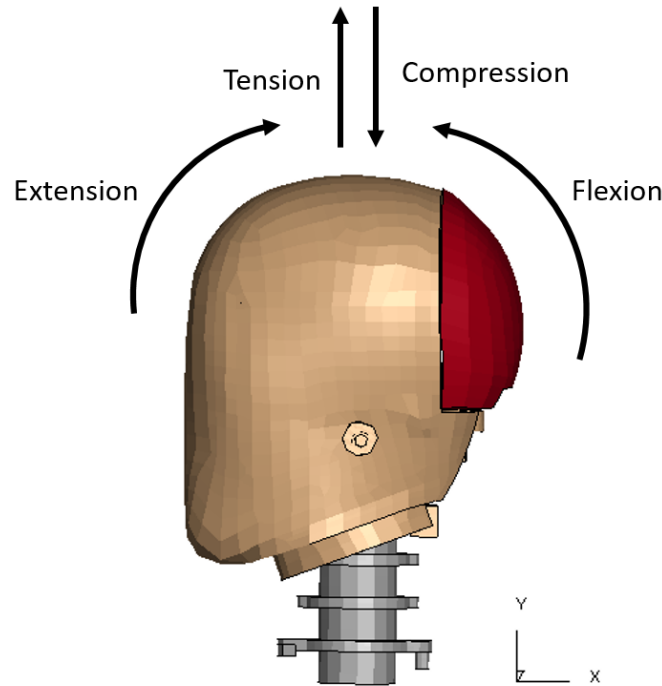


Figure 2.27: Neck Loading Modes

ID 706373), upper right (element ID 706378), lower left (element ID 706383) and lower right (element ID 706388). The injury criterion is defined as the maximum value of the deflection of any of the load cells.

#### *Femur Force*

The force acting on the femur  $F_{femur}$  is the compression force that is transmitted axially on each femur of the dummy. (Cichos et al., 2015)

The risk curves used for the frontal NCAP criteria are described below, after the definition of injury severity.

## 2.8.2 Injury Severity

The Abbreviated Injury Scale (AIS) was designed to simply classify injuries by body region and rank them by severity. The aim was to make sure that the same outcome is understood for the same injury. In Gennarelli and Wodzin (2006), the following definition is given:

“The AIS is an anatomically based, consensus derived, global severity scoring system that classifies each injury in every body region according to its relative importance on a 6 point ordinal scale.”

This six point ordinal scale is listed in Table 2.2.

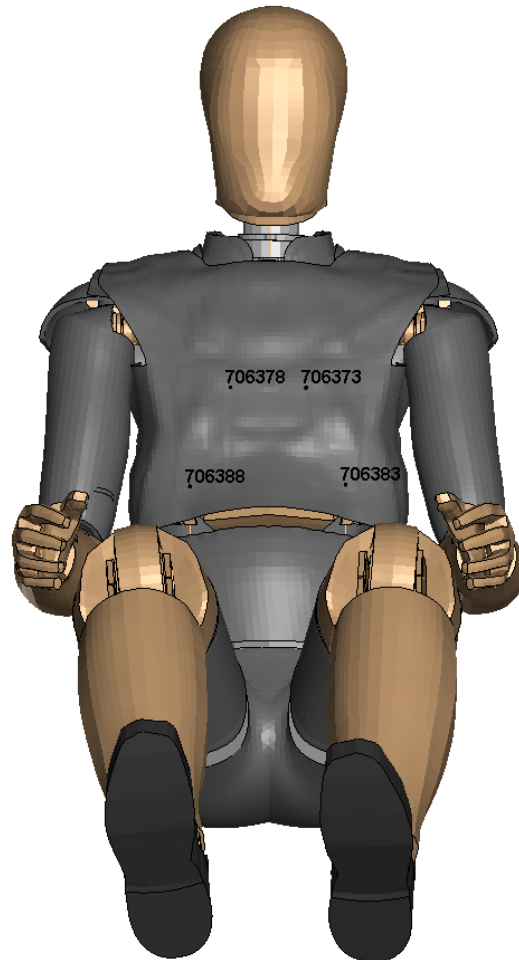


Figure 2.28: Chest Deflection - Load Cells in the THOR Dummy

Table 2.2: AIS Levels, (AAAM, 2015)

Level	Severity
AIS1	Minor
AIS2	Moderate
AIS3	Serious
AIS4	Severe
AIS5	Critical
AIS6	Maximal (currently untreatable)

### 2.8.3 Injury Risk Curves

On the basis of the frontal NCAP injury criteria, the probability of injury can be determined for each body region as the so called injury risk curve. The risk curves used are AIS 3+ and AIS 2+ (serious and moderate), with the plus expressing that all higher severities are implied. This means vehicle performance focuses on more frequently occurring injuries than just severe (AIS 4+) or critical (AIS 5+) injuries. (U.S. Department of Transportation, 2008)

For the load case of a frontal rigid wall test with 100% overlap at 56 km/h, as it is described in Section 2.2.1 and used for the evaluation of the principle, the following injury risk curves are defined for the 50th percentile male Hybrid III driver, according to U.S. Department of Transportation (2008).

**Table 2.3:** Injury Risk Curves, (U.S. Department of Transportation, 2008)

Region	Criterion	Risk Curve
Head	$HIC_{15}$	$P_{head}(AIS3+) = \Phi\left(\frac{\ln(HIC15) - 7.45231}{0.73998}\right)$ where $\Phi$ is the cumulative normal distribution.
Neck	$N_{ij}$	$P_{neck_{Nij}}(AIS3+) = \frac{1}{1 + e^{3.2269 - 1.9688N_{ij}}}$
	$F_{z,Tension}$	$P_{neck_{Tens}}(AIS3+) = \frac{1}{1 + e^{10.9745 - 2.375Neck_{Tension}}}$
	$F_{z,Compression}$	$P_{neck_{Comp}}(AIS3+) = \frac{1}{1 + e^{10.9745 - 2.375Neck_{Compression}}}$
		$P_{neck} = \max(P_{neck_{Nij}}, P_{neck_{Tens}}, P_{neck_{Comp}})$
Chest	Chest Deflection	$P_{chest}(AIS3+) = \frac{1}{1 + e^{10.5456 - 1.568*(ChestDeflection)^{0.4612}}}$
Lower Extremities	$F_{Femur}$	$P_{femur}(AIS2+) = \frac{1}{1 + e^{5.795 - 0.5196F_{femur}}}$

For the femur, an AIS 2+ risk curve is used because this is how most femur fractures are classified. In addition, it ensures the consideration of debilitating multi-fragmentary patellar fractures. (U.S. Department of Transportation, 2008)

As mentioned, NHTSA intends to change both, their rating scheme as well as the used ATD for the frontal NCAP. For the THOR 50th percentile male the proposed injury risk curves planned to be used are listed in U.S. Department of Transportation (2015). Merely the definition for the head risk curve remains unchanged. Nevertheless, the evaluation in this thesis is based on NHTSA' process in U.S. Department of Transportation (2008) and therefore, the included risk curves were applied within this study. The aim was to compare model variants to each other rather than the individual rating assessment.

## 2.8.4 Joint Probability of Injury

The overall probability of injury can be obtained by combining the individual risk curves from Table 2.3 and assuming, that the injuries to different body regions are independent events. This leads to

$$P_{joint} = 1 - (1 - P_{head}) \times (1 - P_{neck}) \times (1 - P_{chest}) \times (1 - P_{femur}) \quad (2.6)$$

which is the probability of serious injury for an occupant. (U.S. Department of Transportation, 2008)

### 2.8.5 Relative Risk

The relative risk (RR) estimates the occupant's risk of an injury compared to a baseline injury risk. It is computed by putting the joint injury risk  $P_{joint}$  in relation to the baseline injury risk  $base$ :

$$RR = \frac{P_{joint}}{base} \quad (2.7)$$

The baseline risk of injury as an approximation of the fleet average injury risk is set to 15%. The  $15 \pm 5\%$  represent the average risk of injury to the driver in all 2008 model year vehicles in the NCAP frontal tests. (U.S. Department of Transportation, 2008)

### 2.8.6 Star Rating Scheme

The star rating scheme was developed to improve the consumers' understanding and to give a quick and simple comparison between different vehicles concerning occupant safety. Important to mention is that it only compares vehicles of the same weight class. (Hershman, 2001)

Depending on the relative risk, the corresponding number of stars is assigned in accordance to Figure 2.29. This correlation was developed based on NCAP frontal crash test data for the 50th percentile male Hybrid III dummy. (U.S. Department of Transportation, 2008)

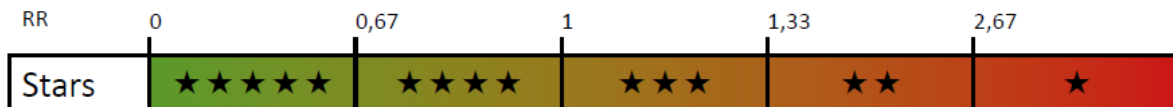


Figure 2.29: Star Rating by means of the Relative Risk, (CARHS, 2020)

Hershman (2001) explains the star rating in frontal collisions as follows:

- ★ ★ ★ ★ ★ 10% or less chance of serious injury
- ★ ★ ★ ★ 11% to 20% chance of serious injury
- ★ ★ ★ 21% to 35% chance of serious injury
- ★ ★ 36% to 45% chance of serious injury
- ★ 46% or greater chance of serious injury

### 2.8.7 Combined Crashworthiness Rating

The overall crashworthiness rating that NHTSA uses combines the results of the frontal, side and rollover tests. The combination process is described in Figure 2.30. However, this research discusses the frontal test procedure and therefore only uses part of this overall rating which is marked in orange.



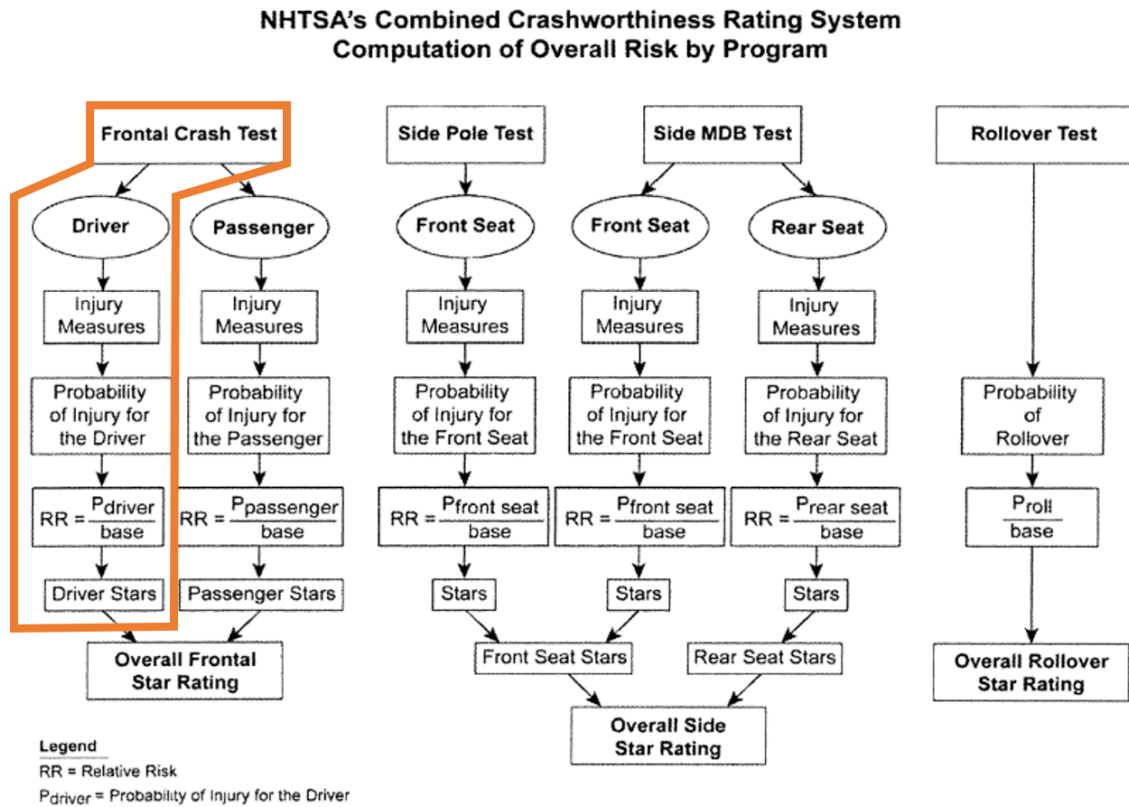
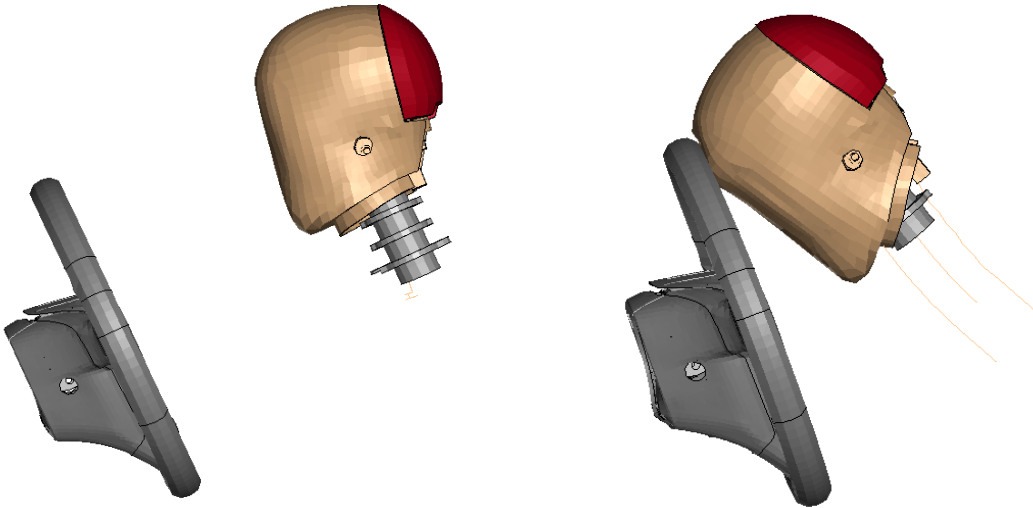


Figure 2.30: Combined Crashworthiness Rating, (U.S. Department of Transportation, 2008)

## 2.8.8 Applied Rating System

The aim of this thesis is to analyse the potential of a principle to reduce the occupant loads in highly automated vehicles. Therefore, the longitudinally adjusted seat position (RearPosHOT) was identified. To show a variation in results, the BaselineHOS and BaselineHOT model were considered for comparison.

A reduction of loads was defined as a lower joint probability of injury, compared to the initial seat position. Different energy management characteristics were evaluated with regard to the U.S. NCAP star rating (Figure 2.29) for the 50th percentile adult male driver. In addition to these frontal NCAP criteria, the  $a_{3ms}$ , BrIC and UBrIC (head) as well as abdomen deflection (chest) were evaluated. Also, the minimum distance between dummy forehead and steering wheel was considered to ensure that no head impact occurred when the airbag was deflating. For clarification, the dummy head and accordingly the steering wheel is considered as the parts seen in Figures 2.31, with an impact shown on the right.



**Figure 2.31:** Distance between Dummy Head and Steering Wheel

The previously defined injury criteria and injury risk curves are valid for the Hybrid III 50th percentile male dummy. However, this study works with the THOR dummy model which is also proposed to be used in the full frontal test by NHTSA in the future (U.S. Department of Transportation, 2015). Therefore and since most of the criteria are based on general biomechanical threshold levels, for the evaluation process within this thesis the injury criteria and injury risk curves for the Hybrid III were adopted for the THOR 50th percentile male.

With NHTSA's intention to introduce a new rating scheme, they already proposed limiting values for the injury criteria for the THOR dummy (NHTSA, 2015). The combinations of the used injury criteria and their respective limits for the THOR 50th percentile male are summed up in Table 2.4.

The critical values partly represent the proposed U.S. NCAP limits and are equivalent to the FMVSS No. 208 regulatory limits. The limit for the head acceleration value  $a_{3ms}$  is taken from the Euro NCAP, whereas the particular neck limits for  $F_{z,Tension}$  and  $F_{z,Compression}$  appear in Kleinberger et al. (1998). The maximum UBrIC value is set by definition (Gabler et al., 2018). Moreover, these values represent the biomechanical limits.

**Table 2.4:** Adopted Injury Criteria with Limits, (NHTSA, 2015)

Region	Criterion	Limit
Head	HIC15	700
	$a_{3ms}$	80 g
	BrIC	1.05
	UBrIC	1
Neck	$N_{ij}$	0.85
	$F_{z,Tension}$	3300 N
	$F_{z,Compression}$	-4000 N
Chest	Chest Deflection	52.3 mm
	Abdomen Deflection	88.6 mm
Lower Extremities	$F_{Femur}$	8588 N

The assessment of injury risk for all, baseline models and with in-crash-movable variations, was conducted via the Tool Dynasaur (Schachner et al., 2018). The obtained files included the critical values as well as diagrams which were visualized in Mutant (Luttenberger et al., 2019). The received data was put together into a rating sheet in Microsoft Office Excel, which assessed the achieved probability of injury and resulting stars for every simulation. The evaluation of the simulations is presented in the next chapter.



## 3 Results

In this chapter the evaluation of the simulation output based on the U.S. NCAP rating is done. At the beginning, the results for the full vehicle model are stated in order to compare and approve the simplified sled model results for BaselineHOS and BaselineHOT. With the introduction of the new seat position, the injury assessment reference values (IARVs) for the Rear-PosHOT model are presented. They pose the initial values that need improvement through adaptations, which concern the airbag deployment time, shoulder belt force limiter scaling and, finally, the principle for energy dissipation. These modifications are explained in detail and documented with their results in the following.

### 3.1 Full Vehicle Model

As described in Section 2.2, the full vehicle simulation model was adapted with regard to airbag deployment time (10 ms) and size of the vent area (radius of 28 mm). The evaluation of the model with these settings in the simulated test procedure of the rigid wall test can be seen in Figure 3.1. The respective diagrams are attached in Appendix B. In the U.S. NCAP star rating the vehicle reached four stars which is equivalent to a joint probability of injury of 14.21% and a relative risk of 0.9476.

### 3.2 Simplified Sled Model

With transformation into the simplified sled model, a new evaluation of the model became necessary. The BaselineHOS and BaselineHOT models were simulated in the frontal NCAP load case. The results for these baseline models are shown in the rating sheet in Figure 3.1, combined with the appropriate values for the full vehicle model for better comparability. The appropriate diagrams can be found in Appendix B.

			Simplified Sled Model		
			Full Vehicle Model	BaselineHOS	BaselineHOT
Region	Criterion	Limit			
Head	HIC <sub>15</sub>	700	500	544	520
	a <sub>3ms</sub>	80	70.3	71.6	71.6
	BRIC	1.05	0.87	0.78	0.80
	uBRIC	1	0.34	0.29	0.30
Neck	N <sub>ij</sub>	0.85	0.29	0.30	0.36
	F <sub>z,tension</sub>	3300	307.0	528.3	849.0
	F <sub>z,compr.</sub>	-4000	-1545.1	-1809.5	-1837.9
Chest	Chest Defl.	52.3	21.3	16.6	26.9
	Abdomen Defl.	88.6	8.5	5.8	4.6
Lwr Ex	F <sub>Femur</sub>	8588	3663.5	4077.2	3953.3
Head-SW	min. distance	> 0 mm	70.9	82.7	50.1

Results - U.S. NCAP Rating				
P <sub>Head</sub>		4.72%	5.95%	5.28%
P <sub>Chest</sub>		1.61%	0.81%	3.25%
P <sub>Femur</sub>		2.00%	2.47%	2.32%
P <sub>Neck</sub>		6.62%	6.64%	7.47%
P <sub>Joint</sub>		14.21%	15.06%	17.17%
Rel. Risk		0.9476	1.0040	1.1448
Stars		★★★★	★★★	★★★

Figure 3.1: Baseline Rating Sheet

The simplified sled model produced slightly different IARVs due to the modifications made. Overall the simplification process can be approved with regard to the joint probability of injury and relative risk.

Comparing the BaselineHOS and BaselineHOT models, it is interesting to see that the HIC15 is a little higher when the dummies hands were positioned on the steering wheel, whereas the chest deflection rose from 17 to 27 mm with the merely adaptation of the arm position.

The formatting in Figure 3.1 is used in all rating sheets. Cells with a red background indicate that the inscribed value is higher than the limit value. Red type poses a safety margin and stands for values that exceed 80% of the biomechanical limits.

### 3.3 New Seat Position

The new seating position with the seat adjusted 400 mm to the rear transforms the BaselineHOT model into the model RearPosHOT, as described in Section 2.5. Through assessment of

the injury criteria very high head loads and chest deflection emerged (Figure 3.2). The joint probability of injury is clearly affected by these with a very high value of 46.20%.

This is the initial situation that was investigated and aimed to improve with this thesis. Therefore, adaptations of the model were conducted to reduce the appearing occupant loads.

			Simplified Sled Model	
			BaselineHOT	RearPosHOT
Region	Criterion	Limit		
Head	HIC <sub>15</sub>	700	520	1021
	a3ms	80	71.6	108.6
	BRIC	1.05	0.80	0.67
	uBRIC	1	0.30	0.24
Neck	Nij	0.85	0.36	0.54
	F <sub>z,tension</sub>	3300	849.0	1054.1
	F <sub>z,compr.</sub>	-4000	-1837.9	-2630.8
Chest	Chest Defl.	52.3	26.9	46.4
	Abdomen Defl.	88.6	4.6	20.0
Lwr Ex	F <sub>Femur</sub>	8588	3953.3	1308.7
Head-SW	min. distance	> 0 mm	50.1	52.4

Results - U.S. NCAP Rating			
P <sub>Head</sub>		5.28%	23.95%
P <sub>Chest</sub>		3.25%	20.65%
P <sub>Femur</sub>		2.32%	0.60%
P <sub>Neck</sub>		7.47%	10.30%
P <sub>Joint</sub>		17.17%	46.20%
Rel. Risk		1.1448	3.0797
Stars		★★★	★

Figure 3.2: BaselineHOT & RearPosHOT Rating Sheet

## 3.4 Adaptations

### 3.4.1 Airbag Deployment Time

Because the seat is moved to the back, the dummy is positioned further away from the airbag. This circumstance suggests that the airbag might be partly deflated by the time the dummy plunges into it, resulting in the high loads and IARVs. Therefore, an analysis of the influence of the airbag deployment time was conducted.

In Figure 3.3, the position of the dummy relative to the airbag at the time of full airbag inflation is shown for various deployment times. Based on the previous video analysis from Chapter 2, it was estimated that the airbag takes 40 ms to be fully inflated. The initially set deployment time was 10 ms.

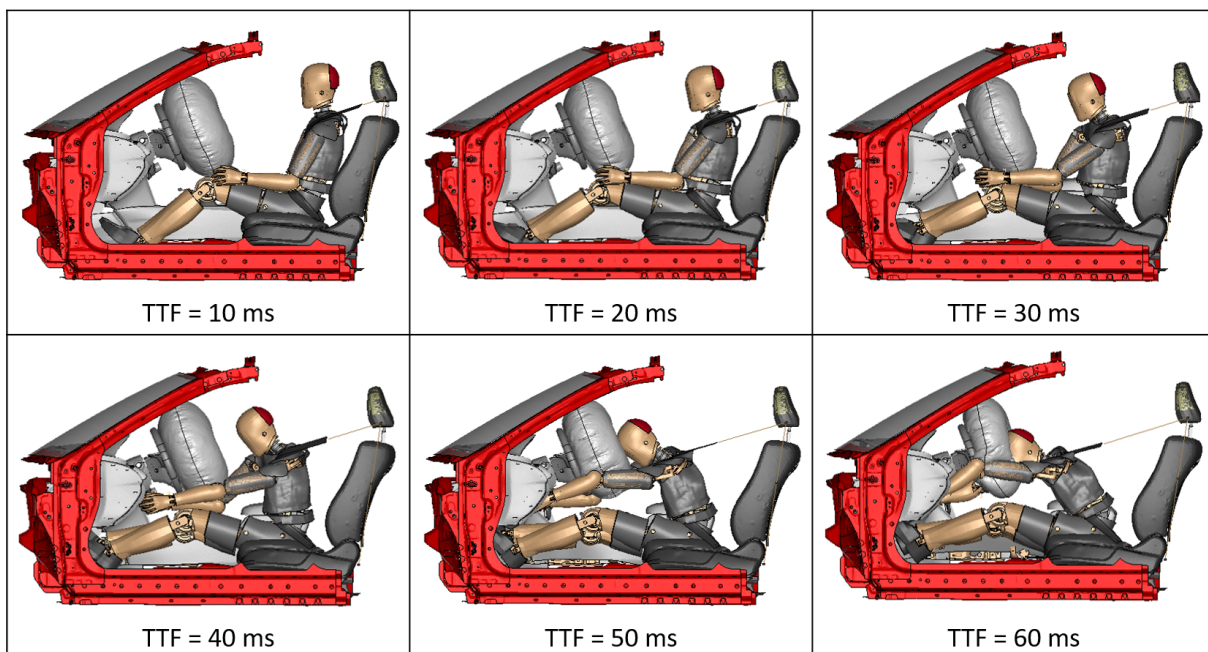


**Figure 3.3:** Airbag Deployment Times - Analysis of Dummy Position at Time of Full Inflation

The most critical and therefore investigated injury criteria were HIC15 and chest deflection, which are plotted according to the deployment times in Figure 3.4.

An airbag deployment of 20 ms shows the best HIC15 and chest deflection. However, at a simulation time of 60 ms, which is the time of full airbag inflation for this case (depicted in Figure 3.3), the distance between dummy head and airbag is 335.8 mm. In comparison, with a time to fire of 30 ms, the distance measured is 249.2 mm and the crucial IARVs similarly exceed the biomechanical limits. With the aim that the dummy is seated almost upright and not positioned too far from the airbag, the difference of about 85 mm is quite decisive.

Because the assessed critical values for all optional deployment times are high in any case, the decision was made to set the new deployment time to 30 ms, which is 20 ms delayed compared to the previous settings.

The adaptation of the deployment time resulted in an overall better relative risk, as can be seen



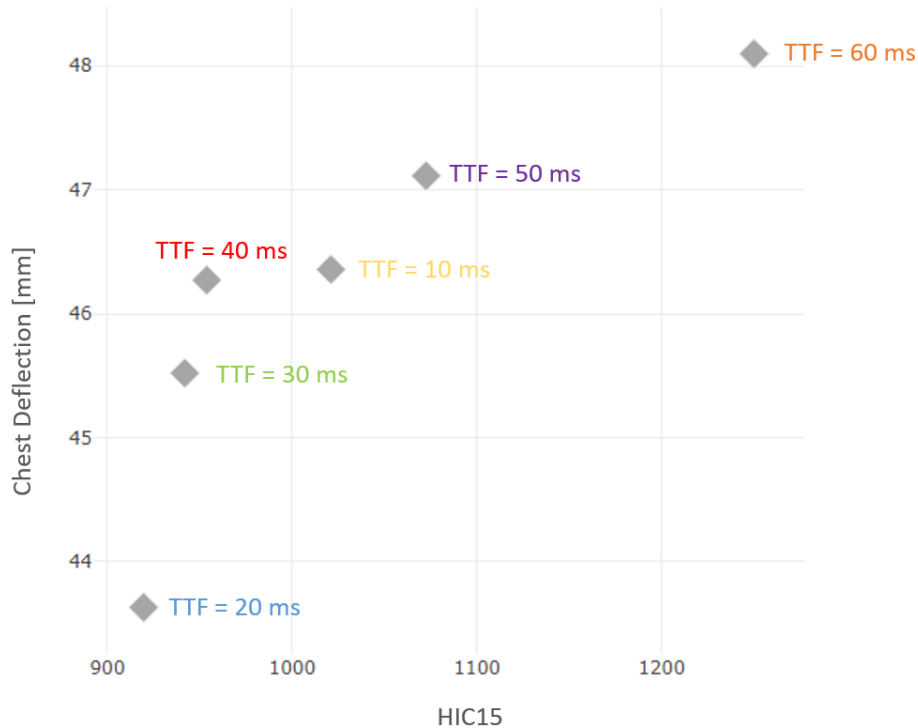


**Figure 3.4:** Airbag Deployment Times - Analysis of HIC15 and Chest Deflection

in the rating sheet in Appendix C. Still, the HIC15 and chest deflection did not show enough improvement, which is why further adjustments to the model were performed.

### 3.4.2 Belt Force Scaling

Too high loading to the upper body and head region might be reduced by reduction of shoulder belt force. This is suggested in a study from Mroz et al. (2018), where load limiters at seat track, seat, seat back, and lap belt were investigated to determine their effect on pelvis and lumbar spine loading of a human body model.

Therefore, a scaling of the seat belt load limiter curve was conducted, which is referred to as belt force (BF) scaling. The scaling factor was, after analysis, set to 0.7. This reduced the occurring maximum shoulder belt force from 5.65 kN to 4.4 kN in the RearPosHOT model (Table 3.1).

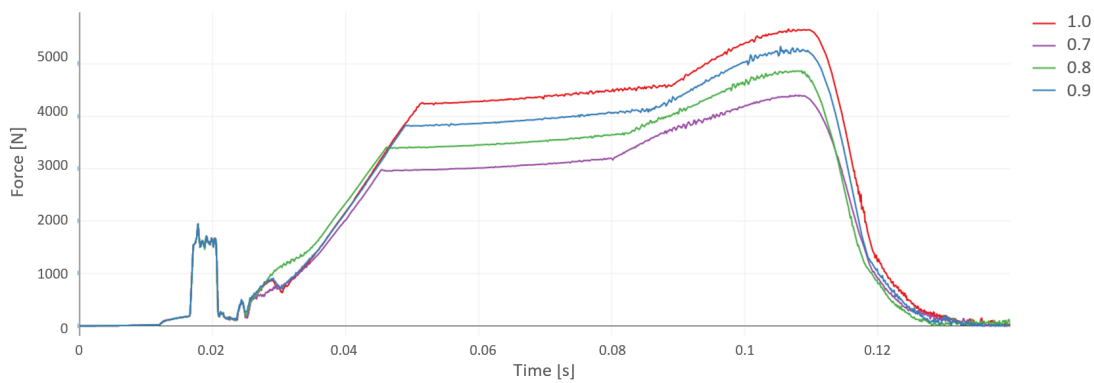
Furthermore, the simulation showed shoulder belt forces that were well within the values of a study from Keon (2016). He investigated occupant response in different vehicles in the NCAP frontal impact test. Equal to the simulated test procedure in this thesis, the restraint system he used included a seat belt pretensioner and frontal airbag. The ATD for the driver was a THOR 50th percentile male.

Figure 3.5 shows the analysed shoulder belt force for the simulation model, whereas the loads for different vehicles from the study are depicted in Figure 3.6.

The prescribed load curves for the unscaled and scaled seat belt load limiter are attached in Appendix D.

**Table 3.1:** Maximum Belt Forces - RearPosHOT Model

Region	Unscaled	BF-Scaling = 0.9	BF-Scaling = 0.8	BF-Scaling = 0.7
Shoulder Belt Force	5651.6 N	5275.7 N	4863.6 N	4395.1 N
Lap Belt Force	8688.0 N	8790.8 N	9417.8 N	9491.7 N



**Figure 3.5:** Shoulder Belt Force for different BL-Scaling Factors - Simulation

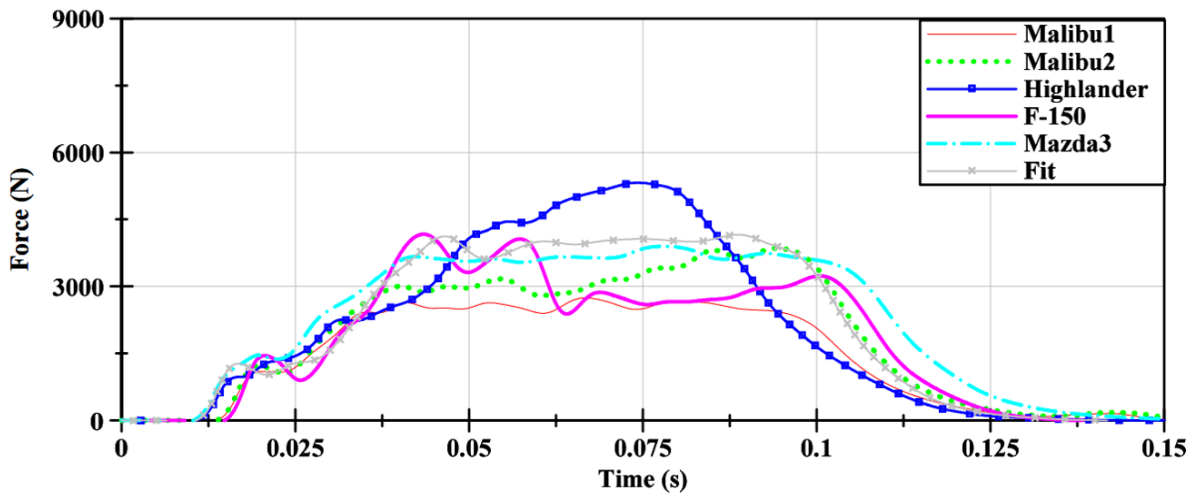


**Figure 3.6:** Shoulder Belt Force in different Vehicle Models, (Keon, 2016)

Since this was a major change in occupant restraint, the simulation of the full vehicle model in the load case of the rigid wall test was redone with the new scaling of the load limiter curve. The assessment showed, that the results were well within the biomechanical limits and were even improved compared to the unscaled version of the full vehicle model. The newly derived relative risk is decreased to 0.8028 which is equivalent to a joint probability of injury of 12.04% (compared to 14.21% with the unscaled model). The maximum shoulder belt force was reduced

from 4.4 kN to 3.1 kN.

Therefore, the adaptation conducted for the RearPosHOT model was approved.

The evaluation of the full vehicle model with scaled seat belt load limiter curve in comparison with the unscaled model can be found in Appendix E.

The adaptation of the belt force scaling resulted in a much better HIC15 as well as reduced chest deflection (Figure 3.7). Still, the joint probability of injury was too high for occupants to withstand, which is why further investigation was necessary.

RearPosHOT			
TTF = 30 ms BF unscaled	TTF = 30 ms BF-Scaling = 0.9	TTF = 30 ms BF-Scaling = 0.8	TTF = 30 ms BF-Scaling = 0.7
0.140	0.140	0.140	0.140

Region	Criterion	Limit				
Head	HIC <sub>15</sub>	700	942	849	824	668
	a3ms	80	100.1	97.7	95.0	85.6
	BRIC	1.05	0.64	0.69	0.85	0.90
	uBRIC	1	0.23	0.25	0.31	0.34
Neck	Nij	0.85	0.56	0.58	0.59	0.51
	F <sub>z,tension</sub>	3300	786.3	704.2	1079.7	1129.3
	F <sub>z,compr.</sub>	-4000	-2076.0	-2205.8	-2461.0	-2671.4
Chest	Chest Defl.	52.3	45.5	43.1	42.9	42.3
	Abdomen Defl.	88.6	19.9	19.4	20.3	19.1
Lwr Ex	F <sub>Femur</sub>	8588	2311.2	1312.0	1323.4	1646.8
Head-SW	min. distance	> 0 mm	68.5	63.9	58.5	46.3

Results - U.S. NCAP Rating					
P <sub>Head</sub>		20.70%	16.94%	15.93%	10.00%
P <sub>Chest</sub>		19.42%	16.07%	15.81%	15.05%
P <sub>Femur</sub>		1.00%	0.60%	0.60%	0.71%
P <sub>Neck</sub>		10.65%	10.98%	11.32%	9.82%
P <sub>Joint</sub>		43.48%	38.31%	37.61%	31.54%
Rel. Risk		2.8984	2.5543	2.5076	2.1026
Stars		★	★★	★★	★★

Figure 3.7: RearPosHOT Rating Sheet - Variation of Belt Force Scaling

### 3.4.3 Principle for Energy Dissipation

The idea of this thesis was to combine the sled model with a principle for energy management, as it is explained in Sections 2.6 and 2.7. The resulting simulation model is the RearPosSMED model. The forward movement of the seat is designed to dissipate energy to further improve the occupant loads. This energy was pre-estimated as follows.

With a given initial velocity in the rigid wall test of 56 km/h and 400 mm of available space that the seat can move, the mean acceleration is

$$\bar{a} = \frac{v^2}{2s} \quad (3.1)$$

The mass of the seat and the THOR dummy were measured within the simulation program:  $m_{Seat} = 31.6$  kg and  $m_{THOR} = 78.1$  kg. Considering only the dummies lower body that is placed on the seat and can theoretically be restrained by the lap belt alone, the reduced mass is  $m_{THOR_{red}} = 40.7$  kg. The force can then be calculated by

$$F = (m_{Seat} + m_{THOR}) * a \quad (3.2)$$

and gives  $F = 33.2$  kN or rather  $F_{red} = 21.9$  kN. With the formula

$$E = F * s \quad (3.3)$$

this results in an estimated energy of  $E = 13.3$  kJ and  $E_{red} = 8.8$  kJ.

For the force-displacement-characteristic, three simple mathematical functions were considered. All of them are variable up to the displacement of 400 mm followed by a strongly linear increase to the final load of ten times the force level. This ensures the stopping of the seat at the maximum displacement.

In the following, the tested functions within the RearPosSMED model with according simulation results are described.

#### Constant-Linear

The graph in Figure 3.8 is at a constant force for the full displacement of 400 mm. Considering the estimated energy of about 9 kJ, the starting force level was adopted at 22.5 kN. Based on the resulting IARVs, a higher variation with 25 kN and adaptations with lower forces were simulated. The according rating sheet is shown in Figure 3.9.

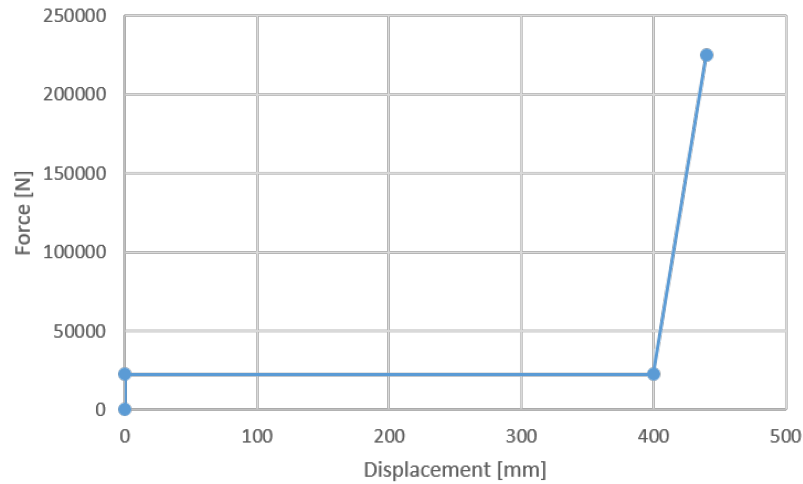


Figure 3.8: Constant-Linear Force-Displacement-Characteristic

Constant-Linear FD-Characteristic			RearPosSMED				
			TTF = 30 ms BL-Scaling = 0.7 f(x): const-lin F = 25,000 N	TTF = 30 ms BL-Scaling = 0.7 f(x): const-lin F = 22,500 N	TTF = 30 ms BL-Scaling = 0.7 f(x): const-lin F = 20,000 N	TTF = 30 ms BL-Scaling = 0.7 f(x): const-lin F = 18,750 N	TTF = 30 ms BL-Scaling = 0.7 f(x): const-lin F = 17,500 N
Region	Criterion	Limit					
Head	HIC <sub>15</sub>	700	521	504	435	417	396
	a3ms	80	70.1	67.4	64.9	63.7	63.2
	BRIC	1.05	0.53	0.53	0.51	0.54	0.49
	uBRIC	1	0.20	0.20	0.19	0.20	0.18
Neck	Nij	0.85	0.42	0.38	0.28	0.26	0.24
	F <sub>z,tension</sub>	3300	748.6	637.0	289.8	291.9	339.0
	F <sub>z,compr.</sub>	-4000	-1338.3	-1215.1	-1090.9	-1080.0	-1062.2
Chest	Chest Defl.	52.3	39.8	39.7	39.5	38.0	36.1
	Abdomen Defl.	88.6	10.8	11.1	10.6	9.7	9.1
Lwr Ex	F <sub>Femur</sub>	8588	313.0	295.7	499.6	1362.3	2307.4
Head-SW	min. distance	> 0 mm	24.0	20.6	14.8	11.6	3.3

Results - U.S. NCAP Rating						
P <sub>Head</sub>		5.30%	4.82%	3.13%	2.75%	2.34%
P <sub>Chest</sub>		12.20%	12.14%	11.87%	10.42%	8.73%
P <sub>Femur</sub>		0.36%	0.35%	0.39%	0.61%	1.00%
P <sub>Neck</sub>		8.32%	7.71%	6.45%	6.23%	5.99%
P <sub>Joint</sub>		24.04%	23.10%	20.45%	18.82%	17.04%
Rel. Risk		1.6027	1.5398	1.3630	1.2546	1.1363
Stars		★★	★★	★★	★★★	★★★

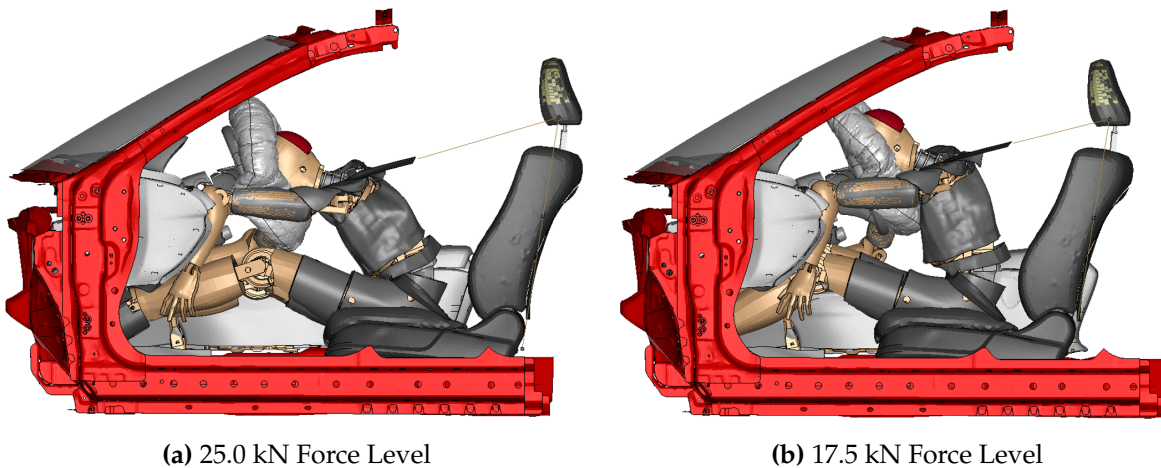
Figure 3.9: RearPosSMED Rating Sheet - Comparison of Constant-Linear-Characteristics

With a higher force level, the HIC15 and chest deflection are increased and the a3ms value even exceeds the 80% safety margin. This is also reflected in a joint probability of injury of more than 20%. Simulation with force levels of 30 kN and 40 kN were also assessed but showed chest and head IARVs higher than the biomechanical thresholds.

A lower constant force and therefore lower dissipated energy decreases the injury potential for

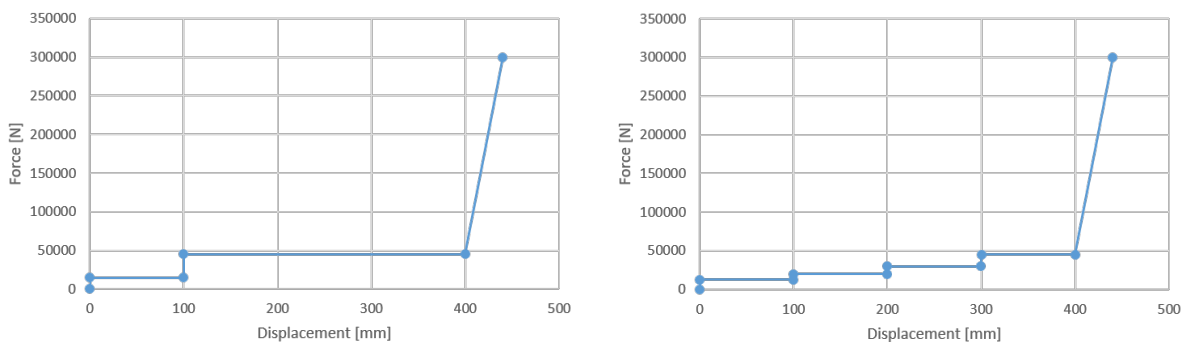
head, chest and neck. The HIC15 for a force level of 17.5 kN, for example, is already at a very good value compared to the starting model RearPosHOT. However, the distance between head and steering wheel shrinks to a minimum which suggests that an impact between the dummy head and the steering wheel might occur. Examination of the simulation model confirms the value of the measured minimum distance, which means that it is close to an impact. Also, the femur force rises with the decline of the force level. This can be explained with a closer look at the kinematics.

Figure 3.10 shows the RearPosSMED model at a simulation time of 0.12. The left side belongs to the higher force level of 25.0 kN whereas the right side is appropriate for the 17.5 kN force level. It is easy to observe that the seat with the higher force level is around 20 cm further behind the other. Therefore, the torso is bent forward and the head dips into the airbag further below than the dummy head in the right figure. Another result of the seat being closer to the front is that the legs touch the dashboard, leading to the increased femur force.



**Figure 3.10:** Kinematic Analysis - RearPosSMED with Constant-Linear-EM-Characteristic

The idea of multiple constant sequences was considered (Figure 3.11) but only led to higher head accelerations and therefore higher head IARVs. With the obviously greater amount of alterable parameters, the main influences remained unidentified. Thus, the approach was not pursued any further and a different kind of mathematical function was looked at instead.



**Figure 3.11:** Constant-Linear Force-Displacement-Characteristics with various Force Levels

### Linear-Linear

The linear-linear force-displacement-characteristic (Figure 3.12) was meant to move the seat forward more gently. The estimated energy suggested a force of 45 kN at a displacement of 400 mm. Simulation was done with a spread spectrum of force levels as can be seen in the rating sheet in Figure 3.13. This was due to the fact that none of the simulations was sufficient.

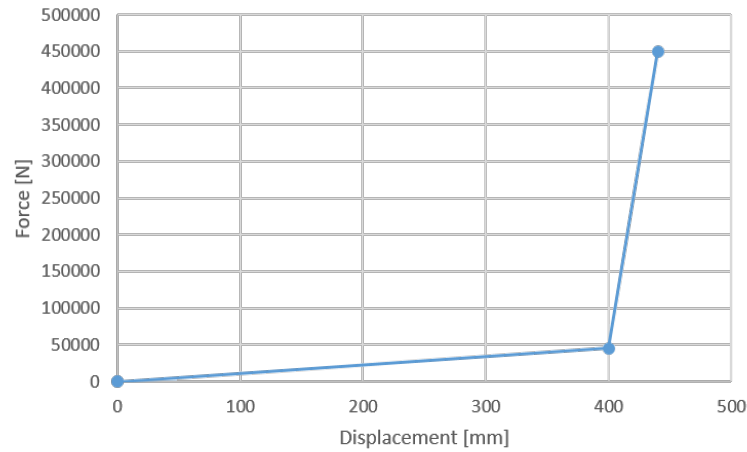


Figure 3.12: Linear-Linear Force-Displacement-Characteristic

Linear-Linear FD-Characteristic			RearPosSMED					
			TTF = 30 ms BF-Scaling = 0.7 f(x): lin-lin F = 95,000 N	TTF = 30 ms BF-Scaling = 0.7 f(x): lin-lin F = 75,000 N	TTF = 30 ms BF-Scaling = 0.7 f(x): lin-lin F = 50,000 N	TTF = 30 ms BF-Scaling = 0.7 f(x): lin-lin F = 40,000 N	TTF = 30 ms BF-Scaling = 0.7 f(x): lin-lin F = 37,500 N	TTF = 30 ms BF-Scaling = 0.7 f(x): lin-lin F = 25,000 N
Region	Criterion	Limit						
Head	HIC <sub>15</sub>	700	556	518	1131	1495	1583	1463
	a3ms	80	78.3	74.8	82.0	102.9	90.4	89.6
	BRIC	1.05	0.54	0.64	0.56	0.61	0.62	0.70
	uBRIC	1	0.19	0.22	0.20	0.21	0.21	0.24
Neck	Nij	0.85	0.46	0.44	0.34	0.27	0.24	0.37
	F <sub>z,tension</sub>	3300	288.8	2279.7	1874.6	1456.3	1409.9	1689.7
	F <sub>z,comp.</sub>	-4000	-2146.3	-2359.6	-2015.7	-1549.1	-1281.1	-2285.6
Chest	Chest Defl.	52.3	40.6	40.4	40.9	35.1	34.4	40.0
	Abdomen Defl.	88.6	9.7	10.4	8.9	7.7	5.3	12.3
Lwr Ex	F <sub>Femur</sub>	8588	1044.6	847.5	604.5	1934.2	2317.1	8792.3
Head-SW	min. distance	> 0 mm						

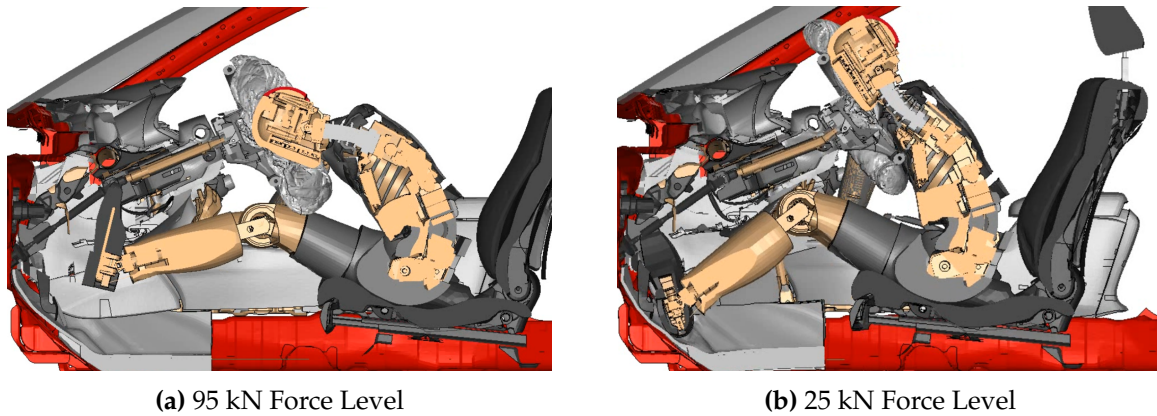
  

Results - U.S. NCAP Rating							
P <sub>Head</sub>		6.30%	5.21%	28.46%	42.38%	45.40%	41.22%
P <sub>Chest</sub>		13.07%	12.88%	13.46%	7.90%	7.39%	12.45%
P <sub>Femur</sub>		0.52%	0.47%	0.41%	0.82%	1.00%	22.68%
P <sub>Neck</sub>		8.99%	8.67%	7.22%	6.34%	5.99%	7.63%
P <sub>Joint</sub>		26.26%	24.94%	42.80%	50.71%	52.94%	63.24%
Rel. Risk		1.7507	1.6625	2.8533	3.3805	3.5294	4.2163
Stars		★★	★★	★	★	★	★

Figure 3.13: RearPosSMED Rating Sheet - Comparison of Linear-Linear-Characteristics

The minimum distance for all of the simulations is zero since they showed a major impact

between dummy and steering wheel and no significant improvement was to be found. There were, however, differences in the kinematics that can be attributed to the force level. Figure 3.14 shows the moment of impact between dummy and steering wheel for the two extremal values.



**Figure 3.14:** RearPosSMED - Impact between Dummy and Steering Wheel

Same as in the constant-linear case, the higher force causes the dummy torso to be more leaned forward and the head to dip into the airbag at a lower point. This leads to an impact with the central part of the steering wheel, which can be seen in Figure 3.14a. Contrary to that is Figure 3.14b for the very low force level. The dummy crashes into the steering wheel with his full torso with the effect that the complete steering unit is pushed to the front. The head severely touches the rim of the steering wheel while the right foot and knee crash into the carpet respectively dashboard, explaining the high femur injury risk. These effects are explainable by the fact that the force level at 400 mm is too low, the seat decelerates suddenly and additionally accelerates the torso and dummy head.

Even though the higher forces lead to an improvement of the assessed injury reference values, the overall evaluation for the energy management with linear-linear-functions is redundant and was not further considered within this thesis.

As an adaptation to the linear-linear-characteristic, an initial force level as in Figure 3.15 was introduced.

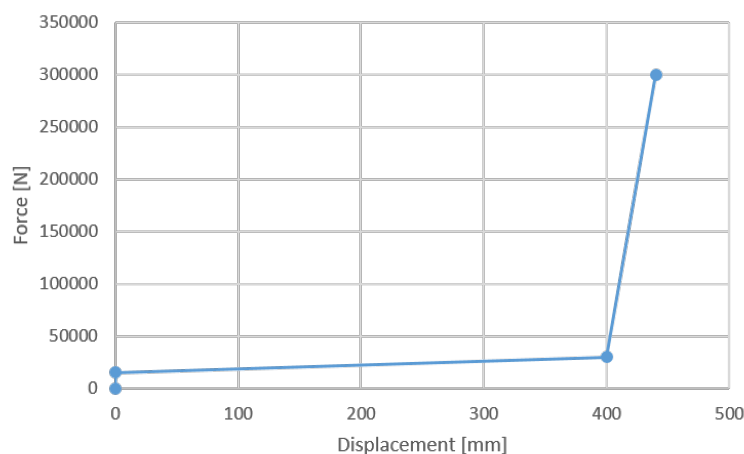
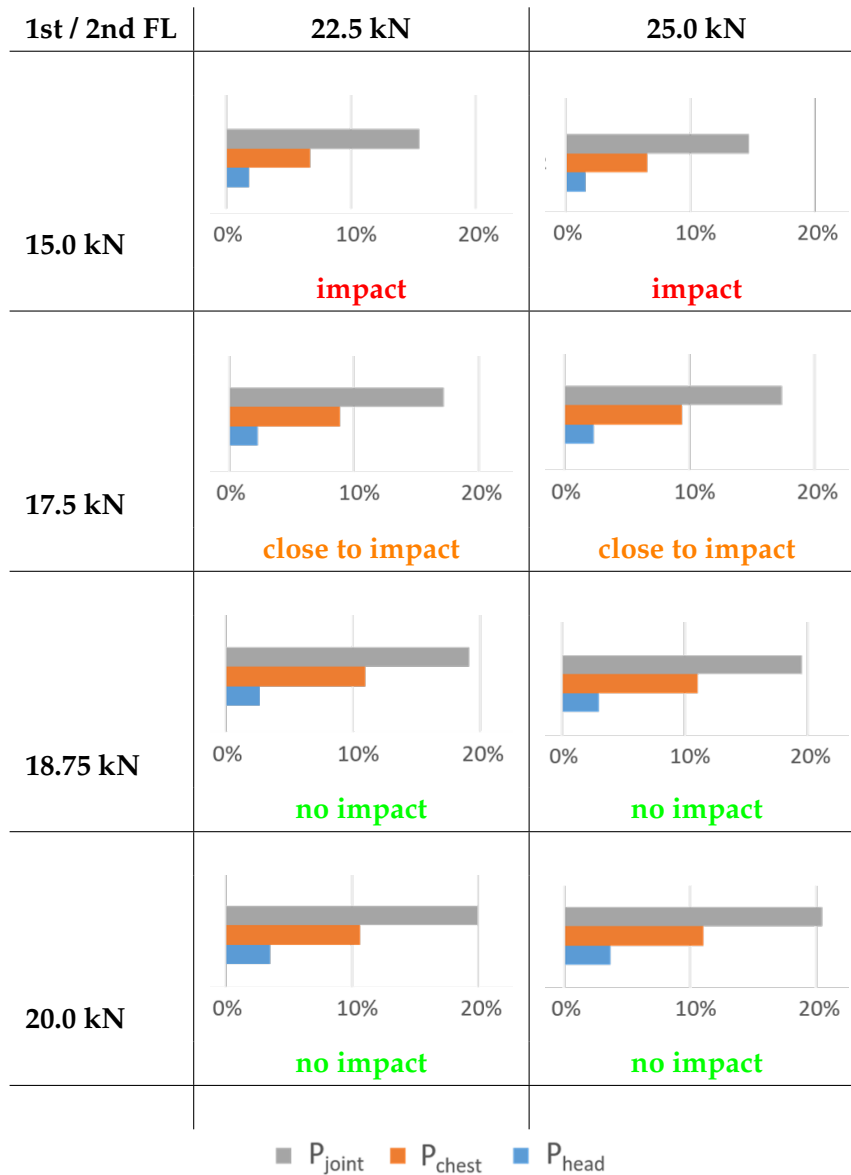


**Figure 3.15:** Linear-Linear Force-Displacement-Characteristic with initial Force Level



Derived from the energy estimation, different simulations with various gradients within the displacement of 400 mm were conducted. Table 3.2 shows a matrix with evaluation of the probability of injury for the most critical body regions head and chest, as well as the joint probability of injury and a statement concerning the impact between dummy head and steering wheel.

**Table 3.2:** Matrix for the Linear-Linear-Characteristic with initial Force Level (FL)



The first force level was set rather low in order to make the seat move forward with the beginning of the frontal crash scenario. Even though the IARVs resulted in a remarkably good rating of injury risk, an initial force of 15 kN led to an impact between the dummy forehead and the steering wheel. It can also be seen in the rating sheet in Appendix F that the value of the second force level did not seem to effect this circumstance. Furthermore, this adjustment hardly changed the assessed reference values and the relative risk remained almost the same throughout the assessed variants. An improvement was not derived unless the second force level was set to 45 kN or higher.

A higher second force level made the seat stop earlier and more gentle, which slightly reduced the femur injury risk. However, the side effect was a rise of HIC15 and particularly chest deflection so that a too high setting was counterproductive.

With increase of the first force level, the injury risk for the head and again, especially for the chest rose. Whereas the chest deflection was approximately 33 mm for the lowest level, it rose to around 38 mm for a force of 20 kN, that is a chest injury potential of 6.57% and 11.06%, respectively, for the more declining characteristic.

Further force levels were tested and their evaluation is attached in the appendix.

### Linear-Constant-Linear

The third mathematical function is a combination of the previous, namely a linear-constant-linear force-displacement-characteristic with an initial force level, see Figure 3.16.

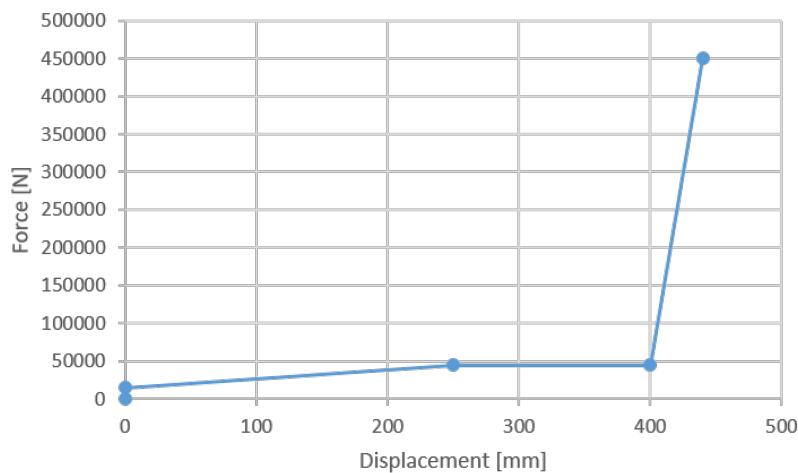


**Figure 3.16:** Linear-Constant-Linear Force-Displacement-Characteristic with initial Force Level

The idea was to have an immediate forward movement of the seat through the initial force level, a linear sequence for a steady movement and the constant part for a smooth stopping. Therefore, the displacement point of change was set to 200 and 250 mm. Based on the previous estimation, the initial force level was set to 15 kN which gave, with a second level of 25 kN, an energy of 8.75 kJ. The second force level was varied, as was the deployment time for one of the options. Figure 3.17 shows the appropriate rating sheet.

The simulations with a second force level of 25 kN showed very good IARVs with joint probability of injury values of about 15%. All options, however, showed a minor impact between dummy forehead and steering wheel rim. Neither the displacement point of change nor a 10 ms delay of airbag deployment led to an improvement of the respective minimum distance. The prevention of the impact was only reached by rising the second force level. The consequences were higher head and chest reference values which were almost and even transcending the 80%-safety margin.

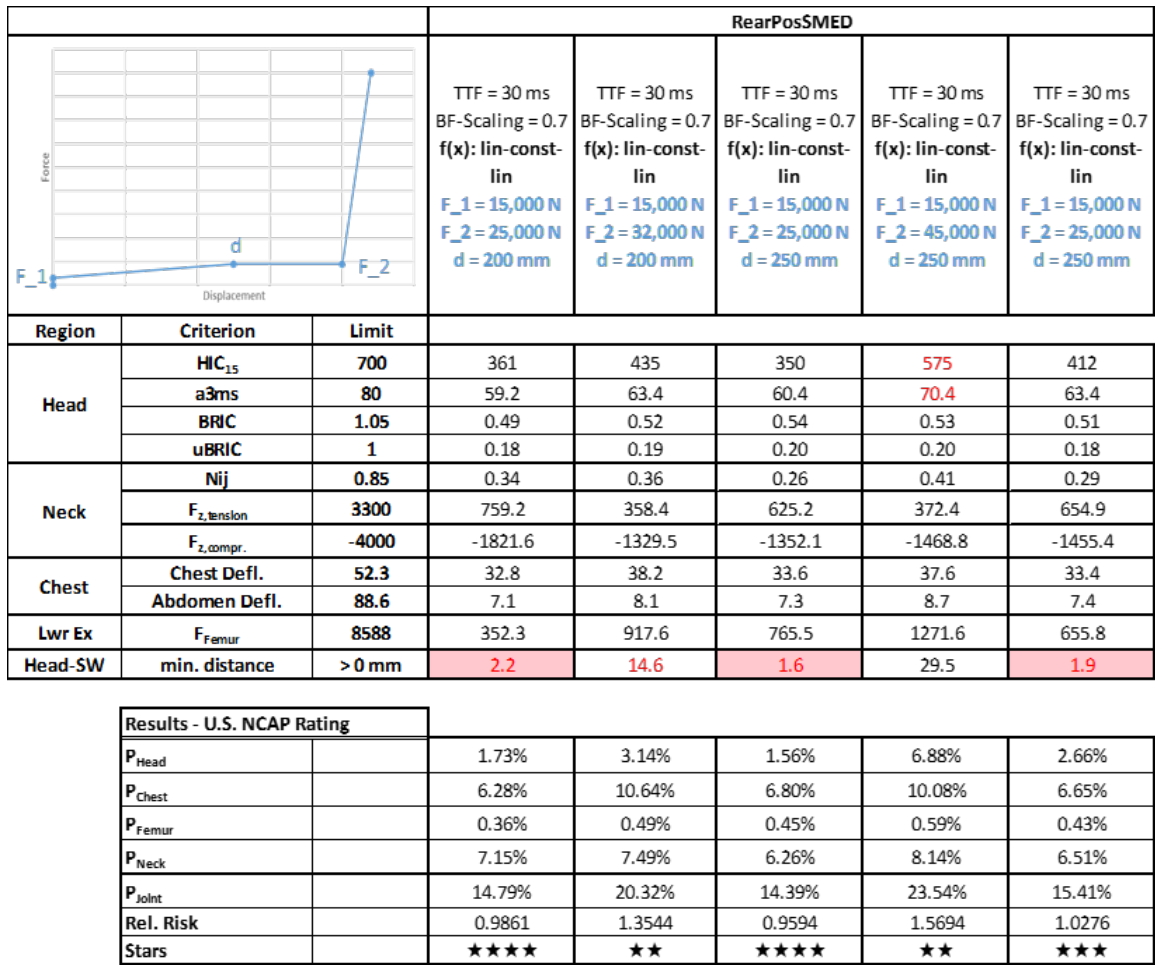


Figure 3.17: RearPosSMED Rating Sheet - Comparison of Linear-Constant-Linear-Characteristics

None of the adapted parameters, showed significant improvement which was also due to the fact that only a small amount of options was tested.

Overall, an improvement to the initial situation, the RearPosHOT model, was reached with adaptation and modification into the RearPosSMED model. A first reduction of occupant loads was achieved with different force-displacement-characteristics which has further potential through continuing investigation.

The next chapters discuss the obtained results and give possible outlooks for the future.



## 4 Discussion

A simplified sled model was derived from a publicly available FE model and simulated with the load case of a rigid wall test. Adaptations and the integration of an energy dissipating principle by means of a seat with in-crash movement were analysed to reduce the occupant loads and improve the evaluated IARVs for a seat position further back.

The source model was developed for use with the oblique moving deformable barrier test. This is why all settings, as for example the airbag inflation curve, were validated for this specific load case. Throughout the process of this thesis various modifications and simplifications were made. In addition, the models were only evaluated by numerical simulation and not verified by mechanical sled tests. Therefore, these limitations have to be kept in mind when considering the outcomes.

With the seat being able to move forward, the seatbelt anchorage had to be adapted. The mounting in the b-pillar was changed into an integral seat belt anchorage, which was tested according to legislation but still limits the validity of the modified simulation model. Since the aim was to use existing restraint systems, the comparability to current conventional vehicles and systems is however maintained.

For the results to be suitable for various future interior concepts, the main focus of this study was the standard seating position with longitudinal adjustment. This describes a seat with upright back rest, moved 400 mm to the rear. With the adequate analysis of this position, reclined respectively sleeping positions might be examined in further research.

The adjustment of the seat was set to 400 mm in order to have an analysed principle and results applicable for all shorter displacements. However, the adjustment range of the future seat systems might not be designed for this seating layout.

Since a THOR 50th percentile male dummy was already included in the open source vehicle model, all results derived are valid for this anthropometry. The consideration of, for example the 5th percentile female dummy, would entail a process of gravity settling and positioning the dummy model onto the seat as well as fitting the seatbelt model onto the dummy. Therefore, the study was restricted to the 50th percentile male dummy which limits the conclusions drawn within this thesis.

The new seat position enlarges the space between the dummy and the steering wheel respectively dashboard. Therefore, the support for the dummy's knees is no longer within range. A resulting effect that usually occurs is submarining, a situation where the lap belt slips over the anterior superior iliac spine of the iliac wings of the pelvis and subsequently loads the ab-

domen (Rawska et al., 2020).

Visual inspection of the results showed that this phenomenon did not occur within the study of the energy dissipating principle. This may be due to the upright seating position, as submarining mainly results from reclined backrests (Rawska et al., 2020). Another influencing factor could be the THOR version 2.1 simulation model since it may be less biofidelic than newer updated versions or the physical dummy and therefore might not be capable of realistic prediction of results.

The adjustment of the seat and dummy further to the back of the vehicle involved a new arm position. The scope was to investigate situations, where the occupant is released from the driving task and therefore, does not actively hold on to the steering wheel. The evaluation of the BaselineHOS (hands on steering wheel) and BaselineHOT (hands on thighs) models suggested, that this adaptation of the seating position has an impact on the IARVs. Specifically, the chest deflection increased from 31.7% of the biomechanical limit to 51.4%. This is reflected in the chest injury risk and led to a rise of the joint probability of injury by 2%.

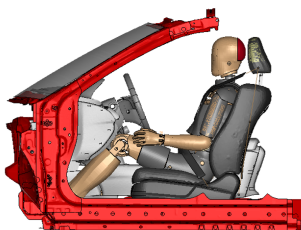
Often, passengers assume different sitting positions in critical driving scenarios compared to the dummy positioning in crash test procedures (Morvan et al., 2007). The difference in chest deflection of 62% that resulted from the modification of the hands being on the dummy's thighs instead of the steering wheel shows that just slightly altered seating can have a significant impact on the injury risk.

For the evaluation of the model and alterations like the just mentioned, an adapted version of the U.S. NCAP rating was used. The assessment with the so-called star-rating is more or less irrelevant but the resulting injury risks, critical values and joint probability of injury allows a robust comparison of the simulated variants.

To show the effects of the individual modifications explained in the previous chapters, the reached percentage of the limiting values for the assessed injury reference values is plotted in Figure 4.1 for some simulations. A comparison of their assessed injury reference values plotted over simulation time is shown in the diagrams in Appendix B.

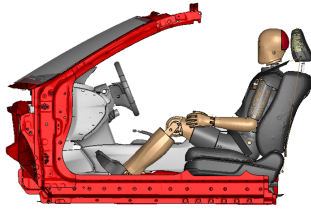
The considered variants are:

- BaselineHOT as the values that are aimed to reach,



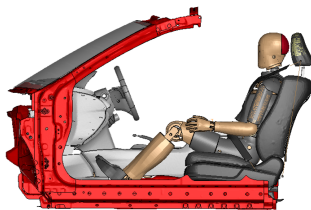
simplified sled model in standard seat position with hands on thighs

- RearPosHOT as the initial values that need improvement,



simplified sled model with seat position 400 mm adjusted to the rear and hands on thighs

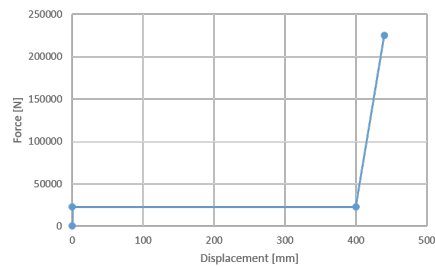
- RearPosHOT with adapted airbag deployment time,
- RearPosHOT with adapted airbag deployment time and belt load scaling,
- RearPosSMED with adapted airbag deployment time and belt load scaling



simplified sled model with seat position 400 mm adjusted to the rear and hands on thighs (= Rear-PosHOT) with energy dissipation through the seat with in-crash-movement

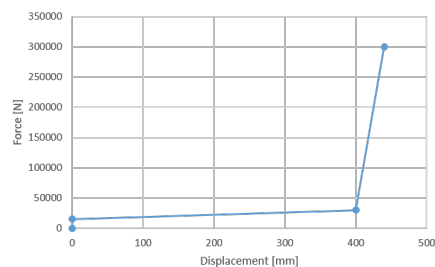
with the principle for energy dissipation defined through a

- constant-linear function with an 18.75 kN force level,

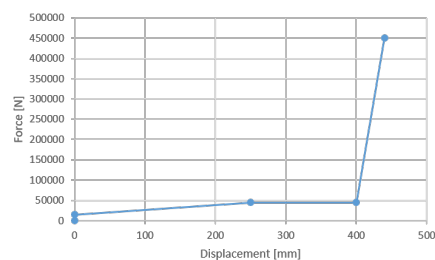


- constant-linear function with a 20.0 kN force level,

- linear-linear function with an incline from an 18.75 to a 22.5 kN force level,



- linear-constant-linear function with an incline from a 15.0 to a 32.0 kN force level within a displacement of 200 mm, remaining at a constant force level of 32 kN.



As a matter of fact, not all simulated RearPosSMED variants led to good results. Moreover, some functions and force levels changed the outcoming injury risk for the worse and significantly downgraded the IARVs.

The listed force-displacement-characteristics for the principle for energy dissipation were chosen as the best variants from the attained results. The particular rating sheets led to the assumption, that HIC15 and chest deflection are the most critical injury criteria when a seat position further back is adopted. In addition, the a3ms value of the head acceleration was increased for many simulations. It is not considered in the star-rating, which supports the impression that the individual injury criteria give better information about the effectiveness of an adaptation than the overall rating.

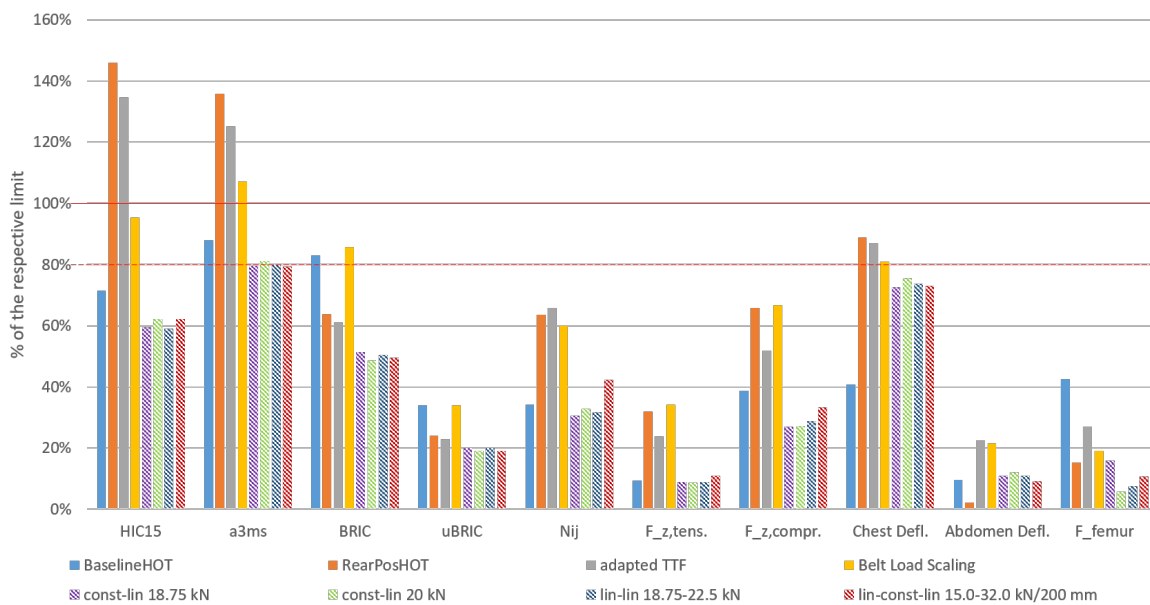


**Figure 4.1:** Reached Percentage of the respective Limits for the considered Variants

Especially the chest deflection was higher in all simulations when the force levels were increased. This effect can also be seen in the diagram in Figure 4.1, where the additional energy dissipation does in fact reduce the chest deflection compared to the RearPosHOT value, but it is not even closely reduced to the percentage of the BaselineHOT model.

In general, the statement that with an increasing force at a displacement of 400 mm, the HIC15 value rises too, can be derived from the evaluations. In addition it could be observed that the higher the force at a displacement of 400 mm was set, the sooner the seat stopped moving forward. This means that the final position of the seat was further behind than it was with a lower set force. As a result, the dummy torso started to lean forward sooner than it did with a lower force level. Thus, the dummy head moved forward sooner and dipped into the airbag at a lower height. In case of an impact, the forehead then hit the steering wheel hub instead of the rim, as it did when the seat stopped later and consequently closer to the steering wheel and airbag.

For these scenarios, the minimum distance between the dummy forehead and the steering

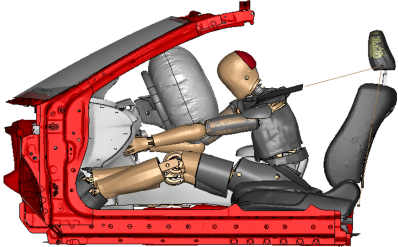
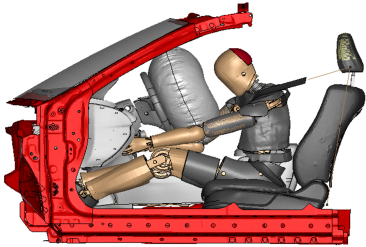
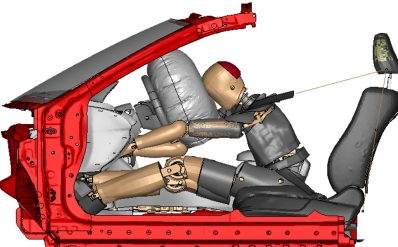
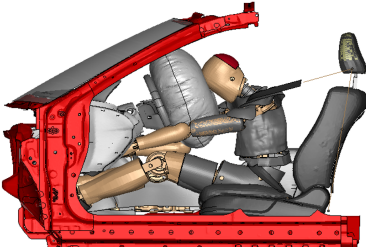
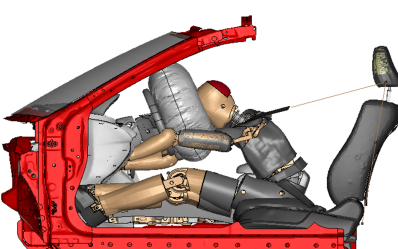
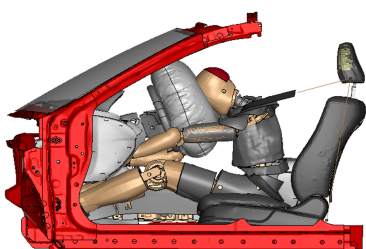
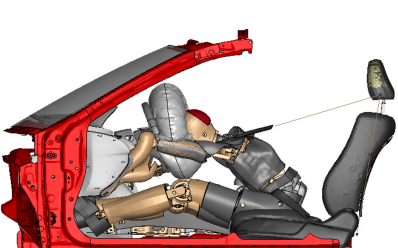
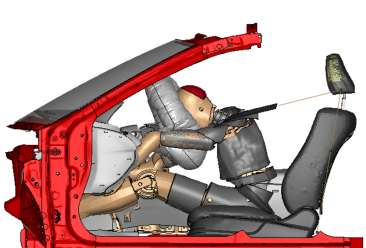
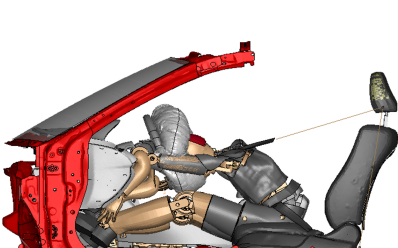
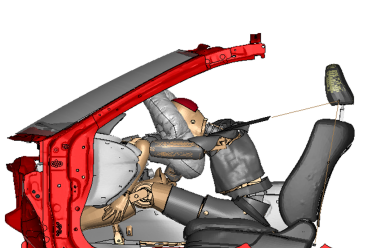


wheel had to be considered. Even though the case of an impact was investigated with a measurement analysis, the evaluation was not excellent. Therefore, the critical values were double-checked in the simulation model. To make a statement whether an impact occurred or not, an evaluated minimum distance higher than 2 mm combined with visual approval was interpreted as no impact.

The adaptation of the airbag deployment time together with the belt load scaling to reduce the shoulder belt force already showed some improvement for most injury reference values compared to the RearPosHOT model (Figure 4.1). Considering the kinematics in the simulations one can see that the dummy dips into the airbag at around 90 ms of simulation time (Table 4.1). For the RearPosHOT model, this is 80 ms after the airbag deployment and around 40 ms after the time of full airbag inflation. For the RearPosSMED model with one of the most promising energy dissipation characteristics this equals 60 ms and 20 ms, respectively. It is visible at a simulation time of 94 ms and 104 ms that the dummy plunges into the airbag at a lower height with the permanently connected seat compared to the seat with in-crash-movement. At 114 ms, the inflation level of the airbag for the RearPosHOT model is already very low, which is why the dummy crashes through the airbag into the steering wheel hub.

This leads to the conclusion that if the airbag was more tightly filled at the time of interaction, the dummy head might not crash through it that easily. In that case, other force-displacement-characteristics that only lacked of enough distance between dummy forehead and steering wheel might lead to improved energy dissipation. This opens up the possibility of further development potential through an additional delay of the airbag deployment time.

Table 4.1: Kinematic Analysis of Interaction between Dummy and Airbag

Time [ms]	RearPosHOT	RearPosSMED - const-lin 18.75 kN
84 ms		
90 ms		
94 ms		
104 ms		
114 ms		

In Section 3.4.3 a pre-estimation of the energy that was aimed to be dissipated with the force-displacement-characteristic was presented. Comparing the derived energy with the effectively

dissipated energy of the mentioned variants (Table 4.2) shows that this approach can not be applied directly. The theoretical calculation sees the dummy as a mass point, that does not take the head, which keeps moving into account. Nevertheless, the approach can be useful to derive an initial force level for the characteristics.

**Table 4.2:** Comparison of Dissipated Energy

Variant	Energy
Pre-estimation	8.8 kJ
const-lin 18.75 kN	7.5 kJ
const-lin 20.0 kN	8.0 kJ
lin-lin 18.75-22.5 kN	8.25 kJ
lin-const-lin 15.0-32.0 kN/200 mm	9.4 kJ

It is impractical for a vehicle with an occupant seated 400 mm further in the back to expect a five-star rating in an evaluation scheme that was not designed for this new seat position. It is rather useful to aim for a safety margin to the biomechanical limits. Apart from chest and abdomen deflection the inclusion of the energy management resulted in thoroughly improved IARVs. Figure 4.1 confirms this assumption especially when compared to the RearPosHOT model, but also when taking into account the initial situation with the BaselineHOT model. This proves that even with very simple force-displacement-characteristics the energy dissipation between seat and vehicle helps to reduce occupant loads in a backwards moved seat position.

Despite the fact that the variety of functions and variants that were investigated was limited, the analysis of potential of the principle for energy dissipation led to a significant reduction of occupant loads and essential conclusions.



## 5 Conclusion

The investigation of a seat position moved 400 mm to the rear within the vehicle cabin resulted in a decrease in joint probability of injury of almost 27% by a seat with in-crash-movement compared to a seat permanently connected to the vehicle. However, this longitudinal adjustment requires an according interior layout in future HAV concepts. Therefore, the demand for an appropriate adjustment range of the seat system arises for a potential implementation of these concepts.

The idea of using existing restraint systems worked well and prevents that a complete re-development becomes necessary. The analysed adaptations to the model simply require modifications of settings and the integration of the seat belt anchorage into the seat structure. Therefore, the comparability to current conventional vehicles and systems is maintained.

Simulation has shown that small alterations of the seating position can have a great impact on the occupant safety. Rearranging the dummy's arms from the steering wheel onto his thighs led to an increase of the joint probability of injury from 15% to 17%. Combined with the seat position moved backwards, this probability reached a level of 46%. The increase in risk of chest injury was 2.4% and 17.4% respectively. This shows the risk associated with seats positioned significantly rearwards compared to the standard position and underlines the importance of the conducted study.

The investigated operating principle fulfils its initial purpose of dissipating energy in a frontal crash scenario and well reduces the occupant loads. Even though the injury assessment reference value for chest deflection is still increased compared to the BaselineHOT model, an approach for its reduction was found within this thesis. Analysis showed that the idea of the seat energy management combined with the adaptation of airbag deployment time and belt load scaling has huge potential, with a reduction of chest injury risk of 11% compared to the RearPosHOT model. In some criteria this concept resulted in even better values than the simulation of the standard seat position in the vehicle with arms on thighs (BaselineHOT) showed. The overall reached joint probability of injury for the variants listed in Chapter 4 affirms the effectiveness of the principle of energy dissipation. The initially reached probability of 17% (BaselineHOT) jumped up to 46% with moving the seat to a backwards position (RearPosHOT). The variants of the energy dissipating principle then managed to reduce this value again to 19% respectively 20%.

For the optimal utilisation of the approach, the interaction of the conducted adaptations made to the sled model with a longitudinally adjusted seat is of great value. Considering the limited amount of analysed force-displacement-characteristics that already led to convincing results, it will be interesting to see the further improvement that can be reached by re-adaptation and optimization of parameters.



## 6 Summary

The aim of this thesis was the analysis of potential of a new type of operating principle to reduce occupant loads in highly automated vehicles. Therefore, the standard seating position adjusted 400 mm to the rear was chosen to be investigated. The principle's mode of operation was a seat with crash-in-movement to dissipate crash energy that burdens the occupant.

Based on a finite element model of a vehicle in an oblique barrier test, an adapted model was obtained. The scenario of a simplified sled model in the load case of a frontal NCAP test was reached through separate consideration of the two submodels full vehicle model and seat model.

The seat model, on the one hand, needed alteration with regard to its movement within the vehicle cabin. The seatbelt anchorage was integrated into the seat back, transforming the standard seat into a belt integral seat. Furthermore, a headrest was added to the seat in order to obtain the possibility to use the simulation model for rear impact research. After an increase of stiffness through addition of a supporting frame as well as some parts made of high-tensile steel, the seat was tested for compliance with the relevant legislation from NHTSA.

On the other hand, the full vehicle model was modified and modelled in the load case of a rigid wall test. It was then reduced and combined with the seat model to result in a simplified sled model. Subsequently, adaptations to longitudinally adjust the seat and alter the position of the dummy's hands were conducted. For the seat to be able to move in a pre-defined way the connections between the seat and the relevant body-in-white parts were changed. This resulted in the simplified model with energy dissipation which was used to analyse the reduction of occupant loads.

Therefore, different force-displacement-characteristics were implemented into the energy dissipating principle. After simulation of the according crash test procedure, the results were evaluated. For the assessment process, part of NHTSA's star rating system was used. Further adaptations led to optimised simulation results that are presented and discussed within the thesis.

The analysis of the operating principle of a seat with in-crash-movement with the aim to reduce the occupant loads led to a reduction of the joint probability of injury of almost 27%. This concludes the great potential of this new type of energy management system for improved occupant protection.





## 7 Outlook

In the future, HAV concepts will be further developed and therefore, more knowledge about the adjustment range of seats might be available. Thereby, the limited examination of the 400 mm adjustment of the seat can be varied and adapted accordingly.

With the introduction of HAVs to the roads the severity of accidents will decrease which makes a development of injury risk curves for lower AIS levels and their integration into the NCAP rating scheme necessary.

Along with the implementation of automated technologies come the new seating concepts described in Chapter 1. The next step after investigation of the longitudinally adjusted seat could be the combination with a reclined backrest. This position will need further research also considering the quite likely occurring effect of submarining.

Another scope of application resulting in the introduction of HAVs is the backwards facing seating concept. The load case of this position equals a rear impact crash procedure in a forward facing seat. This scenario was always considered during the development process of the simplified sled model within this thesis which is why, for instance, headrests were added to the seat.

For the principle of energy dissipation between seat and vehicle, further improvement can be reached in the sense of an optimization and re-adaptation of the parameters in combination with new variants of the force-displacement-characteristic. The interaction of the adaptations seem quite promising to further reduce the occupant loads.

In addition, the research should be extended and simulations redone with different anthropometrics like the 5th percentile female dummy as well as human body models. Variable adaptation based on specific initial conditions, for example the occupant model or seat displacement, might also be a possible field of further study.



## Bibliography

- Development & Validation of a Finite Element Model for the 2012 Toyota Camry Passenger Sedan*, 2016. URL <https://www.ccsa.gmu.edu/wp-content/uploads/2016/06/2012-toyota-camry-tech-summary-v5.pdf>.
- AAAM. Abbreviated injury scale, 2015. URL <https://www.aaam.org/abbreviated-injury-scale-ais/>.
- H.-D. Adomeit, T. Just, and J. Adomeit. Das hohe schutzniveau eines pre-crash rückhaltesystems und seine breitbandige wirkung, 2009.
- CARHS, editor. *Safety Companion 2020*. 2020.
- D. Cichos, M. Otto, S. Zölsch S. Clausnitzer, D. Vetter, and G. Pfeiffer. Crash-analyse: Beschreibung der kriterien: Version 2.4, 2015. URL [www.mdvfs.de](http://www.mdvfs.de).
- Daimler AG. Conditionally automated driving: the s-class leads the field, 2020. URL <https://media.daimler.com/marsMediaSite/en/instance/ko.xhtml?oid=47164442>.
- R. Eppinger, E. Sun, F. Bandak, M. Haffner, N. Khaewpong, M. Maltese, S. Kuppa, T. Nguyen, E. Takhounts, R. Tannous, A. Zhang, and R. Saul. Development of improved injury criteria for the assessment of advanced automotive restraint systems - ii. *nhtsa*, 1999.
- eurostat. Road accident fatalities: statistics by type of vehicle, 2020. URL [https://ec.europa.eu/eurostat/statistics-explained/index.php/Road\\_accident\\_fatalities\\_-\\_statistics\\_by\\_type\\_of\\_vehicle](https://ec.europa.eu/eurostat/statistics-explained/index.php/Road_accident_fatalities_-_statistics_by_type_of_vehicle).
- A. Filatov, J. M. Scanlon, A. Bruno, S. S. K. Danthurthi, and J. Fisher. Effects of innovation in automated vehicles on occupant compartment designs, evaluation, and safety: A review of public marketing, literature, and standards, 2019.
- L. F. Gabler, J. R. Crandall, and M. B. Panzer. Development of a metric for predicting brain strain responses using head kinematics. *Annals of Biomedical Engineering*, 46(7):972–985, 2018. ISSN 1573-9686. doi: 10.1007/s10439-018-2015-9. URL <https://doi.org/10.1007/s10439-018-2015-9>.
- T. A. Gennarelli and E. Wodzin. Ais 2005: a contemporary injury scale. *Injury*, 37(12):1083–1091, 2006. ISSN 0020-1383. doi: 10.1016/j.injury.2006.07.009.
- E. Haug, H.-Y. Choi, and Robin, S. Beaugonin, M. Human models for crash and impact simulation. 12:231–452, 2004. doi: 10.1016/S1570-8659(03)12004-2.
- L. Hershman. The u.s. new car assessment program (ncap): Past, present and future. (390), 2001.

- K. Hessenberger. Strength analysis of seat belt anchorage according to ece r14 and fmvss. In 4th European LS-DYNA Users Conference, editor, *Crash/Automotive Applications II*, 2003.
- A. Huf and S. Sengottu Velavan. Development of occupant restraint systems for future seating positions in fully or semi-autonomous vehicles. In Fraunhofer ICT, editor, *Airbag 2018*. 2018.
- Humanetics Group. Anthropomorphic test devices (atd), 2020. URL <https://humanetics.humaneticsgroup.com/products/anthropomorphic-test-devices>.
- IIHS. Rcar-iiwpg seat/head restraint evaluation protocol, 2008. URL [https://www.iihs.org/media/84f361de-a61a-4614-985c-c420c1d20634/1386701948/Ratings/Protocols/current/rcar\\_iiwpg\\_protocol.pdf](https://www.iihs.org/media/84f361de-a61a-4614-985c-c420c1d20634/1386701948/Ratings/Protocols/current/rcar_iiwpg_protocol.pdf).
- J. Iraeus and M. Lindquist. Development and validation of a generic finite element vehicle buck model for the analysis of driver rib fractures in real life nearside oblique frontal crashes. In *Accident Analysis & Prevention 95*, volume 95, pages 42–56. 2016. doi: 10.1016/j.aap.2016.06.020.
- H. P. Ive, D. Sirkin, D. Miller, J. Li, and W. Ju. "don't make me turn this seat around!" driver and passenger activities and positions in autonomous cars, 2015. URL [file:///M:/VSI-P/050\\_Theses/20\\_MSC\\_Heider/TEC/050\\_Media/050\\_Papers/Driver%20and%20Passenger%20Activities%20and%20Positions%20in%20Autonomous%20Cars.pdf](file:///M:/VSI-P/050_Theses/20_MSC_Heider/TEC/050_Media/050_Papers/Driver%20and%20Passenger%20Activities%20and%20Positions%20in%20Autonomous%20Cars.pdf).
- S. Jorlöv, K. Bohman, and A. Larsson. Seating positions and activities in highly automated cars – a qualitative study of future automated driving scenarios. In International Research Council on the Biomechanics of Injury, editor, *2017 IRCOBI Conference Proceedings*, IRCOBI Conference Proceedings. IRCOBI, 2017. ISBN 2235-3151.
- T. Keon. Alternative approaches to occupant response evaluation in frontal impact crash testing, 2016. URL <https://www.nhtsa.gov/sites/nhtsa.dot.gov/files/keon04-06-2016-rev.pdf>.
- M. Kleinberger, E. Sun, R. Eppinger, S. Kuppa, and R. Saul. Development of improved injury criteria for the assessment of advanced automotive restraint systems, 1998.
- F. Laakmann, L. Zink, and M. Seyffert. New interior concepts for occupant protection in highly automated vehicles. *ATZ worldwide*, 121(4):48–53, 2019. ISSN 2192-9076. doi: 10.1007/s38311-019-0012-8.
- T. R. Laituri, S. Henry, K. Pline, G. Li, M. Frankstein, and P. Weerappuli. New risk curves for nhtsa's brain injury criterion (bric): Derivations and assessments. *Stapp Car Crash Journal*, 60: 1–64, 2016. ISSN 1532-8546.
- P. Luttenberger, L. Schlacher, M. Schachner, and W. Sinz. Mutant - analysis tool - group assessment report, 2019. URL <https://gitlab.com/VSI-TUGraz/mutant>.
- T. Matsushita, H. Saito, C. Sunnevang, M. Östling, A. Vishwanatha, and A. Tabhane, editors. *Evaluation of the protective performance of a novel restraint system for highly automated vehicles (HAV)*, 26th ESV Conference Proceedings, 2019. URL <https://www-esv.nhtsa.dot.gov/Proceedings/26/26ESV-000321.pdf>.

- H. Morvan, K. H. Tan, F. Robache, M. P. Pacaux, and P. Drazetic. Pre-crash investigation using a driving simulator and numerical analyses to determine the influence of the arms positions. *International Journal of Crashworthiness*, 12(5):531–539, 2007. ISSN 13588265. doi: 10.1080/13588260701483862.
- K. Mroz, M. Östling, R. Richardson, J. Kerrigan, J. Forman, B. Gepner, N. Lubbe, and B. Pipkorn. Effect of seat and seat belt characteristics on the lumbar spine and pelvis loading of the safer human body model in reclined postures. In International Research Council on the Biomechanics of Injury, editor, *2018 IRCOBI Conference Proceedings*, IRCOBI Conference Proceedings. IRCOBI, 2018. ISBN 2235-3151.
- National Center for Statistics and Analysis. 2018 fatal motor vehicle crashes: Overview. traffic safety facts research note., 2019. URL <https://crashstats.nhtsa.dot.gov/Api/Public/ViewPublication/812826>.
- NHTSA. Laboratory test procedure for fmvss 210: Seat belt assembly anchorages, 1994. URL <https://www.law.cornell.edu/cfr/text/49/571.210>.
- NHTSA. Nhtsa, 2012. URL [file:///M:/VSI-P/050\\_Theses/20\\_MSC\\_Heider/TEC/050\\_Media/040\\_0ther/NHTSA\\_Test\\_Reports/NHTSA%20NVS%20%20%20Vehicle%20Crash%20Test%20Database%20-%20Test%20Detail%20Information.html](file:///M:/VSI-P/050_Theses/20_MSC_Heider/TEC/050_Media/040_0ther/NHTSA_Test_Reports/NHTSA%20NVS%20%20%20Vehicle%20Crash%20Test%20Database%20-%20Test%20Detail%20Information.html).
- NHTSA. Nhtsa, 2014a. URL <https://www-nrd.nhtsa.dot.gov/database/VSR/veh/TestDetail.aspx?LJC=8789>.
- NHTSA. Moving barrier to vehicle crash test in support of nhtsa’s frontal oblique offset program: Research moving deformable barrier into left front of a 2014 honda accord: Final report, 2014b.
- NHTSA. New car assessment program: Request for comments, 2015.
- NHTSA. Crash simulation vehicle models, 2018. URL <https://www.nhtsa.gov/crash-simulation-vehicle-models>.
- NHTSA. Automated vehicles for safety, 2020a. URL <https://www.nhtsa.gov/technology-innovation/automated-vehicles>.
- NHTSA. Nhtsa, 2020b. URL <https://www.nhtsa.gov>.
- M. Östling and A. Larsson. Occupant activities and sitting positions in automated vehicles in china and sweden. In *Proceedings of 26th International Technical Conference on the Enhanced Safety of Vehicles*. 2019.
- M. B. Panzer, J. S. Giudice, and D. Parent. Thor 50th male finite element model user manual: Model version 2.1 for ls-dyna, 2015.
- K. Rawska, B. Gepner, D. Moreau, and J. R. Kerrigan. Submarining sensitivity across varied seat configurations in autonomous driving system environment. *Traffic Injury Prevention*, pages 1–6, 2020. ISSN 1538-957X. doi: 10.1080/15389588.2020.1791324.

- M. P. Reed, S. M. Ebert, M. L. H. Jones, and J. J. Hallman. Prevalence of non-nominal seat positions and postures among front-seat passengers. *Traffic Injury Prevention*, pages 1–6, 2020. ISSN 1538-957X. doi: 10.1080/15389588.2020.1793971.
- SAE International. Taxonomy and definitions for terms related to driving automation systems for on-road motor vehicles, 2014. URL [https://saemobilus.sae.org/content/j3016\\_201609/](https://saemobilus.sae.org/content/j3016_201609/).
- M. Schachner, J. Micorek, P. Luttenberger, R. Greimel, and C. Klug. Dynasaur, 2018. URL <https://gitlab.com/VSI-TUGraz/Dynasaur>.
- H. Singh, V. Ganesan, J. Davies, M. Paramasuwom, and G. Lorenz. Vehicle interior and restraints modeling development of full vehicle finite element model including vehicle interior and occupant restraints systems for occupant safety analysis using thor dummies: Report no. dot hs 812 545, 2018.
- Statistik Austria. Straßenverkehrsunfälle jahresergebnisse 2018: Straßenverkehrsunfälle mit personenschaden, 2019.
- E. G. Takhounts, M. J. Craig, K. Moorhouse, J. McFadden, and V. Hasija. Development of brain injury criteria (bric). *Stapp Car Crash Journal*, 57:243–266, 2013. ISSN 1532-8546.
- Torque. Volkswagen i.d. buzz concept is the world’s first fully autonomous mpv, 2017. URL <https://www.torque.com.sg/news/volkswagen-d-buzz-concept-worlds-first-fully-autonomous-mpv/>.
- U.S. Department of Transportation. Consumer information; new car assessment program; notice, 2008. URL <https://www.govinfo.gov/content/pkg/FR-2008-07-11/pdf/E8-15620.pdf>.
- U.S. Department of Transportation. New car assessment program: Notice: Request for comments, 2015. URL <https://www.govinfo.gov/content/pkg/FR-2015-12-16/pdf/2015-31323.pdf>.
- Volkswagen Group. Individual mobility redefined: Autonomous driving at the touch of a button, 2017. URL [https://www.volkswagenag.com/en/news/2017/03/Autonomous\\_driving.html](https://www.volkswagenag.com/en/news/2017/03/Autonomous_driving.html).
- Volvo. 360c: A new way to travel, 2018. URL <https://www.volvocars.com/intl/cars/concepts/360c?redirect=true>.
- Volvo Car Group. Volvo cars ceo urges governments and car industry to share safety-related traffic data, 2017. URL <https://www.media.volvocars.com/global/en-gb/media/pressreleases/207164/volvo-cars-ceo-urges-governments-and-car-industry-to-share-safety-related-traffic-data>.

## A Appendix - List of Submodels

- Barrier,
- Driver and Passenger Dummy,
- Driver and Passenger Airbag,
- Curtain Airbag (Driver),
- Front and Rear Suspension,
- Body in White,
- Front and Rear Door,
- Powertrain,
- Battery,
- Radiator,
- Wheels,
- Fenders,
- Front and Rear Sub Frame,
- Front and Rear Fascia,
- Instrument Panel, Dashboard, Washer Bottle and Carpets,
- Front Bumper,
- Hood,
- Rear Trunk,
- Steering Column and Steering Wheel,
- Seats and Seatbelts,
- Materials,
- Contacts, Time History, Connections, Control Cards, Accelerometer and Mass.





## B Appendix - evaluated Diagrams

### Head Acceleration

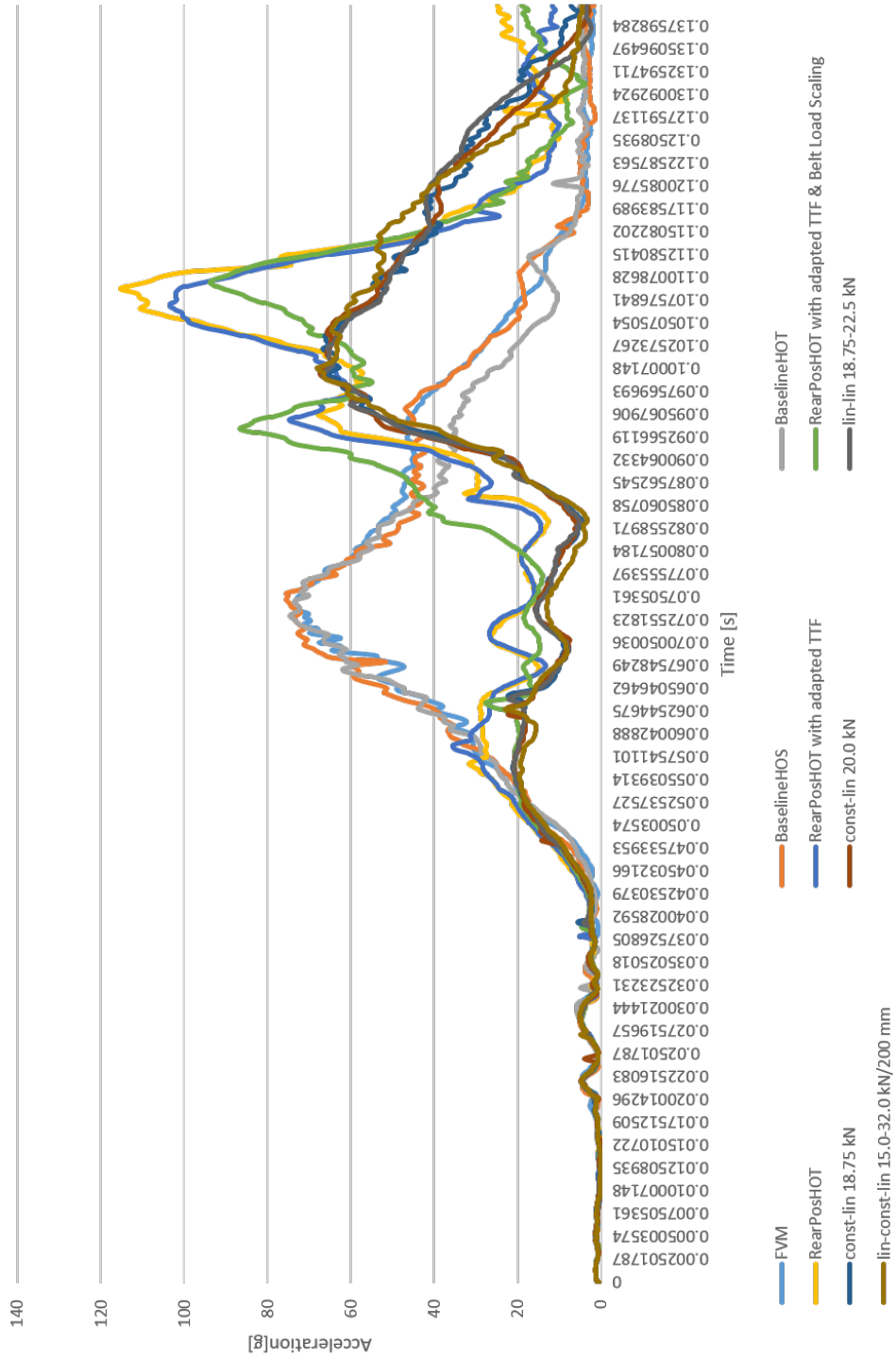


Figure B.1: Comparison of the Head Acceleration

# Neck Axial Force

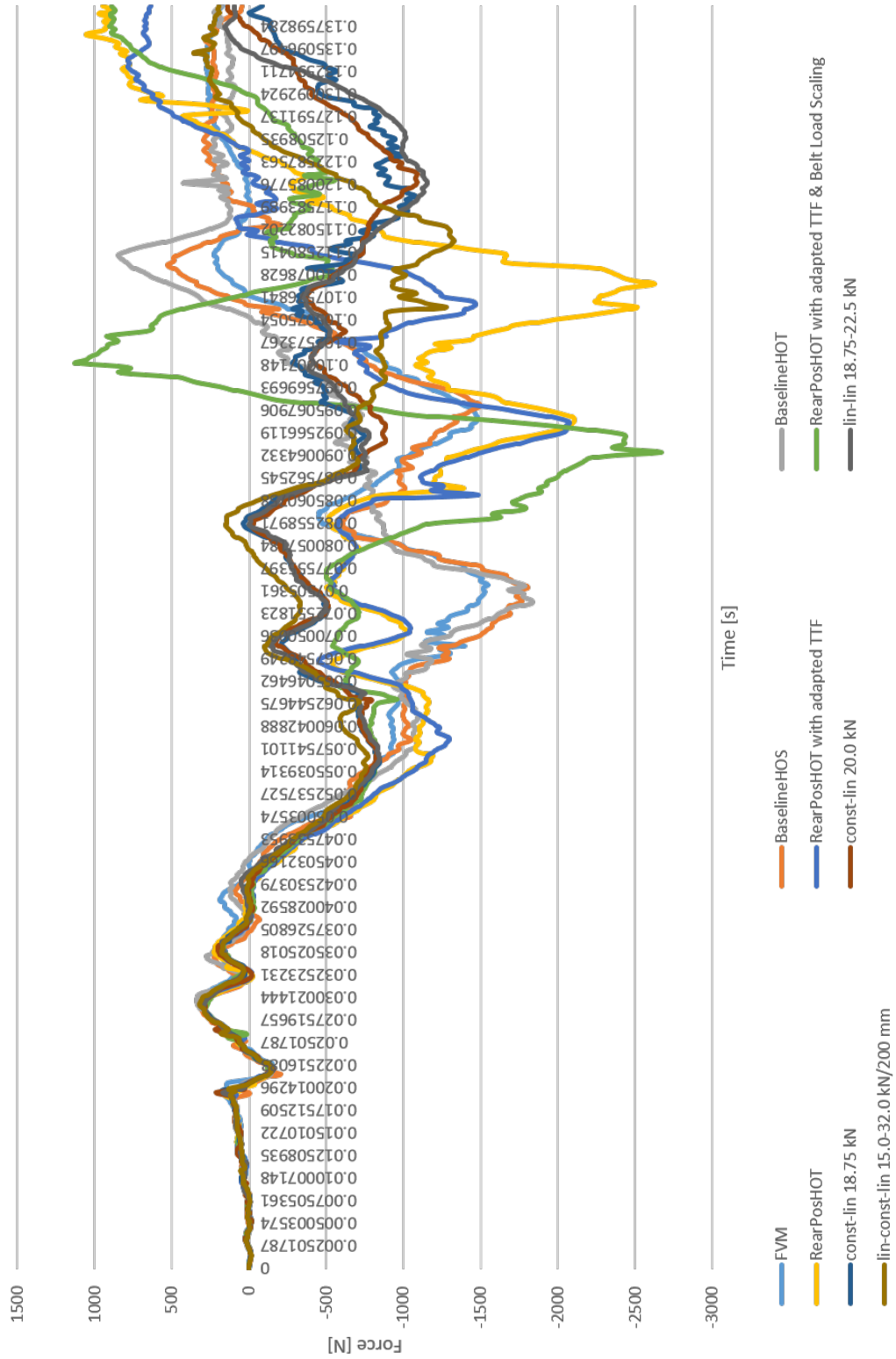


Figure B.2: Comparison of the Neck Axial Force

# Neck Shear Force

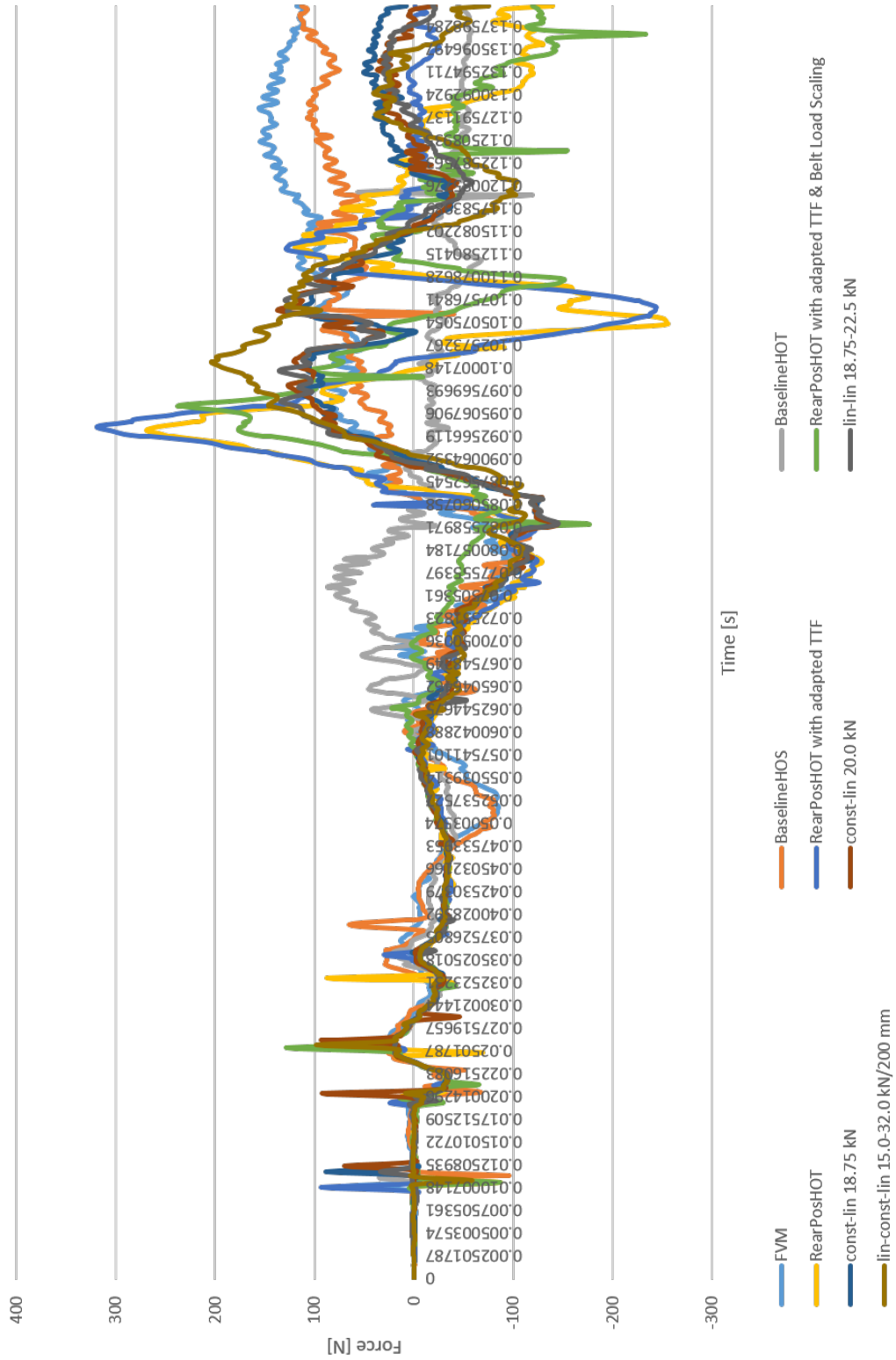


Figure B.3: Comparison of the Neck Shear Force

# Neck Moment

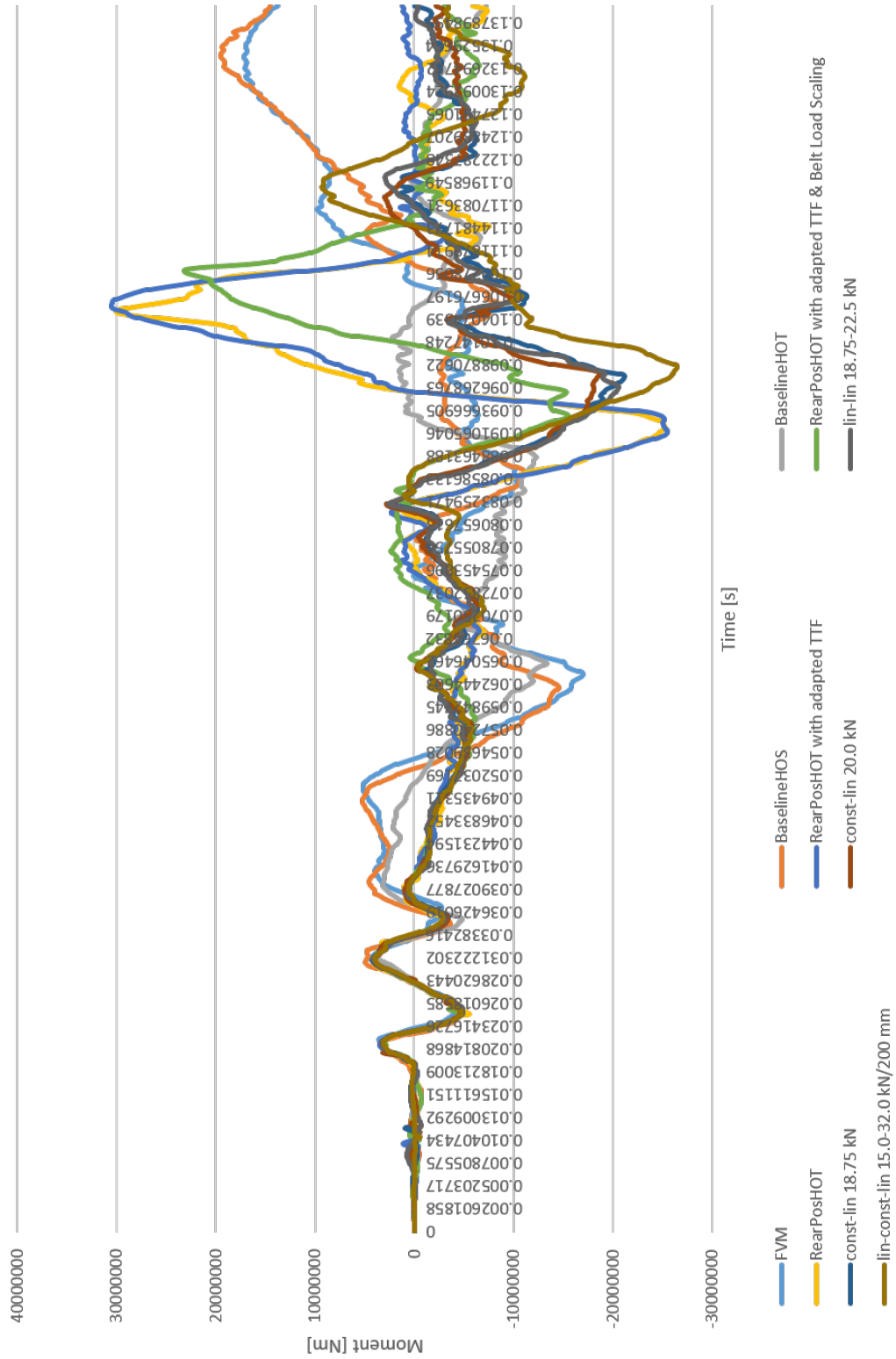


Figure B.4: Comparison of the Neck Moment

# Femur Compression Force Left

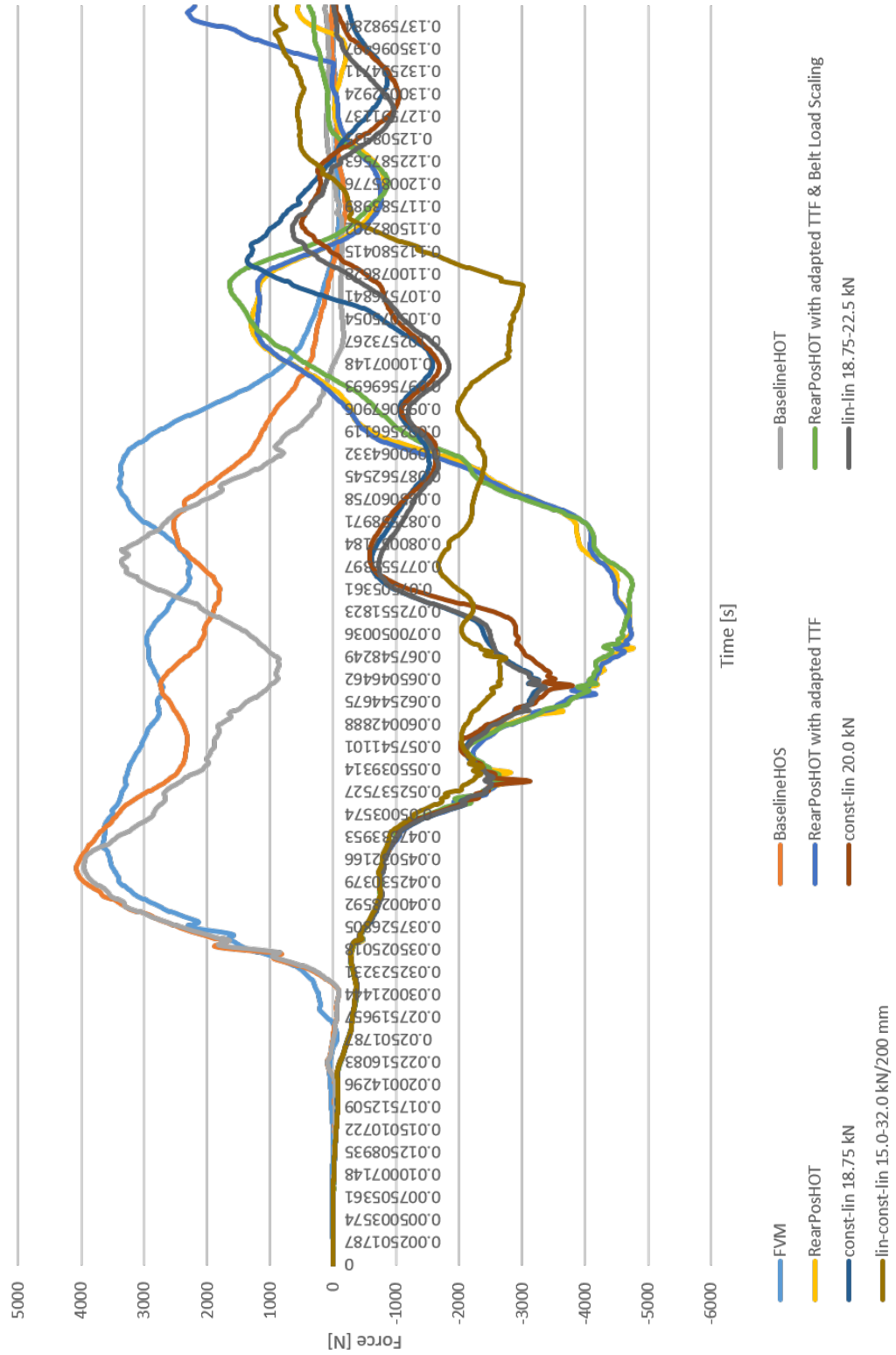


Figure B.5: Comparison of the Femur Compression Force Left

# Femur Compression Force Right

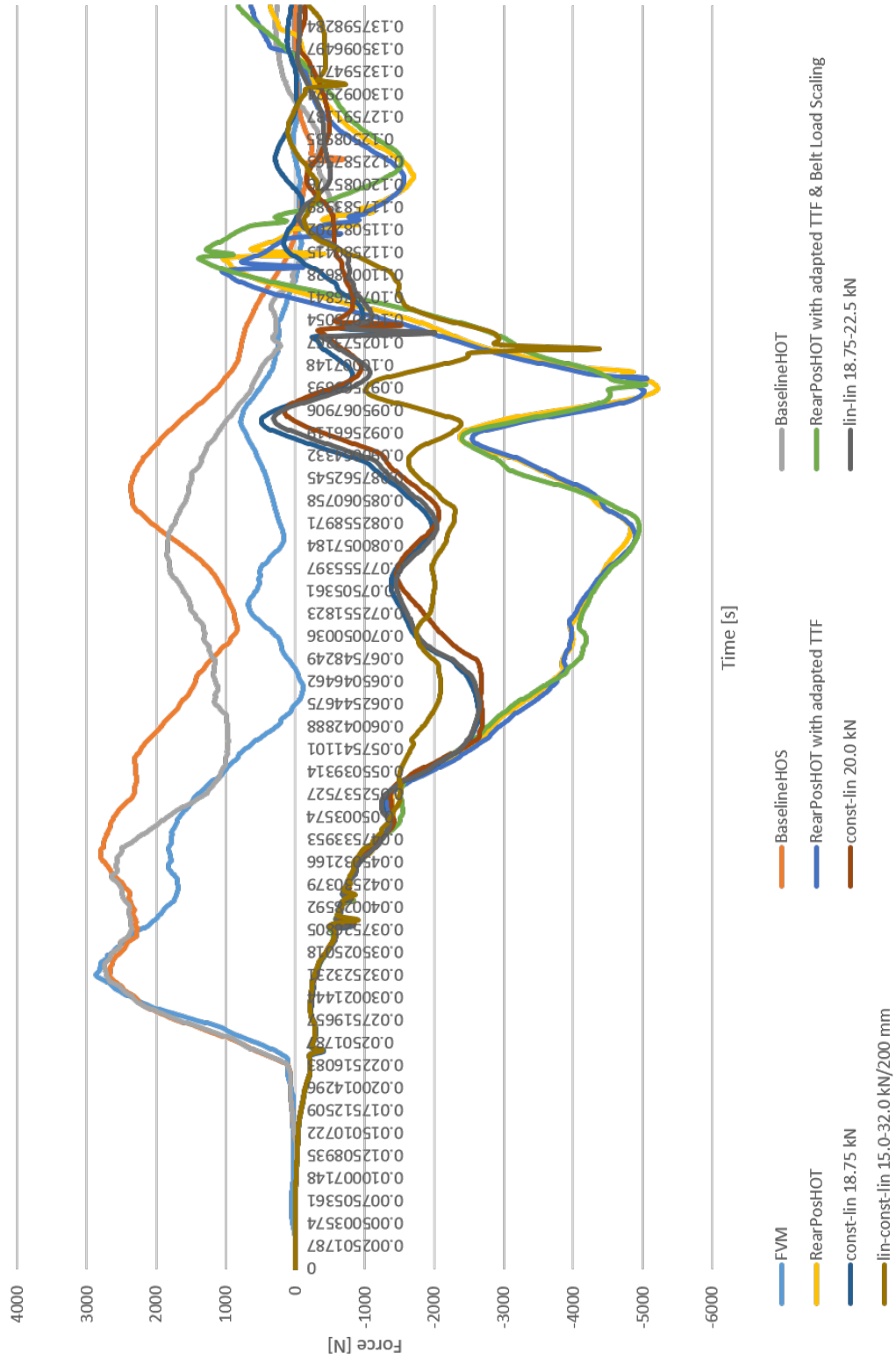


Figure B.6: Comparison of the Femur Compression Force Right

# Chest Deflection Upper Left Load Cell

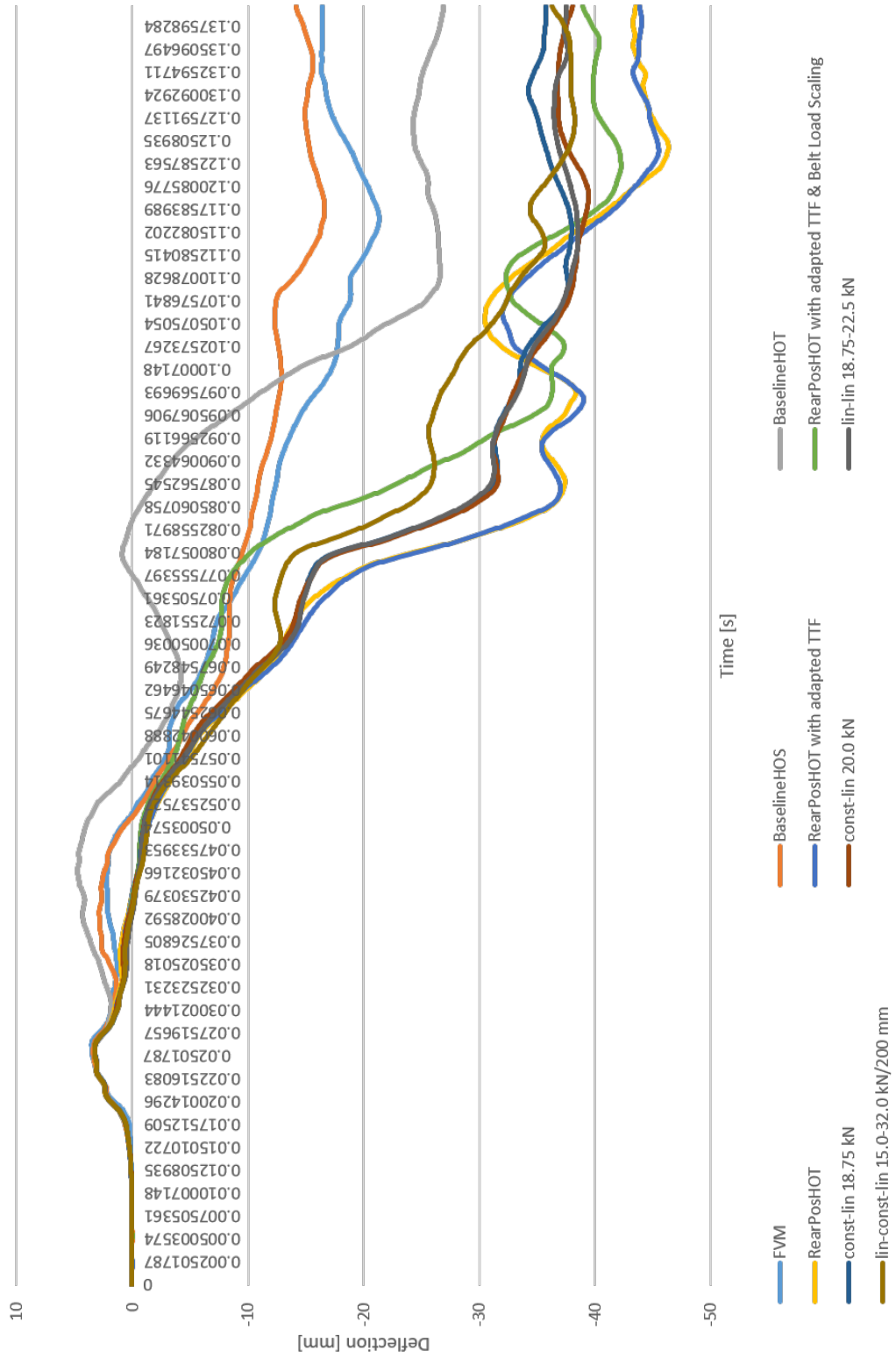


Figure B.7: Comparison of the Chest Deflection UL

# Chest Deflection Upper Right Load Cell

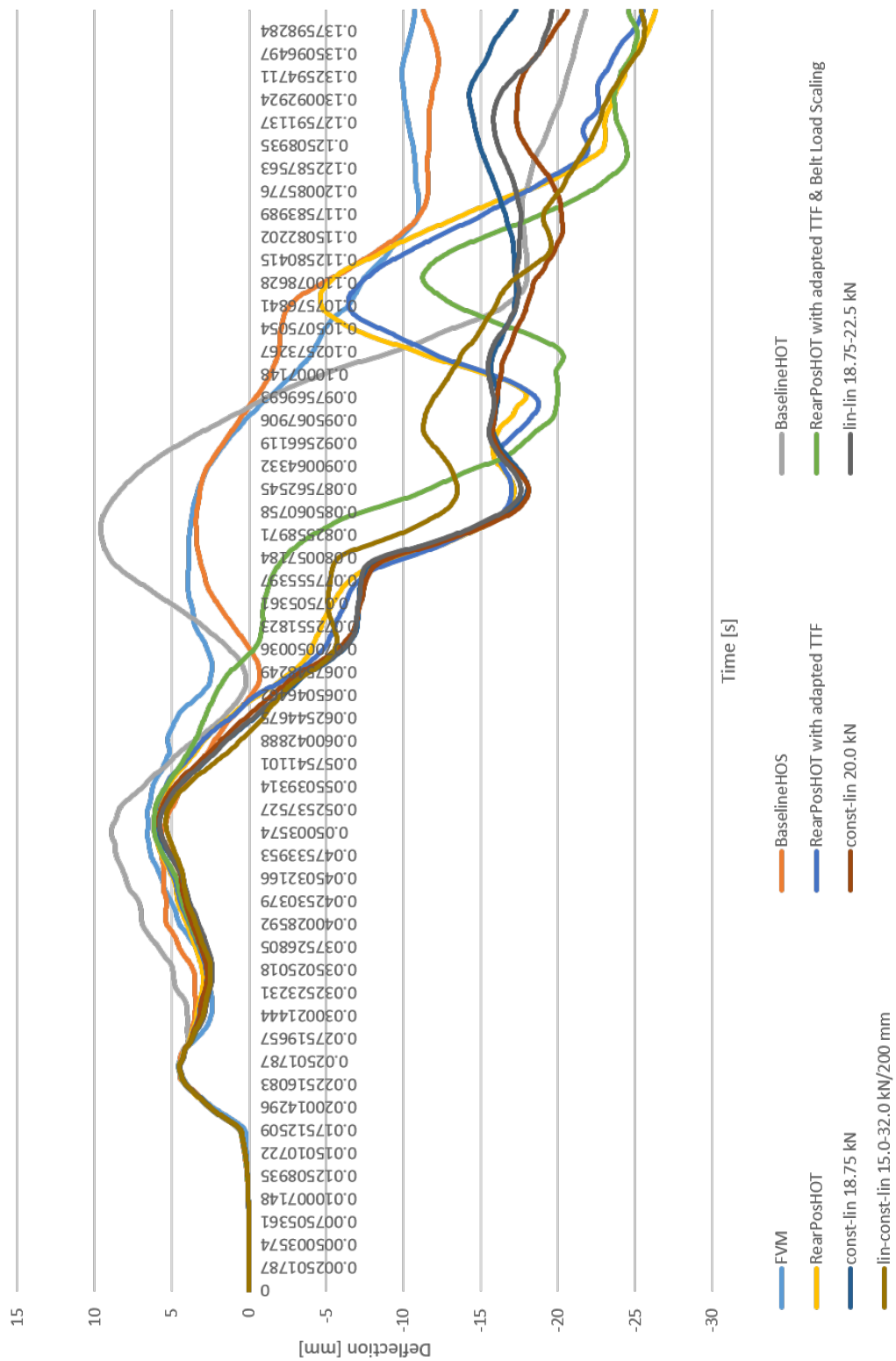


Figure B.8: Comparison of the Chest Deflection UR



# Chest Deflection Lower Right Load Cell

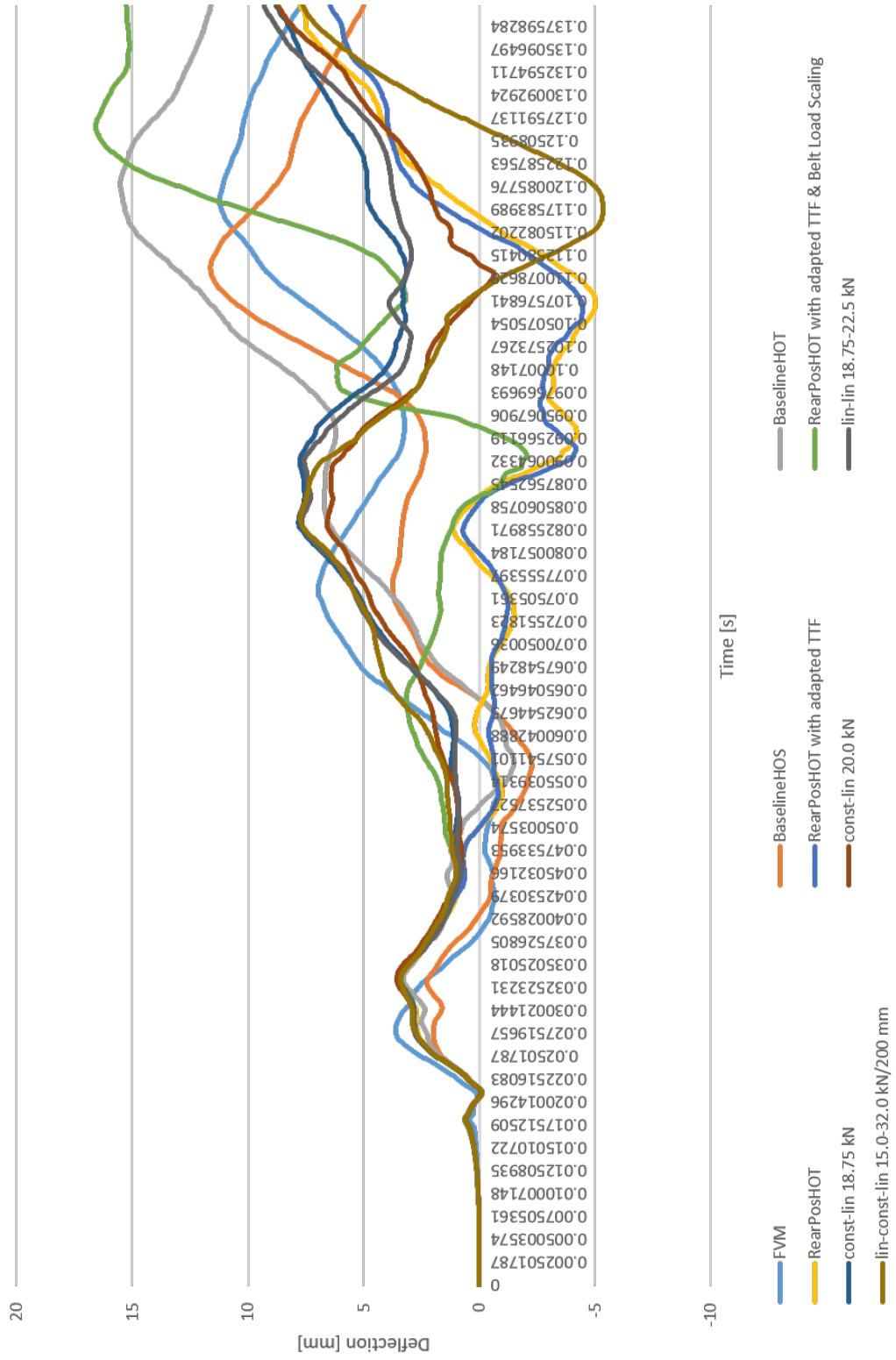


Figure B.9: Comparison of the Chest Deflection LR

# Chest Deflection Lower Left Load Cell

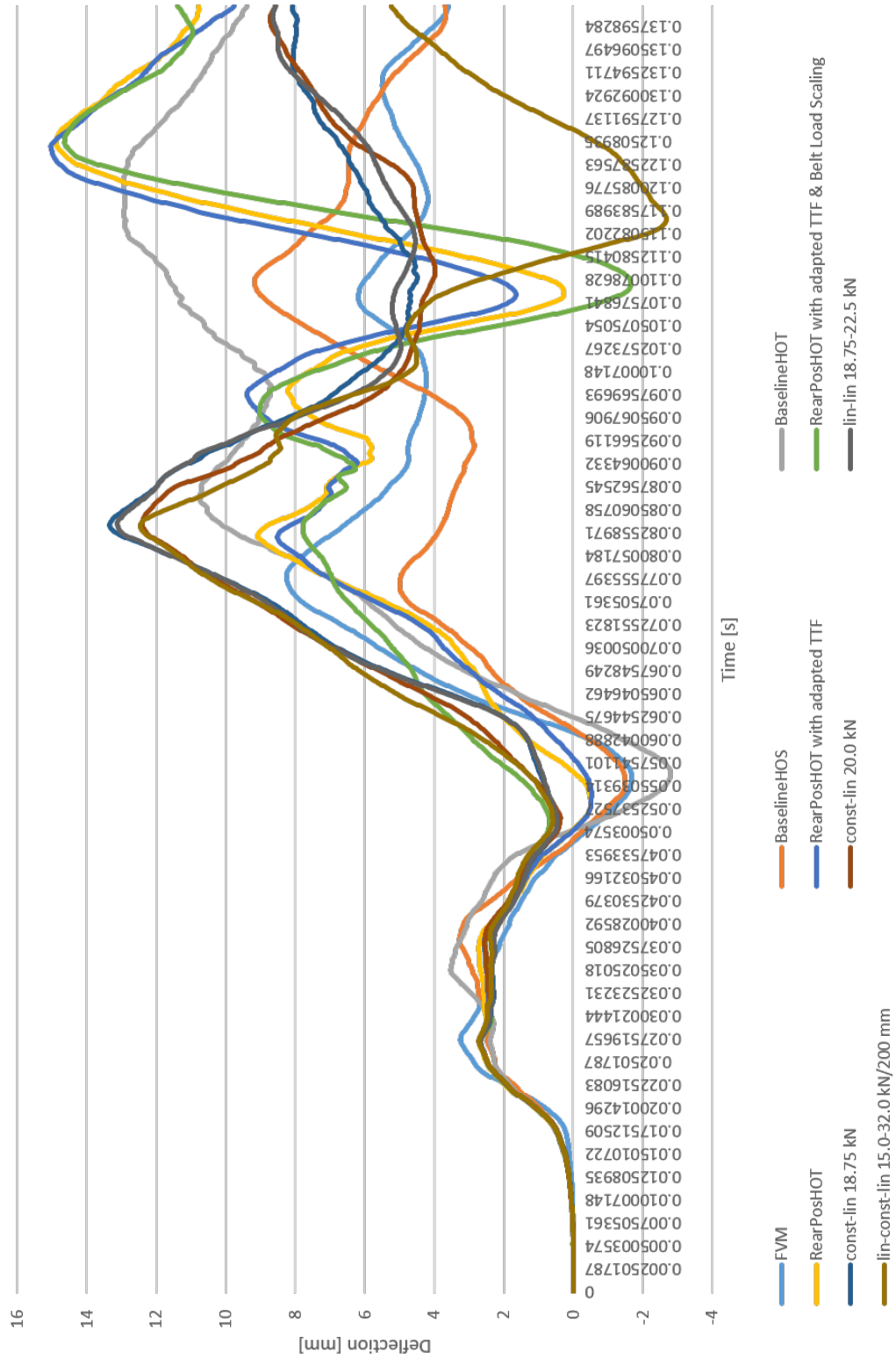


Figure B.10: Comparison of the Chest Deflection LL

# Abdomen Deflection Left

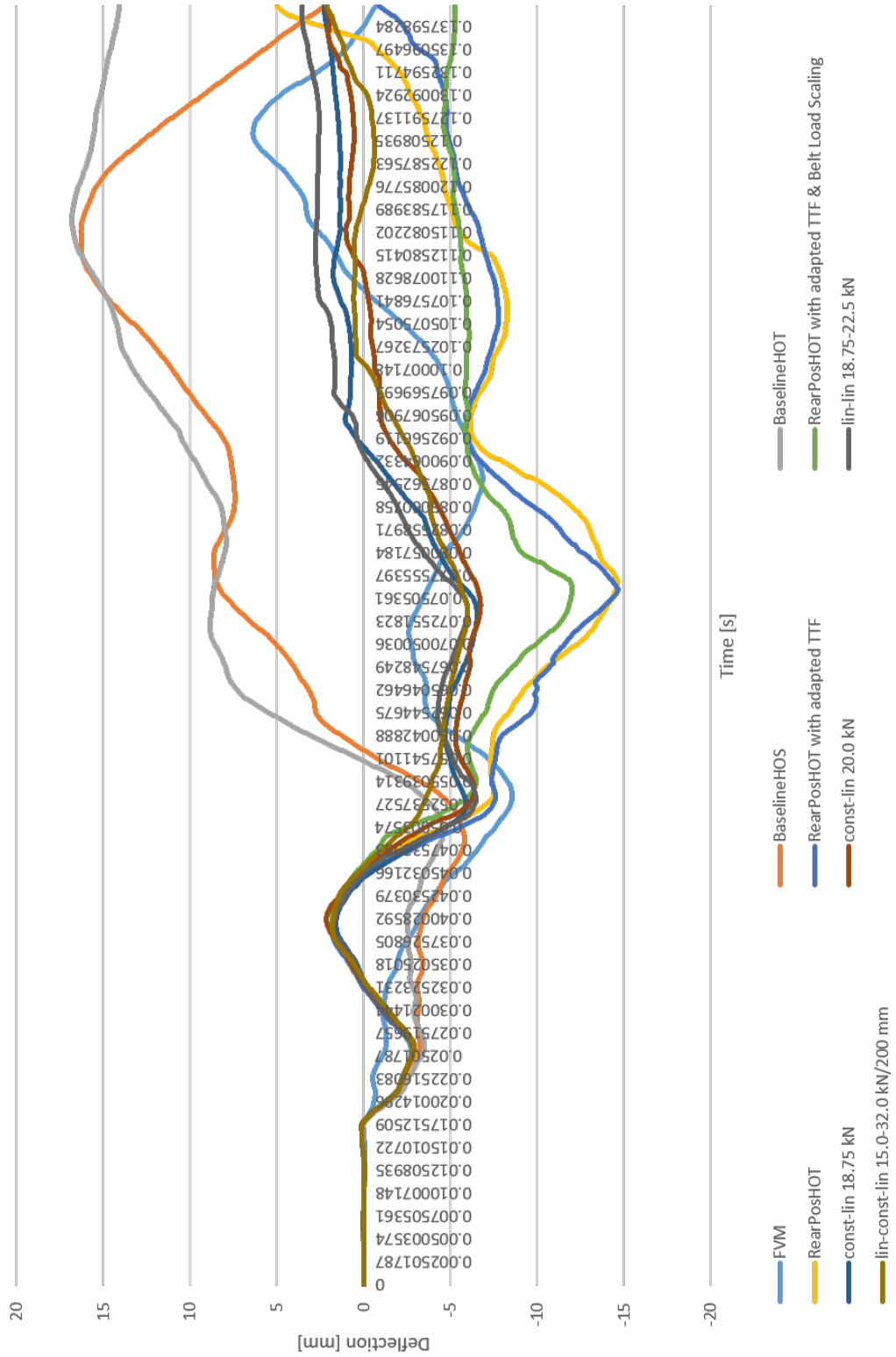


Figure B.11: Comparison of the Abdomen Deflection Left

# Abdomen Deflection Right

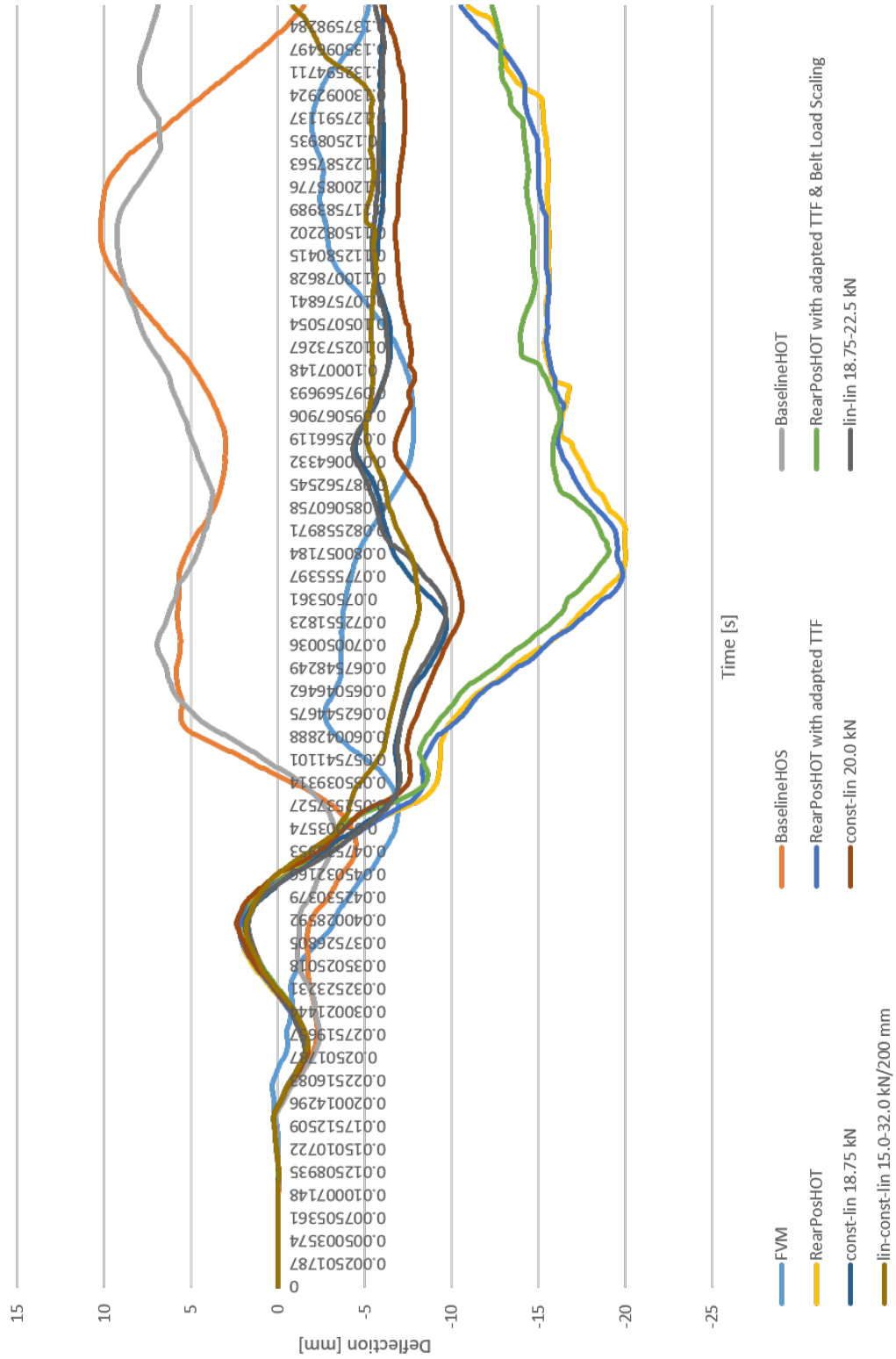


Figure B.12: Comparison of the Abdomen Deflection Right

# Shoulder Belt Force

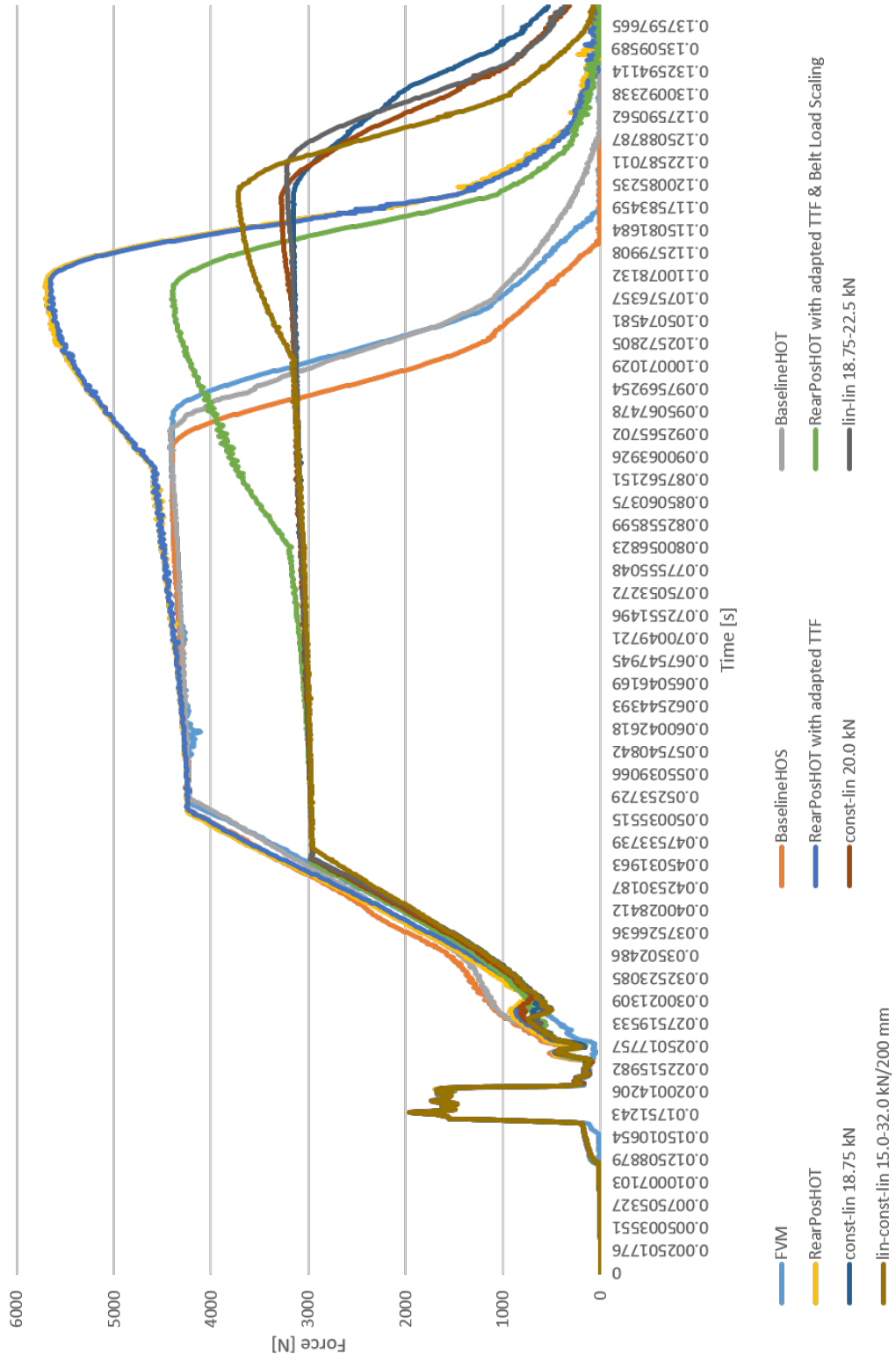


Figure B.13: Comparison of the Shoulder Belt Force

# Pelvis Belt Force

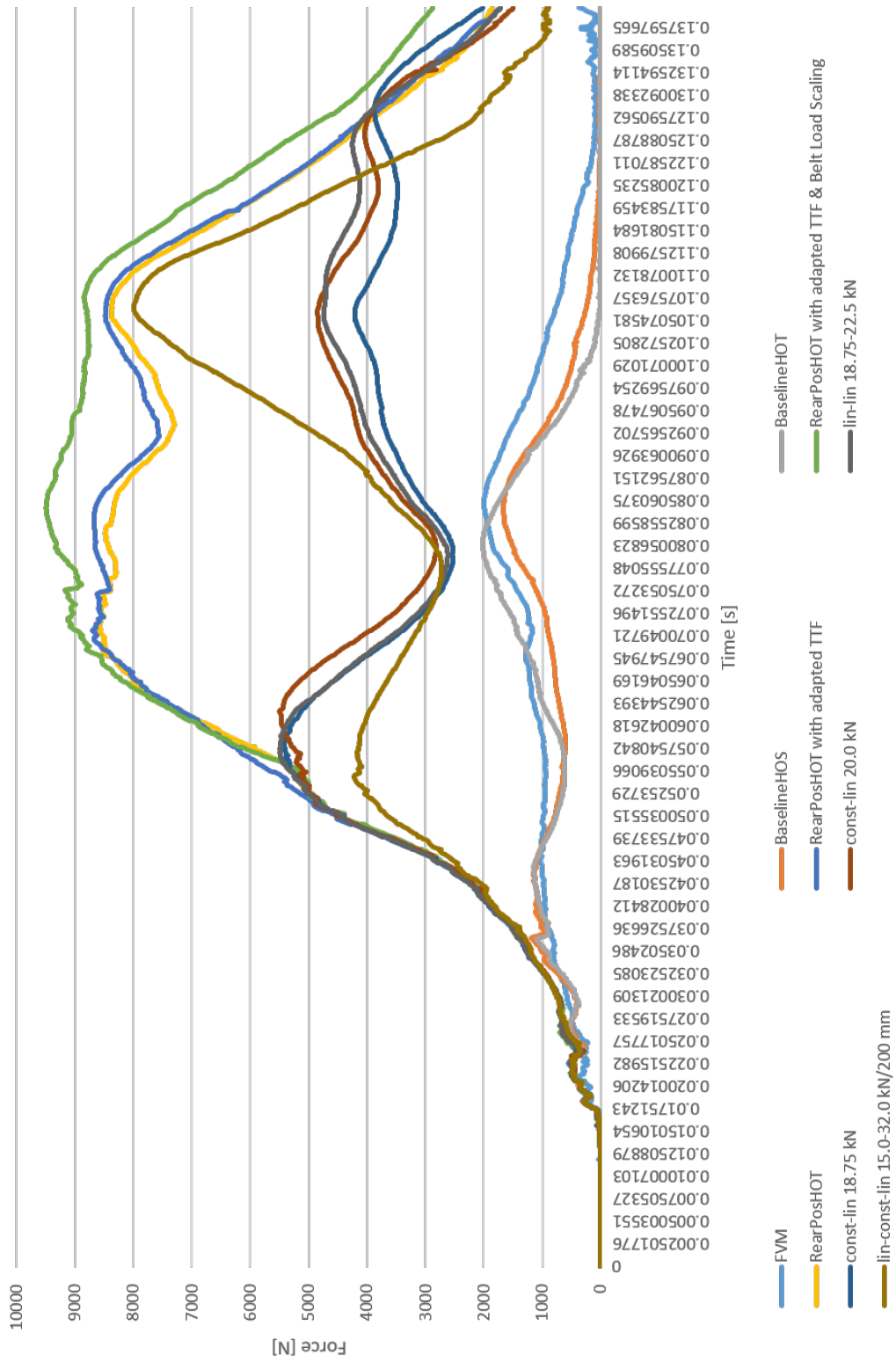


Figure B.14: Comparison of the Pelvis Belt Force

# C Appendix - Simplified Sled Model

## Rating Sheet for various Airbag Deployment Times

RearPosHOT					
TTF = 10 ms	TTF = 20 ms	TTF = 30 ms	TTF = 40 ms	TTF = 50 ms	TTF = 60 ms
0.140	0.140	0.140	0.140	0.140	0.140

Region	Criterion	Limit						
Head	HIC <sub>15</sub>	700	1021	920	942	954	1073	1250
	a3ms	80	108.6	100.6	100.1	100.2	103.9	109.8
	BRIC	1.05	0.67	0.68	0.64	0.58	0.55	0.57
	uBRIC	1	0.24	0.25	0.23	0.21	0.19	0.21
Neck	Nij	0.85	0.54	0.52	0.56	0.53	0.54	0.53
	F <sub>z,tension</sub>	3300	1054.1	1017.8	786.3	880.1	1738.8	2432.7
	F <sub>z,compr.</sub>	-4000	-2630.8	-1981.4	-2076.0	-1809.3	-2016.3	-1841.4
Chest	Chest Defl.	52.3	46.4	43.6	45.5	46.3	47.1	48.1
	Abdomen Defl.	88.6	20.0	19.3	19.9	19.4	19.3	19.3
Lwr Ex	F <sub>Femur</sub>	8588	1308.7	1412.5	2311.2	1366.6	1487.0	1390.1
Head-SW	min. distance	> 0 mm	52.4	62.9	68.5	74.4	84.6	85.4

Results - U.S. NCAP Rating							
P <sub>Head</sub>		23.95%	19.79%	20.70%	21.19%	26.07%	33.20%
P <sub>Chest</sub>		20.65%	16.80%	19.42%	20.52%	21.80%	23.35%
P <sub>Femur</sub>		0.60%	0.63%	1.00%	0.62%	0.65%	0.62%
P <sub>Neck</sub>		10.30%	10.02%	10.65%	10.06%	10.34%	10.13%
P <sub>Joint</sub>		46.20%	40.33%	43.48%	44.01%	48.50%	54.27%
Rel. Risk		3.0797	2.6888	2.8984	2.9340	3.2335	3.6182
Stars		★	★	★	★	★	★

Figure C.1: RearPosHOT Rating Sheet - Variation of Airbag Deployment Time





## D Appendix - Diagrams for the Seat Belt Load Limiter Curve

Unscaled

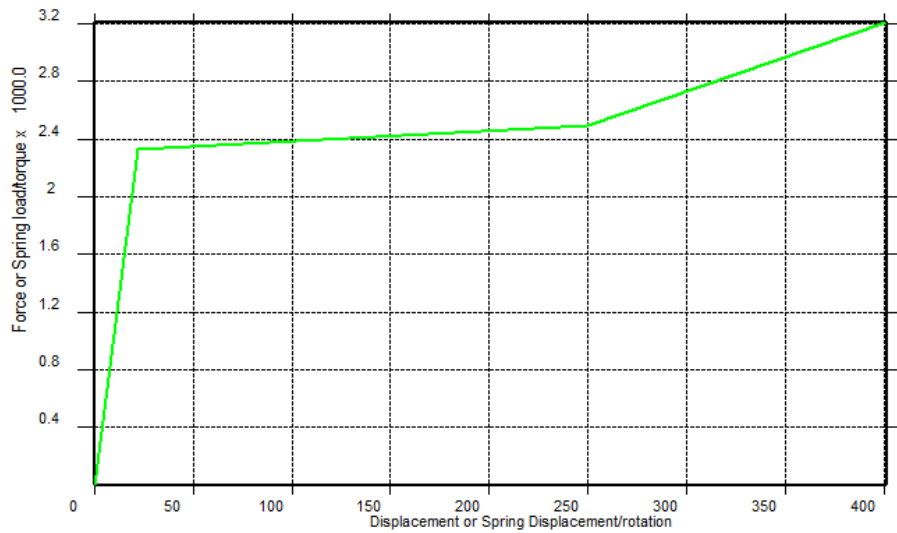


Figure D.1: Unscaled Seat Belt Load Limiter Curve

Scaled

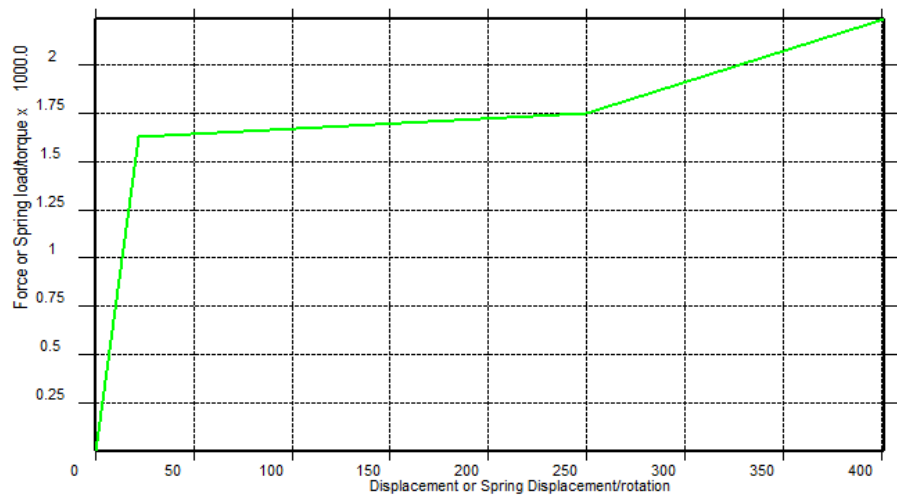


Figure D.2: Scaled Seat Belt Load Limiter Curve - Scaling Factor 0.7



# E Appendix - Full Vehicle Model

## Rating Sheet for Belt Force Scaling

			Full Vehicle Model	
			Unscaled	LL-Scaling = 0.7
Region	Criterion	Limit		
Head	HIC <sub>15</sub>	700	500	399
	a3ms	80	70.3	62.6
	BRIC	1.05	0.87	0.95
	uBRIC	1	0.34	0.36
Neck	Nij	0.85	0.29	0.29
	F <sub>z,tension</sub>	3300	307.0	368.6
	F <sub>z,compr.</sub>	-4000	-1545.1	-1391.5
Chest	Chest Defl.	52.3	21.3	19.9
	Abdomen Defl.	88.6	8.5	7.4
Lwr Ex	F <sub>Femur</sub>	8588	3663.5	3909.2
Head-SW	min. distance	> 0 mm	70.9	46.8

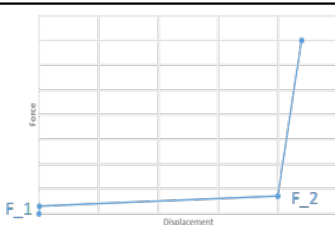
Results - U.S. NCAP Rating			
P <sub>Head</sub>		4.72%	2.40%
P <sub>Chest</sub>		1.61%	1.32%
P <sub>Femur</sub>		2.00%	2.27%
P <sub>Neck</sub>		6.62%	6.56%
P <sub>Joint</sub>		14.21%	12.04%
Rel. Risk		0.9476	0.8028
Stars		★★★★	★★★★

Figure E.1: Full Vehicle Model Rating Sheet - Comparison of Belt Force Scaling



# F Appendix - RearPosSMED

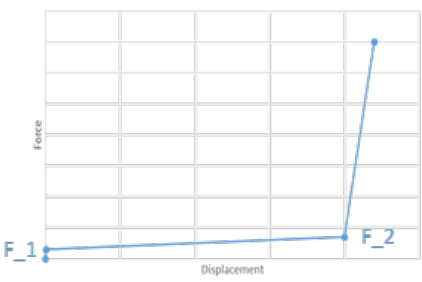
## Rating Sheet for linear-linear Force-Displacement-Characteristics with an Initial Force Level

Linear-Linear FD-Characteristic			RearPosSMED						
			TTF = 30 ms BF-Scaling = 0.7 f(x): lin-lin F_1 = 20,000 N F_2 = 25,000 N	TTF = 30 ms BF-Scaling = 0.7 f(x): lin-lin F_1 = 20,000 N F_2 = 22,500 N	TTF = 30 ms BF-Scaling = 0.7 f(x): lin-lin F_1 = 18,750 N F_2 = 25,000 N	TTF = 30 ms BF-Scaling = 0.7 f(x): lin-lin F_1 = 18,750 N F_2 = 22,500 N	TTF = 30 ms BF-Scaling = 0.7 f(x): lin-lin F_1 = 17,500 N F_2 = 25,000 N	TTF = 30 ms BF-Scaling = 0.7 f(x): lin-lin F_1 = 17,500 N F_2 = 22,500 N	TTF = 30 ms BF-Scaling = 0.7 f(x): lin-lin F_1 = 17,500 N F_2 = 20,000 N
Region	Criterion	Limit							
Head	HIC <sub>15</sub>	700	458	454	430	413	398	394	404
	a3ms	80	64.7	65.0	63.8	64.0	62.2	62.7	62.3
	BRIC	1.05	0.50	0.49	0.52	0.53	0.52	0.51	0.49
	uBRIC	1	0.19	0.18	0.20	0.20	0.19	0.19	0.18
Neck	Nij	0.85	0.31	0.29	0.28	0.27	0.26	0.28	0.23
	F <sub>z, tension</sub>	3300	440.3	330.7	317.3	294.9	540.2	291.3	308.8
	F <sub>z, compr.</sub>	-4000	-1209.8	-1289.4	-1232.9	-1155.3	-1292.4	-1101.5	-1083.7
Chest	Chest Defl.	52.3	38.7	38.2	38.6	38.5	36.9	36.3	36.3
	Abdomen Defl.	88.6	9.5	10.1	10.3	9.7	9.8	8.9	9.0
Lwr Ex	F <sub>Femur</sub>	8588	476.7	907.3	187.3	647.6	650.6	1201.6	2062.7
Head-SW	min. distance	> 0 mm	27.3	19.1	15.9	13.7	8.8	9.8	7.5

Results - U.S. NCAP Rating									
P <sub>Head</sub>		3.66%	3.56%	3.03%	2.68%	2.37%	2.30%	2.50%	
P <sub>Chest</sub>		11.06%	10.63%	11.02%	10.95%	9.42%	8.91%	8.89%	
P <sub>Femur</sub>		0.39%	0.49%	0.33%	0.42%	0.42%	0.56%	0.88%	
P <sub>Neck</sub>		6.78%	6.61%	6.39%	6.32%	6.17%	6.38%	5.91%	
P <sub>Joint</sub>		20.44%	19.90%	19.50%	19.16%	17.38%	17.16%	17.15%	
Rel. Risk		1.3626	1.3266	1.2999	1.2774	1.1587	1.1441	1.1435	
Stars		★★	★★★	★★★★	★★★★	★★★	★★★★	★★★★	

Figure F.1: RearPosSMED Rating Sheet - Comparison of Linear-Linear-Characteristics with an Initial Force Level

Linear-Linear FD-Characteristic			RearPosSMED				
			TTF = 30 ms BF-Scaling = 0.7 <b>f(x): lin-lin</b> <b>F_1 = 15,000 N</b> <b>F_2 = 45,000 N</b>	TTF = 30 ms BF-Scaling = 0.7 <b>f(x): lin-lin</b> <b>F_1 = 15,000 N</b> <b>F_2 = 35,000 N</b>	TTF = 30 ms BF-Scaling = 0.7 <b>f(x): lin-lin</b> <b>F_1 = 15,000 N</b> <b>F_2 = 27,500 N</b>	TTF = 30 ms BF-Scaling = 0.7 <b>f(x): lin-lin</b> <b>F_1 = 15,000 N</b> <b>F_2 = 25,000 N</b>	TTF = 30 ms BF-Scaling = 0.7 <b>f(x): lin-lin</b> <b>F_1 = 15,000 N</b> <b>F_2 = 22,500 N</b>
Region	Criterion	Limit					
Head	HIC <sub>15</sub>	700	438	371	342	353	366
	a3ms	80	63.7	59.1	61.2	60.7	59.8
	BRIC	1.05	0.52	0.51	0.52	0.53	0.52
	uBRIC	1	0.19	0.19	0.19	0.20	0.19
Neck	Nij	0.85	0.31	0.27	0.29	0.24	0.25
	F <sub>z,tension</sub>	3300	327.6	432.4	751.1	424.5	599.7
	F <sub>z,comp.</sub>	-4000	-1474.4	-1395.3	-1579.8	-1456.0	-1441.3
Chest	Chest Defl.	52.3	38.6	35.2	32.3	33.2	33.4
	Abdomen Defl.	88.6	7.2	7.3	7.2	7.4	7.3
Lwr Ex	F <sub>Femur</sub>	8588	640.5	334.8	1899.9	2891.1	3386.1
Head-SW	min. distance	> 0 mm	13.8	1.8	1.9	1.3	0.8

Results - U.S. NCAP Rating						
P <sub>Head</sub>		3.20%	1.89%	1.44%	1.60%	1.82%
P <sub>Chest</sub>		11.01%	8.01%	5.98%	6.51%	6.70%
P <sub>Femur</sub>		0.42%	0.36%	0.81%	1.35%	1.74%
P <sub>Neck</sub>		6.75%	6.38%	6.52%	6.03%	6.09%
P <sub>Joint</sub>		20.02%	15.81%	14.08%	14.72%	15.47%
Rel. Risk		1.3344	1.0539	0.9386	0.9815	1.0311
Stars		★★	★★★	★★★★	★★★★	★★★

Figure F.2: RearPosSMED Rating Sheet - Comparison of Linear-Linear-Characteristics with an Initial Force Level